* DORIN LELEA *
DORIN.LELEA@UPT.RO
LOCAL 12.06.2025 15:27
20.01.2025 20:28 - 20.01.2028 20:28
UNIVERSITATEA POLITEHNICA DIN TIMISOARA
Angajat UPT
20110420940401bd89332de2924a2697

Structural Strengthening of Historic Masonry Buildings Using Mesh Reinforced Composite Materials

A Thesis Submitted for obtaining
the Scientific Title of PhD in Engineering
from
Politehnica University Timișoara
in the Field of Civil Engineering
by

Arch. Dragoș Petru BOCAN

PhD Committee Chair:	prof. univ. dr. ing. Raul Dan ZAHARIA
PhD Supervisor:	prof. univ. dr. ing. Adrian Liviu CIUTINA
Scientific Reviewers:	prof. univ. dr. ing. Antonio FORMISANO
	prof. univ. dr. ing. Marcela Florina PRADA
	conf. univ. dr. ing. Sorin-Codruț FLORUȚ
	prof. univ. dr. ing. Marius MOȘOARCĂ

Date of the PhD Thesis Defense: 30th of April 2025

BUPT

The PhD thesis series of UPT are:

1.Automation
2.Chemistry
3.Energetics
4.Chemical Engineering
5.Civil Engineering
6.Electrical Engineering
7.Electronic Engineering and Telecommunications
8.Industrial Engineering
9.Mechanical Engineering
10.Computer Science and Information Technology
11.Science and Material Engineering
12.Systems Engineering
13.Energy Engineering
14.Computers and Information Technology
15.Materials Engineering
16.Engineering and Management
17.Architecture
18.Civil Engineering and Installations
19.Electronics, Telecommunications and Information Technologies

Politehnica University Timișoara, Romania, initiated the above series to disseminate the expertise, knowledge and results of the research carried out within the doctoral school of the university. According to the Decision of the Executive Office of the University Senate No. 14/14.07.2006, the series includes the doctoral theses defended in the university since October 1, 2006.

Copyright © Editura Politehnica – Timișoara, Romania, 2021

This publication is subject to copyright law. The multiplication of this publication, in whole or in part, the translation, printing, reuse of illustrations, exhibit, broadcasting, reproduction on microfilm or any other form is allowed only in compliance with the provisions of the Romanian Copyright Law in force and permission for use obtained in writing from the Politehnica University Timișoara, Romania. The violations of these rights are under the penalties of the Romanian Copyright Law.

Romania, 300223 Timișoara, Bd. Vasile Pârvan no. 2B
Tel./fax +40-(0)256 404677
e-mail: editura@upt.ro

BUPT

Foreword

Going through the steps of this doctoral research has been a long journey that would not have been possible without the help received from the persons around me. I would like to thank them all for their assistance. The events of these years saw my work being supervised by two helpful persons, Prof. PhD. Eng. Adrian-Liviu Ciutina who closely assisted me with finishing the work. He was preceded by Prof. PhD. Eng. Marius Moșoarcă, who helped me start the works and introduced me to doing research and publishing results.

Cătălina Bocan as my wife and colleague has been a wonderful support and has provided me with strength to see the work done. Her contribution was complemented to that of our design studio Atelier CAAD that invested in my research and allowed me to take time to do the work.

Lect. PhD. Arch. Alexandra Keller deserves my gratitude providing me with close support at every step and answering lots of my questions. Alongside her a group of colleagues, Lect. PhD. Eng. Mihai Fofiu, PhD. student Arch. Emanuel Tămaș, Lect. PhD. Arch. Iasmina Onescu from the Faculty of Architecture and Urbanism provided me with help and information and deserve my thanks. Other colleagues pushed me in the right direction and kept me on my tracks.

The INCD URBAN-INCERC team led by Ing. Aurelian Gruin and complemented by researcher Ion Alexandru and machinist Mihai Moldovan also deserve my thanks providing me with research hardware and knowledge.

Making possible the experimental part of my work, Kerakoll S.P.A. through Product Manager Paolo Casadei and Eng. Rareș Brădean supported my work providing materials and guidance for the test specimens.

Most of the results interpretation and much of the text work was done under the roof of Reykjavik University that offered me a calm place to study and guidance through Prof. Eyþór Rafn Þórhallsson and Prof. Jónas Þór Snæbjörnsson.

Not least, Prof. PhD. Arch. Yohei Endo assisted by student Yusuke Kuwabara from Endo Research Group and Drd. Ing. Giovanna Longobardi provided me with help on matters that were at the time less known to me.

Timișoara, November 2024 Dragoș Bocan

BUPT

BOCAN, Dragos Petru

Structural Strengthening of Historic Masonry Buildings Using Mesh Reinforced Composite Materials

PhD theses of UPT, Series X, No. YY, Editura Politehnica, 200Z, 151 pages, 100 figures, 14 tables.

ISSN:

ISBN:

Keywords

Historic masonry structures, Mesh Reinforced Composite Materials, Seismic retrofit, Architectural conservation

Abstract

The conservation and restoration of historic buildings is a complex topic that should be approached in an interdisciplinary manner to improve the structural behaviour while maintaining the authenticity and aesthetics of the structure. Therefore, the research is trying to explore structural strengthening solutions that align with urban, building conservation and social principles. Thus, the main aim of the study was to test and understand the behaviour strengthening solutions, which can also ensure the authenticity of historic buildings and limit the strengthening intervention to the more adapted surfaces while preserving the original decorations and building aspect. This could only be achieved by using compatible materials with the original structure from a historical and physico-chemical point of view. During the study, the emphasis was placed on the structural behaviour of historic masonry brick wall samples built using recovered bricks and reconstructed with lime-based mortar under in-plane shear loads. Since the main purpose was to discover acceptable strengthening options that would lead to structural retrofit of historic masonry buildings while preserving their architectural value, steel mesh reinforcements with a lime-based matrix applied on one or both sides were considered. The specimens were tested for shear strength in laboratory conditions according to the ASTM E519/E519M – 15 and the recorded results were analysed to observe the performances of the proposed solutions in terms of resistance, stiffness and ductility. Subsequently, numerical simulations were made on masonry wallets and a sample structure to understand the effect of the strengthening solutions in a global analysis.

BUPT

CONTENTS

SYMBOLS AND ABBREVIATIONS 7

FIGURE INDEX 9

LIST OF TABLES 13

1 HERITAGE BUILDINGS AND INTERVENTIONS IN TIMISOARA 14

1.1 Context 14
1.2 Structural Systems 14
1.3 Geographic Location and Implication 17
1.4 Typical Façade Decoration of Historical Buildings and Contextual Orientation 18
1.5 Property Features 21
1.6 Need for Intervention 22
1.7 Research Goals 26

2 STRENGTHENING OF HISTORIC BRICK MASONRY IN SEISMIC AREAS (STATE OF THE ART) 28

2.1 Introduction 28
2.2 Analysis of Load-Bearing Masonry Structures by Period 28
2.3 Masonry Block Types 30
2.4 Mortar and Masonry Bond 31
2.5 Wall Thickness 33
2.6 Evolution of Composite Materials Used for Masonry Walls Reinforcement 33
2.7 Strategies for Numerical Analysis of Proposed Solutions 36
2.8 Combining Seismic Retrofit with Thermal Retrofit Opportunities 39
2.9 Conclusion 39

3 EXPERIMENTAL INVESTIGATION ON MASONRY SPECIMENS 41

3.1 Analysis of Load-Bearing Masonry Structures 41
3.2 Considerations For Choosing the Case-Study 43
3.3 Presentation of the Testing Programme 44
3.4 Testing Set-up and Loading Protocol 49
3.4.1 Testing Set-up and Interpretation of Results 49
3.4.2 Loading Protocol 55
3.5 Material Properties 56
3.5.1 Brick 56
3.5.2 Lime-based Mortar 59
3.5.3 Masonry 61
3.5.4 Strengthening Materials 61
3.6 Testing Results 64
3.6.1 Unreinforced Specimen 1NA 64
3.6.2 Double-sided Strengthened Specimen 71
3.6.3 Single-sided Strengthened Specimen 78
3.6.4 Failure Modes 89
3.7 Discussion of Testing Results and Comparison 92
3.8 Conclusions of the Experimental Study 97

BUPT

4 FINITE ELEMENT INVESTIGATIONS 99

4.1 FE Modelling of Wallet Specimens 99
4.1.1 Macro-Modelling Approach 99
4.1.2 Input Data and Procedure 100
4.1.3 Numerical Results 101
4.2 Structural FE Model 103
4.2.1 Calibration at Specimen Scale 103
4.2.2 Structural Simulation Context 107
4.2.3 Seismic Characteristics and Material Model 108
4.2.4 Global Structural Behaviour 109
4.2.5 Interpretation of Numerical Results 112
4.3 Conclusions of the FE Simulations 117

5 CONCLUSIONS 118

5.1 General Conclusions 118
5.2 Practical Applications 118
5.3 Personal Contributions 119
5.4 Future Developments 119
5.5 Published Papers 121
5.5.1 Papers in Web of Science Indexed Journals 121
5.5.2 Papers in Web of Science Indexed Proceedings 121
5.5.1 Papers in International Database Indexed Proceedings 121

6 BIBLIOGRAPHY 122

7 ANNEX A FAILURE MODES OF TESTED SPECIMENS 133

7.1 Unreinforced Specimen 133
7.2 Double-sided strengthened specimen 138
7.3 Single-sided Strengthened Specimen 146

BUPT

SYMBOLS AND ABBREVIATIONS

Symbols

M_w – Seismic Moment magnitude
M_L – Seismic Local magnitude scale
L – length
w – width of the specimen
h – height of the specimen
t - thickness of the specimen
s_s – shear stress (according to ASTM E519/E519M – 15 [1])
A_n – net area of the specimen
P – diagonally applied load
n - percent of the specimen area that is solid expressed as a decimal
γ - shear strain (according to ASTM E519/E519M – 15 [1])
Δx – shortening in the direction parallel to loading, mm
Δy – extension in the direction perpendicular to loading, mm
g – gage length in the direction parallel to the loading force
G – modulus of rigidity for shear
f_k – characteristic compressive strength of masonry [N/mm^2]
K – constant used in the calculation of the compressive strength of masonry
f_b – normalised mean compressive strength of a masonry unit [N/mm^2]
f_m – compressive strength of masonry mortar [N/mm^2]
ρ – density, kg/m^3
δ – drift percent
ΔS - displacement on the horizontal axis (perpendicular to the piston force)
ΔS_1 - displacement on the horizontal axis (perpendicular to the piston force) – face 1
ΔS_2 - displacement on the horizontal axis (perpendicular to the piston force) – face 2
ΔV - displacement along the vertical axis (along the piston force)
ΔV_1 - displacement along the vertical axis (along the piston force) – face 1
ΔV_2 - displacement along the vertical axis (along the piston force) – face 2
α - angle of the diagonal
L_0 - initial distance between the displacement tracers' supports
R - virtual radius of the circle that the deformation curve was approximated
α - angle made regarding the circle center by the LVD support rods
ΔH - horizontal deformation on the non-reinforced side
ΔH_1 - horizontal deformation in the displacement tracer direction on the non-reinforced side
ΔH_2 - horizontal deformation in the displacement tracer direction on the reinforced side
δ_u - maximum drifts
δ_b - cracking drifts
E - Young's Modulus [N/mm²]
f_t – tensile strength [MPa]
G_{ft} – the fracture energy in tension [N/m]
c – masonry cohesion [MPa]
ϕ – friction angle [rad]
G_{fs} – the fracture energy related to shear [N/m]

BUPT

f_c – compressive strength [MPa]
G_{fc} - the fracture energy in compression [N/m]

Abbreviations

NHL - Natural Hydraulic Lime
FRP – fibre reinforced polymers
FRCM - fibre reinforced cementitious matrix
TRM - textile reinforced mortar
SFRP - steel fibre reinforced polymers
CRM – composite reinforced mortar
CLT - cross-laminated timber
FEA - finite element analysis
DEM - discrete element modeling
ICF - insulated concrete forms
SIP - structurally insulated panels
URM – unreinforced masonry
ETICS – External Thermal Insulation Composite System
URM – unreinfroced masonry
OS – one-sided stregthening system
DS - double-sided stregthening system

FIGURE INDEX

Fig. 1.1 Roof structure example from Timisoara 15
Fig. 1.2 Roof structure example from Arad 16
Fig. 1.3 Location of Banat Region and Timisoara (After Google Earth) [12] 17
Fig. 1.4 Typical cross-section for a historical building in Timișoara: section on a partially collapsed building 19
Fig. 1.5 Typical decoration for the region – front facades 20
Fig. 1.6 Stucco decoration pieces (examples used in re-decoration) 20
Fig. 1.7 Difference in decoration towards street vs. courtyard on the same building (example) 21
Fig. 1.8 Water infiltration damage 22
Fig. 1.9 Foundation settlement 23
Fig. 1.10 Response spectrum of Banloc 1991 seismic motion S-W[21] 24
Fig. 1.11 Accelerograms for the Banat seismic events from 1991 (a) X-direction, b) Y-direction, c) vertical direction) (after [22]) 24
Fig. 1.12 Damage examples from comparable shallow earthquake 1 (Gorj 2023) - photo by prof. Marius Mosoarca. Red – hear and diagonal tension cracking; Yellow – Shear Sliding; Purple - Crushing 25
Fig. 1.13 Damage examples from comparable shallow earthquake 2 (Gorj 2023) - photo by prof. Marius Mosoarca. Red – shear and diagonal tension cracking; Yellow – Shear Sliding; Purple - Crushing 26
Fig. 2.1 Ancient masonry structural solutions - a) Agrigento (6th century B.C.); b) Pompeii; c) Domus Augustana (1st century AD) 29
Fig. 2.2 Medieval masonry structural solutions - a) Rouen Cathedral (10th-19th century); b) Piazza del Campo, Siena - Palazzo Pubblico (13th century) and Torre del Mangia (14th century); c) Wrocław Town Hall (13th century) 29
Fig. 2.3 Masonry structural solutions starting with the 19th century - a) Clayton Hotel Amsterdam American (19th century); b) Guinness Storehouse, Dublin (20th century); c) Vienna Gasometers (19th century) 30
Fig. 2.4 Contemporary masonry buildings designed by the author 30
Fig. 2.5 Masonry structures – a) stone masonry; b) limestone masonry; c) clay brick masonry 30
Fig. 2.6 Masonry blocks – a) clay bricks [39]; b) contemporary multi-cellular clay block [40]; Autoclaved aerated concrete [41] c) Concrete block [42] 31
Fig. 2.7 Masonry bond patterns – a) English; b) Flemish; Running bonds – c) Stretcher bond; d) Header bond 32
Fig. 2.8 FRP fabrics – a) uni-directional carbon fibres; b) bi-directional carbon fibres; c) quadri-directional carbon fibres; d) uni-directional glass fibres [62] 34
Fig. 2.9 FRCM strengthening solution using glass fibre mesh and fibre reinforced cement mortar [64] 34
Fig. 2.10 Textile reinforced mortar (TRM) strengthening solutions – a) Bi-axial mesh of alkali-resistant glass and aramid fibre [66]; b) Bi-axial mesh of basalt fibre [67] 35

BUPT

Figure Index

Fig. 2.11 Composite reinforced mortar (CRM) composed of a lime-based mortar matrix and a steel fibre mesh [69] 35
Fig. 2.12 Comparative results obtained for a masonry wallet subjected to diagonal compression during a) laboratory testing; b) micro-modelling; c) macro-modelling (performed in the DIANA software) [29] 38
Fig. 3.1 Typical floor plan with bracing walls (CFR hospital Timisoara) 41
Fig. 3.2 Typical failure modes of masonry wallets [88][89] 42
Fig. 3.3 Existing masonry bond on typical historic building (suspended work site, Emanoil Ungureanu street, no. 17 Timisoara) 44
Fig. 3.4 URBAN-INCERC Contract for performing the experimental shear-strength tests on wallets 45
Fig. 3.5 Pallets for construction of specimens 45
Fig. 3.6 Specimens constructed horizontally on pallets 46
Fig. 3.7 Wall specimens – drawing and bond 46
Fig. 3.8 Unreinforced wall specimens 47
Fig. 3.9 Application of reinforcing sheets – a) first layer of reinforcement, b) second layer of reinforcements c) final reinforcement layout 48
Fig. 3.10 Application of reinforcing sheets 49
Fig. 3.11 Design of transportation jig 50
Fig. 3.12 Transportation and rotation using the jig 50
Fig. 3.13 Loading shoe design 51
Fig. 3.14 Displacement Tracer [96]; mounting solution 52
Fig. 3.15 Specimen placement with loading cell (hydraulic actuator) 53
Fig. 3.16 Layout according to "Standard Test Method for Diagonal Tension (Shear) in Masonry Assemblages – ASTM E519/E519M – 15" [97] 54
Fig. 3.17 Brick recovery site 56
Fig. 3.18 Brick transported to lab site 57
Fig. 3.19 Brick dimensions 57
Fig. 3.20 Mortar specimens during testing 60
Fig. 3.21 Mortar used as matrix 62
Fig. 3.22 Reinforcement used for double-sided strengthening specimens 63
Fig. 3.23 Reinforcement used for single-sided strengthening 63
Fig. 3.24 Force by horizontal deformation on face 1 chart of 1NA specimen 64
Fig. 3.25 Force by horizontal deformation on face 2 chart of 1NA specimen 65
Fig. 3.26 Force by vertical deformation on face 1 chart of 1NA specimen 66
Fig. 3.27 Force by vertical deformation on face 2 chart of 1NA specimen 67
Fig. 3.28 Force-drift percent response curve for 1NA URM specimen 68
Fig. 3.29 Shear stress-shear strain chart for 1NA URM specimen 69
Fig. 3.30 1NA Specimen before collapse -2s 70
Fig. 3.31 1NA Specimen after collapse 70
Fig. 3.32 Applied force in the 3A2 test intervals – breaks due to damage assessment 71
Fig. 3.33 Force by horizontal deformation on face 1 charts of 2 of 2A2 and 3A2 specimens 72
Fig. 3.34 Force by horizontal deformation on face 2 charts of 2A2 3A2 specimens 73
Fig. 3.35 Force by vertical deformation on face 1 charts of 2A2 and 3A2 specimens 74

BUPT

Fig. 3.36 Force by vertical deformation on face 2 charts of 2A2 and 3A2 specimens 75
Fig. 3.37 Force-drift percent chart for 2A2 and 3A2 symmetrically strengthened specimens..... 76
Fig. 3.38 Shear stress-shear strain chart for 2A2 and 3A2 symmetrically strengthened specimens 77
Fig. 3.39 Force by horizontal deformation on the non-reinforced face 1 (face 2 for 4A1 specimen) charts of 4A1 and 6A1 specimens..... 79
Fig. 3.40 Force by horizontal deformation on the reinforced face 2 (face 1 for 4A1) charts of 4A1, 5A1, 6A1 specimens – compression shown 80
Fig. 3.41 Force by vertical deformation on the non-reinforced face 1 (face 2 for 4A1) charts of 4A1, 5A1 and 6A1 specimens 81
Fig. 3.42 Force by vertical deformation on the reinforced face 2 (face 1 for 4A1) charts of 4A1, 5A1 and 6A1 specimens 82
Fig. 3.43 Force-drift percent chart for 4A1 and 6A1 one-sided strengthened specimens..... 83
Fig. 3.44 Shear stress-shear strain chart for 4A1 and 6A1 one-sided strengthened specimens..... 84
Fig. 3.45 Deformation on the horizontal diagonal plane 85
Fig. 3.46 Analysis of deformation implications 86
Fig. 3.47 Shear strain and shear modulus corrected values for specimen 6A1 87
Fig. 3.48 Readings from the faulty data and video analysis 88
Fig. 3.49 Example of image measurement 88
Fig. 3.50 1NA specimen failure due to diagonal tension cracking; Red – diagonal tension cracking; Yellow – Shear joint sliding 89
Fig. 3.51 Failure mode of the 2A2 specimen; Red – diagonal tension cracking; Yellow – Shear joint sliding; Purple – crushing; Orange – joint sliding delamination 90
Fig. 3.52 Failure modes of the 3A2 specimen; Red – diagonal tension cracking; Yellow – Shear joint sliding; Purple – crushing; Orange – joint sliding delamination 90
Fig. 3.53 Failure mode of 4A1 specimen; Red – diagonal tension cracking; Yellow – Shear joint sliding; Purple – crushing 91
Fig. 3.54 Failure mode of 5A1 specimen; Red – diagonal tension cracking; Yellow – Shear joint sliding; Purple – crushing 91
Fig. 3.55 Failure mode of 6A1 specimen; Red – diagonal tension cracking; Yellow – Shear joint sliding; Purple – crushing 91
Fig. 3.56 Drift-Shear Stress Graphs..... 93
Fig. 3.57 Drift-Shear Stress Graphs - Enlarged First Part..... 94
Fig. 3.58 Shear strain-stress diagrams for all relevant tested specimens..... 97
Fig. 4.1 Numerical model 99
Fig. 4.2 Tension 100
Fig. 4.3 Shear 100
Fig. 4.4 Compression..... 100
Fig. 4.5 Simulation Results..... 102
Fig. 4.6 Damage location in simulated model and laboratory tested specimen (numerical simulation - a) unreinforced masonry model; b) double-sided reinforced model; c) single-sided reinforced model; laboratory test - d) unreinforced masonry

BUPT

specimen; e) double-sided reinforced specimen; f) single-sided reinforced specimen)..... 102
Fig. 4.7 2D and 3D Projection of virtual specimen test assembly..... 103
Fig. 4.8 Calibrated URM parameters..... 104
Fig. 4.9 Reinforcement Parameters DS (Geosteel G600) Respectively OS (Geosteel G1200)..... 104
Fig. 4.10 Specimen scale simulation results..... 106
Fig. 4.11 Structural perspective and cross-section..... 107
Fig. 4.12 Masonry damage legend..... 109
Fig. 4.13 Wall 4 URM up: final state of panel wall; down: pushover response curve (the pushover curve is presented in black, and the bilinear equivalent in orange) 110
Fig. 4.14 Wall 4 DS up: final state of panel wall; down pushover response curve (the pushover curve is presented in black, and the bilinear equivalent in orange)..... 111
Fig. 4.15 Wall 4 OS up: final state of panel wall; down pushover response curve (the pushover curve is presented in black, and the bilinear equivalent in orange)..... 112
Fig. 4.16 URM Wall 4 at maximum 5.84cm drift..... 113
Fig. 4.17 DS Wall 4 at 5.82cm drift..... 113
Fig. 4.18 OS Wall 4 at 5.84cm drift..... 113
Fig. 4.19 Shear Drift comparison..... 115
Fig. 4.20 Shear Drift Comparison - Enlarged First Part..... 116
Fig. 7.1 Main events during 1NA unreinforced masonry specimen testing..... 137
Fig. 7.2 Main events during 2A2 two-side strengthened specimen testing..... 145
Fig. 7.3 Main events during 4A1 one-side strengthened wall testing..... 156

LIST OF TABLES

Table 1-1 Brick compressive strength in Banat region (specimens) 16
Table 1-2 Reconstructed historic lime mortar strength - D Janotova, Z Slizkova "Lime-based mortars with various binder composition: characterization and freeze-thaw resistance assessment" [11], current study 16
Table 2-1 Physical-mechanical properties of masonry blocks 31
Table 2-2 Physical-mechanical properties of mortar 33
Table 3-1 Testing specimens and the considered strengthening solution 49
Table 3-2 Brick compression tests (scan from report of URBAN-INCERC Timisoara) 58
Table 3-3 Brick density 59
Table 3-4 Masonry mortar density 59
Table 3-5 Mortar testing results 60
Table 3-6 Reinforcing materials properties [93] [69] [94] 63
Table 3-7 Comparison of key data 95
Table 4-1 Material properties used in the macro-scale model 101
Table 4-2 Maximum Shear for 3Muri Specimens 105
Table 4-3 Material properties of the reinforcement materials used in the numerical simulation 109
Table 4-4 Pushover analysis results 114

BUPT

1 HERITAGE BUILDINGS AND INTERVENTIONS IN TIMISOARA

1.1 Context

Central and eastern Europe built environment was transformed by the changes brought by the industrial revolution during the late 19th and the beginning of the 20th century [2]. In many parts of this region fired brick was the material of choice due to local resources and the industrialization. In larger cities hundreds of new buildings were built in a timespan of just a few decades [3]. The very character of these centres was defined by the built environment of this period.

Time passed and a few decades later, after the degradation of these buildings the problem was how to approach their restoration. After the romantic and conservative approaches put forth by Viollet-le-Duc and John Ruskin and the destruction of the world wars a new approach emerged. It was based on the conservation of authenticity, at building scale [4], then at urban scale [5] and with consideration towards local context [6], social implications and changes [7] [8]. The main declarations and charters that summarize this approach are The Venice charter, The Declaration of Amsterdam, The Nara Document of Authenticity, The Burra Charter and the Valletta Principles.

The hazards that these similar structures face are different in respect to their geographical locations, one of the main examples being the seismic actions that they face, as documented by the SHARE Project [9].

The intervention on the structure of the buildings is one of the key aspects of each rehabilitation as degradation occurred in time and the real risks are better understood. Structure is also a key element, and its lack o capacity negates any use of the construction.

The current thesis is focused on the structures of this period and tests a possible answer to the structural maintenance of masonry elements that would preserve as much of the cultural and social significance of the buildings they belong to.

1.2 Structural Systems

The structures of this period present in the Banat region consist of mainly masonry foundations and wall elements. The regular masonry is made of standard compact fired units.

The underground level is generally present, with masonry foundation and walls, with small top windows towards the street. The first floor above the underground level is supported by either masonry vaults or a brick barrel vaulted ceiling supported by steel beams. To obtain a flat floor above it, a light infill is present above the arching vaults. This floor is usually higher than the street level, sometimes with a considerable level difference.

The upper floor walls taper towards the top of the building providing vertical support and exhibiting horizontal exterior ledges. They have standardized thicknesses, 60, 45 and 30 cm resulting from the used brick module. Lime based mortar is predominant, cement mortar being used in the later period together with the introduction of some concrete elements. The walls characteristics vary considerably based on their position and role in the building. The internal walls are largely devoid of openings. The external walls get a classical rhythm of window

BUPT

openings that diminish the active wall area and divide it into piers - and – lintels system. In this case the exterior masonry stresses are higher. This proved to be configuration problem, especially in the seismic areas, as is the western Romania, in which there is a lack of transverse walls perpendicular to the façade. On the longitudinal direction the walls are mostly evenly spaced due to the wood beam elements length. The structures of the floors above the upper levels are built around closely spaced parallel wooden beams that connect the walls at regular intervals, usually at 1 to 2 m. These are covered on both sides with planks, with a filling and parquet finish on top and a reed reinforced plaster ceiling beneath.

The resulting floor structures suggest their elasticity in the horizontal plane, thus the carrying walls share the horizontal seismic loads, regardless of their configuration and relative rigidity. This results in an increased importance of their shear behaviour.

Most roof structures of the mentioned period use queen post truss systems with tie beams firmly connecting the below masonry walls. For taller roofs additional queen posts or even king post trusses are stacked on top of each other [10]. Fig. 1.1, Fig. 1.2Fig. 1.2



Fig. 1.1 Roof structure example from Timisoara

BUPT



Fig. 1.2 Roof structure example from Arad

Specimens of compact fired brick from different buildings in the Banat region tested at the laboratory of Politehnica University Timișoara yield different results Table 1-1.

Table 1-1 Brick compressive strength in Banat region (specimens)

Specimen Code	PFB	GLM	FLD	YS	BJT	PCAC	PIPM	POC
f_b [N/mm²]	15.16	14.82	9.56	16.58	14.41	14.64	8.71	14.93

As for mortars, they are mostly sand-lime, and are harder to replicate today, because the procedure of producing hydrated lime has changed drastically since that time. Because of the need to have mortars compatible for work on historic buildings is high various compositions are being explored including for the specimens built for the present study Table 1-2.

Table 1-2 Reconstructed historic lime mortar strength - D Janotova, Z Slizkova "Lime-based mortars with various binder composition: characterization and freeze-thaw resistance assessment" [11], current study

Specimen source	L[11]	LM[11]	NHL3.5[11]	NHL5[11]	Current Study Specimens Average
f_m [MPa]	1.8	5.9	6.8	6.1	5.38

1.3 Geographic Location and Implication

Timisoara and the Banat Region are found in Eastern Europe, in the western part of Romania[12]. A large part of its surface belongs to the West Plain, a large alluvial plain, part of the Pannonian Basin at the west of the Carpathian Mountains (Fig. 1.3).

This area is characterized by the presence of seismic activity. The earthquakes in this region are characterized by the following characteristics:

- Short periods of vibration (ranging from below 0.2 seconds to up to 0.3 seconds) that impact large masonry structures.
- Pulse actions with a strong initial cycle followed by cycles of reduced intensity.
- Significant components perpendicular to the fault rupture.
- Horizontal and vertical components of similar acceleration.

The most recent significant activity with epicentres in this area dates from 1991 and has reached an intensity of 5.6 on the Richter scale [13].

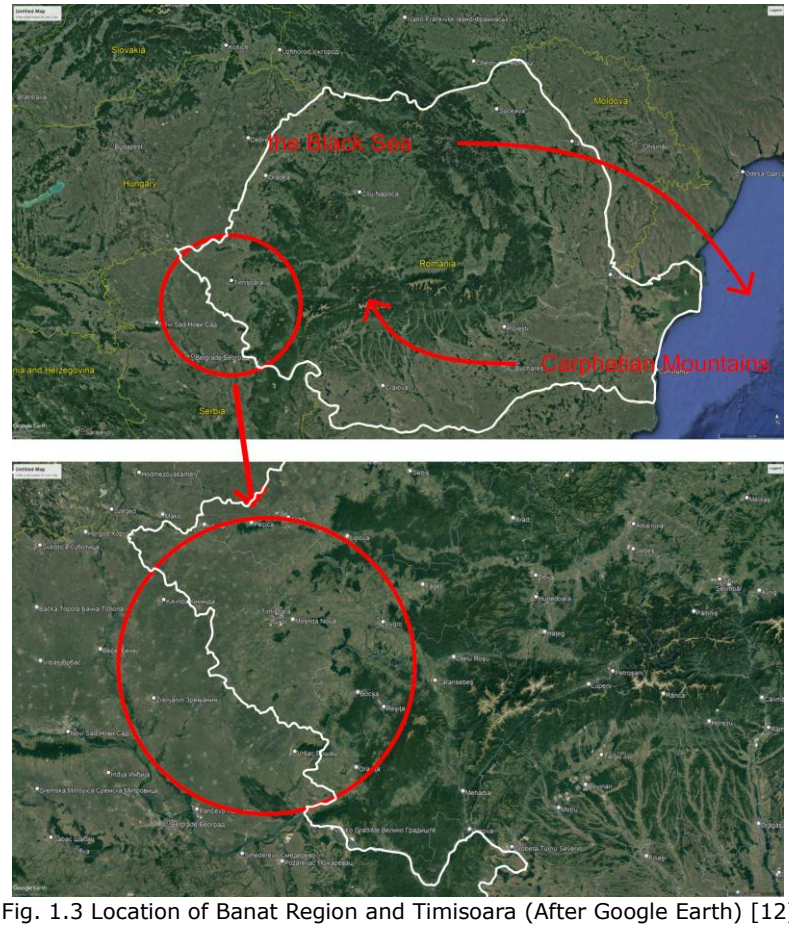


Fig. 1.3 Location of Banat Region and Timisoara (After Google Earth) [12]

Geomorphologically (based on various geotechnical studies), the region belongs to the Banat Plain, specifically the Timiș Plain subdivision, with its horizontal aspect contributing to the stability of the terrain.

Geologically, the area belongs to the Pannonian Basin, with the stratigraphic column comprising a lower layer affected by tectonic activity and a post-tectonic cover.

The lower stratigraphic layer (pre-Senonian) consists of crystalline formations. The upper part of these formations presents an altered zone with variable thickness, generally between 50–100 meters. Occasionally, the metamorphic basement rocks are intersected by eruptive rocks. Above the crystalline formations are Permian and Mesozoic formations, represented mainly by sandstones, conglomerates interbedded with clay, argillaceous-sandy schists and limestones.

Post-tectonic cover begins with Senonian formations, laid transgressively and discordantly over older Mesozoic deposits or directly over the crystalline basement. Senonian deposits exhibit significant diversity, including conglomerates, limestones, chalky limestones, calcareous sandstones, argillaceous schists with coal layers, and microconglomerates. Toward the end of the Senonian period sedimentation resumed. Finally, Quaternary deposits represent alluvial, aeolian, and fluvial deposits distributed across various local geological features.

Around Timișoara recent alluvial Quaternary deposits can be identified. These deposits are part of the fluvial stratigraphy, with variation in thickness depending on natural processes and anthropogenic intervention.

According to seismic zoning, the site is characterized by the following parameters: a_g = 0.20 g; T_c = 0.7 s (as per P100-1/2013). The frost depth is 0.6–0.7 meters (as per STAS 6054/77).

1.4 Typical Façade Decoration of Historical Buildings and Contextual Orientation

After one century and a half of Ottoman ruling, since the 18th century when Timisoara was taken over by Austrian administration, later known as the Austrian Empire, a policy of replacing existing built and urban structures within the city was implemented and pursued [14]. It was continued until 1918 when the Austro-Hungarian Empire collapsed. The ottoman traces were erased and new streets, fortification systems, infrastructure replaced the old ones [15].

The new urban planning system is a designed and cartesian one with squares and continuous built front towards the streets. The facades that make up this front are generally 3 storeys high. The nearby cities in Romania such as Arad, Oradea, Caransebeș, Lugoj have similar developments.

The new structures are made of locally sourced materials. As clay is present, fired bricks are the main masonry material. They make up large parts of the structures. Foundations, vaults, walls are made of fired bricks. Several factories were present in the Banat region, close to Timișoara, in Jimbolia, Kikinda, Lugoj, Sankt Hubert and Charleville [16]. They were not only producing ceramic bricks and roof tiles for local needs but also exporting them.

Other materials involved is local wood, mainly oak and spruce being used for floors and roof structures.

Building systems used are the same encountered throughout the whole Austro-Hungarian Empire at the time of construction. The degree of organization

BUPT

meant that these systems were documented in books as Lothar Abel's Allgemeiner Bauratgeber [17], documents that well illustrates the materials and the technologies used.

The typical construction in the Timisoara city centre generally consists of an underground level that has its upper part higher than the surrounding streets' level, gaining space for small windows or ventilation. The floor above it is built using brick arches and vaults with filling materials on top resulting in a flat usable surface. The foundations and walls are all made of brick masonry with considerable thickness, thicker than the structural walls. The three storeys above it are made of masonry walls and wooden floor slabs with plastered ceilings. The masonry walls are thicker at the ground level and thinner at the upper levels, using standard modular thicknesses of 60 cm, 45 cm, and 30 cm, respectively. The roof structure is a timber framing system that holds a ceramic tile cover with steep slopes of 30, 45 or even 70° angles, the latter value being more typical at the beginning of the 20th century. In some cases, the floor above the ground level is vaulted (Fig. 1.4).



Fig. 1.4 Typical cross-section for a historical building in Timișoara: section on a partially collapsed building

The decoration of the front façades represents a very important feature for the city image of the time, as well as for the character of these historic areas in contemporary times, many of them becoming listed as heritage sites (Fig. 1.5).

The original decorations are generally made of stucco pieces attached both mechanically and with mortar to the masonry (Fig. 1.6). It consists mostly of window

BUPT

perimeter profiles, medallions, and cornices. The rest of the façade is covered in lime plaster with a final coat of paint.

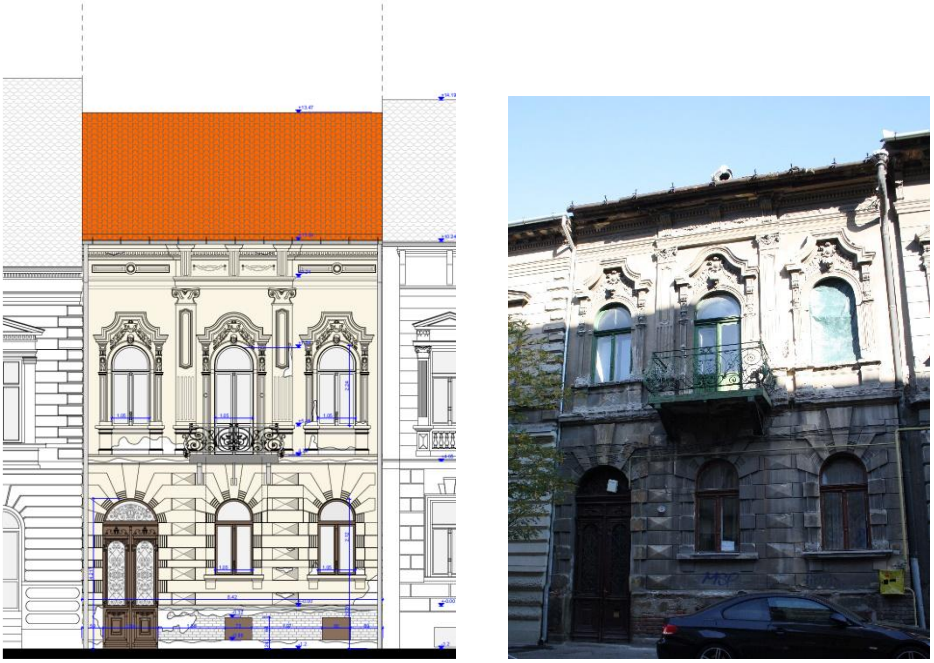


Fig. 1.5 Typical decoration for the region – front facades



Fig. 1.6 Stucco decoration pieces (examples used in re-decoration)

However, the building facades were treated differently by the time-builders: while the front (street) ones get a lot of attention with generally neoclassical or eclectic decoration, the inner courtyards facades are much simpler and are mainly covered by plain plastered surfaces, sometimes coming with curved window jambs (Fig. 1.7).



Fig. 1.7 Difference in decoration towards street vs. courtyard on the same building (example)

These building methods can be found throughout the former Austro-Hungarian Empire. They are present in cities in the western part of Romania, as well as in Hungary, Austria, Serbia, Slovakia, Czech Republic, and other countries.

1.5 Property Features

The Romanian property form in the apartment buildings is highly particular comparing with other countries of Europe. This is due to the recent history and specific events from the 20th century.

During the communist ruling (1947 - 1990), the heritage buildings, as well as other private properties were nationalized. In order to house the important number of workers imported into town, some of the apartment structures were modified or adapted. The new families and individuals were allowed to stay in the apartments for a symbolic rent, assigned to them as they were brought to work in the newly planned industries.

After the 1989 Revolution, several repair procedures were implemented. One procedure involved the restitution of properties to identified former owners. If the former owners could not be identified, the renters were given the opportunity to purchase the apartments they had been occupying before 1989.

The output result of this sequence of decisions is that a staggering 98% of the apartments are privately owned sometimes by individuals in in precarious health and economic state, unable to finance or take care of the building [18].

1.6 Need for Intervention

The necessity for intervention is brought forth by a multitude of factors:

- Climate degradation, gradually in its nature, but which can lead to sudden failure events, like roof or cornice collapses due to roof structure water actions, or even sudden detaching of plaster surfaces and decorations that are loose to a point where a storm or frost make them fall off (Fig. 1.8)



Fig. 1.8 Water infiltration damage

- Foundation settlement, often combined with damaged rainwater collection systems (Fig. 1.9).
- Human intervention degradation, like incompetent removal of structural elements, use of incompatible materials
- Seismic activity degradation.



Fig. 1.9 Foundation settlement

The latter action is very important as its hazardous moment is unforeseeable and can lead to considerable damage to URM (unreinforced masonry) buildings and loss of life. The artistically valuable elements of listed buildings or listed urban areas can also be affected. In Romania, Timisoara and Banat region are known as seismic zone with its own geo-seismic characteristics. This aspect should be thought in the context in which the entire Timișoara city centre is a listed protected area subjected to preservation. The same situation is met in the surrounding important cities.

The Banat earthquakes characteristics are [19], [20]:

- Shallow epicentre 5 to 30 km depth
- Expected peak ground acceleration of 0.2 g
- Short periods of vibration (0.2-0.3 s). This overlaps with the oscillation periods of massive masonry buildings, fact that may lead to resonance effect and possible destructions.
- The recorded accelerograms show powerful first cycles followed by ones of reduced intensity.
- Similar intensities of horizontal and vertical components, thus the vertical accelerations are important.
- The most important movements are perpendicular to the faults.

BUPT

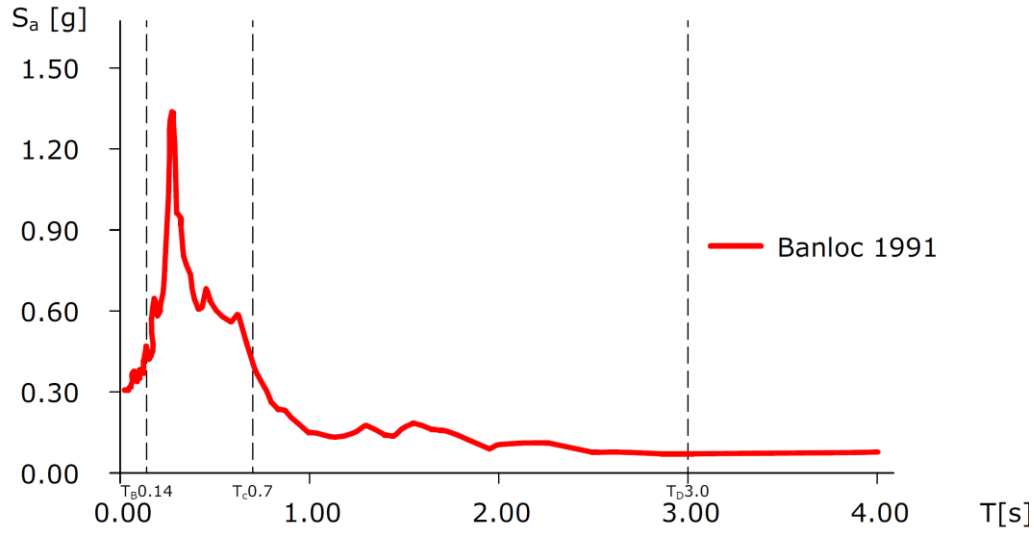


Fig. 1.10 Response spectrum of Banloc 1991 seismic motion S-W[21]

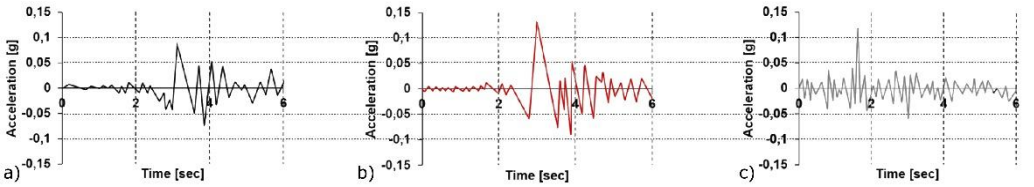


Fig. 1.11 Accelerograms for the Banat seismic events from 1991 (a) X-direction, b) Y-direction, c) vertical direction) (after [22])

The most powerful recent earthquake in the area was of M_w= 5.6 magnitude, with an epicentre near Banloc, South-West of Timisoara [19][23] that generated damage to the nearby buildings and was felt tens of kilometres away (Fig. 1.10). Accelerograms recorded during the seismic event show that the intensities on the horizontal and vertical direction are similar, reaching in both cases up to 0.13 g (Fig. 1.11). This highlights that in this region, both components of the seismic action must be taken into account.

Most recently there was a comparable activity in a nearby area, in Gorj County, where there were several seismic movements in February 2023, the larger of which had a magnitude of M_L5.2 and M_L5.7. The epicentres were also shallow, situated at 16.5 and respectively at 6.3 km of depth. Damage done to masonry buildings was typical by diagonal cracks and can be seen below in Fig. 1.12 and Fig. 1.13, but the buildings also present typical damages which can be connected to the important vertical component of the earthquake [24].



Fig. 1.12 Damage examples from comparable shallow earthquake 1 (Gorj 2023) - photo by prof. Marius Mosoarca. Red – hear and diagonal tension cracking; Yellow – Shear Sliding; Purple - Crushing

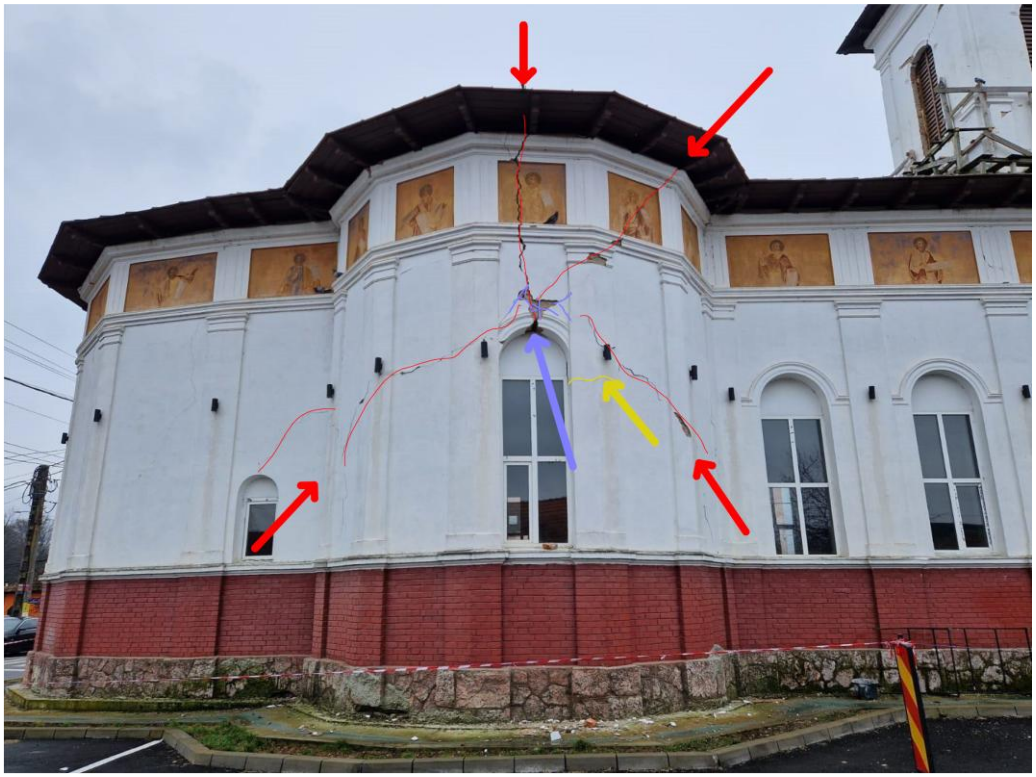


Fig. 1.13 Damage examples from comparable shallow earthquake 2 (Gorj 2023) - photo by prof. Marius Mosoarca. Red – shear and diagonal tension cracking; Yellow – Shear Sliding; Purple - Crushing

The context underscores the pressing need for interventions to strengthen masonry walls in seismic-prone areas. The primary goal is to enhance the shear strength of the weakened walls while preserving the architectural expression and ecological value of historic brick structures. Contemporary conservation philosophy emphasizes minimal alteration to the original behaviour of monuments, thus discouraging the use of very high strength materials and rigid additions, which are deemed inappropriate for such applications [25].

However, the past practice proves that due to the context related to apartment property in Romania, coupled with the reluctance and sometimes impossibility to move out the occupants during the presumptive interventions, one possible structural rehabilitation arises for the interventions made only on the external side of the walls.

1.7 Research Goals

The research presented herein tried to align the need for structural strengthening and align it with the ICOMOS principles [4], [5], [6], [7], [8], [26]. The "International Charter for the Conservation And Restoration Of Monuments And Sites (The Venice Charter 1964)" [4] The Declaration of Amsterdam" [5] highlights that besides the cultural value of heritage structures, it is also essential to consider the social and physical context of the building and, ultimately, the social consequences of

the interventions, mainly in the case of owners and tenants. The "The Nara document on authenticity" [6] represents one step further from the Venice Charter. It acknowledges the importance of considering the cultural, social and historical value of the world heritage and highlights that to preserve the authenticity of heritage, it is crucial to involve multidisciplinary teams in each step, from analysis to monitoring. Ultimately, the "Burra charter" [7].

To this end, researchers and building material companies have developed various materials and techniques. The research goals that can be maintained in this context are:

- Ensuring the authenticity of the materials and design
- Limiting the strengthening intervention to the more adapted surfaces to receiving it, while preserving the original decoration
- Using compatible materials with the original structure from historical but also from physic-chemical point of view
- Considering the environmental impact of the materials and techniques used.

Adapting the intervention to the human and social factor, as in Romania, the context of apartment ownership presents unique challenges for masonry wall strengthening, particularly in seismic-prone areas. Many apartments are owner-occupied, making it impractical to relocate residents during structural interventions. due to financial, logistical, and social reasons. Many residents may also be reluctant to leave their homes, even temporarily, due to personal attachments and security concerns. Consequently, there is a strong preference for carrying out necessary strengthening work exclusively from the exterior.

In the case of historic buildings, preserving the interior aesthetics and original features is crucial. Internal interventions could disrupt these elements, leading to a loss of cultural and historical value. Similarly, for public buildings that have outside highly decorations, the preference might be to conduct the intervention on the inside, especially where the external façade's appearance is critical to the adjacent urban context.

The plaster surfaces of the streets can be used to strengthen the building.

The facades towards the inner courtyards of the city blocks, not being covered by any decoration lend themselves to a greater possibility of intervention, that can easily include strengthening and even thermal upgrades, the extra few centimetres of thickness not altering their aspect in a critical way.

BUPT

2 STRENGTHENING OF HISTORIC BRICK MASONRY IN SEISMIC AREAS (STATE OF THE ART)

2.1 Introduction

Masonry has been throughout history an important material used because of its durability, aesthetics and mainly because of its corresponding load bearing capacity. More than this, it was used in a variety of regions, with or without seismic activity, proving therefore its versatility but also leading to high vulnerabilities over time. Therefore, in order to maintain their structural integrity and ensure the safety of the inhabitants, suitable strengthening solutions have to be found, which could also ensure the protection of the valuable features of the buildings [27]. The solutions should be adapted in function of the building degradations and past interventions; therefore, each building represents a case-study and should be treated independently.

Within the scope of this insight, a detailed evaluation of the development and current condition of masonry structures strengthening solution is provided. The historical analysis, the traditional and contemporary reinforcement materials and techniques, the numerical analytical strategies, and the integration of seismic and thermal retrofitting are the primary areas of attention. The purpose of this analysis is to bring attention to the recent developments in reinforcement techniques and the ways in which these techniques can be used to improve the structural performance of masonry buildings.

2.2 Analysis of Load-Bearing Masonry Structures by Period

Over several centuries, masonry construction techniques have evolved significantly, influenced by advances in technology, architectural styles, engineering knowledge and available materials. Throughout antiquity (Fig. 2.1), massive stone blocks and cement-free construction techniques were used, like in the case of the Egyptian pyramids and Greek temples. The use of precision cutting and interlocking stones reduced the amount of binding materials required [28]. Throughout the mediaeval period (Fig. 2.2), vaults, flying buttresses, and arches made of stone and brick were created to support larger and more complicated structures. For this, mortar has become a more widely used technique for joining stones and bricks [29]. Subsequently, starting with the Renaissance, different solutions suitable for reinforced masonry were developed with the ultimate goal of enhancing the structural performance of buildings considering lime mortars and later Portland cement mortars gained widespread usage [30]. The various building techniques and materials that have been employed throughout history have a significant impact on the load-bearing capacity and structural behaviour of masonry structures (Fig. 2.3,Fig. 2.4). The original constructions were built using large stone blocks, which required a lot of work but provided a lot of strength and stability. The use of brick and mortar enabled more adaptive designs and streamlined the construction process. A thorough understanding of these strategies is required for developing successful reinforcement methods that preserve the original design while increasing performance [31]. Various case studies which focus on the analysis of historic masonry structures highlight that advanced

understanding of these structures and the influence of local seismic and environmental conditions and the way structures were designed [32] [33].



a) b) c)

Fig. 2.1 Ancient masonry structural solutions - a) Agrigento (6th century B.C.); b) Pompeii; c) Domus Augustana (1st century AD)



a) b) c)

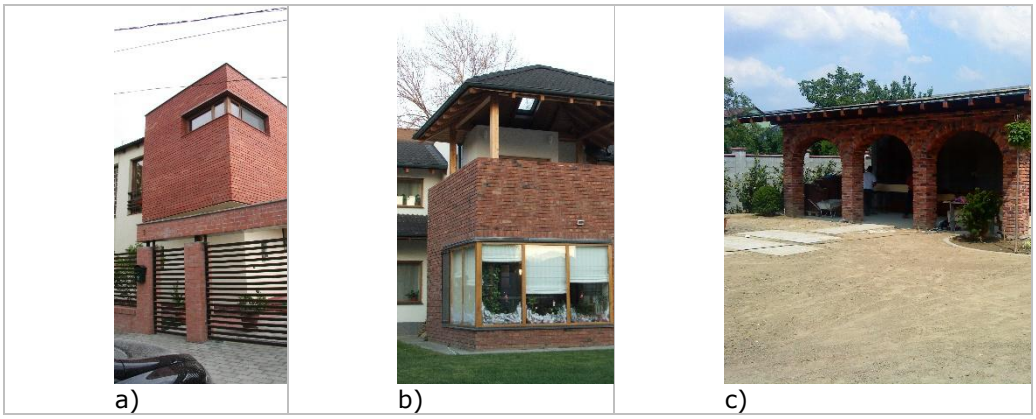
Fig. 2.2 Medieval masonry structural solutions - a) Rouen Cathedral (10th-19th century); b) Piazza del Campo, Siena - Palazzo Pubblico (13th century) and Torre del Mangia (14th century); c) Wrocław Town Hall (13th century)



a) b) c)

BUPT

Fig. 2.3 Masonry structural solutions starting with the 19th century - a) Clayton Hotel Amsterdam American (19th century); b) Guinness Storehouse, Dublin (20th century); c) Vienna Gasometers (19th century)

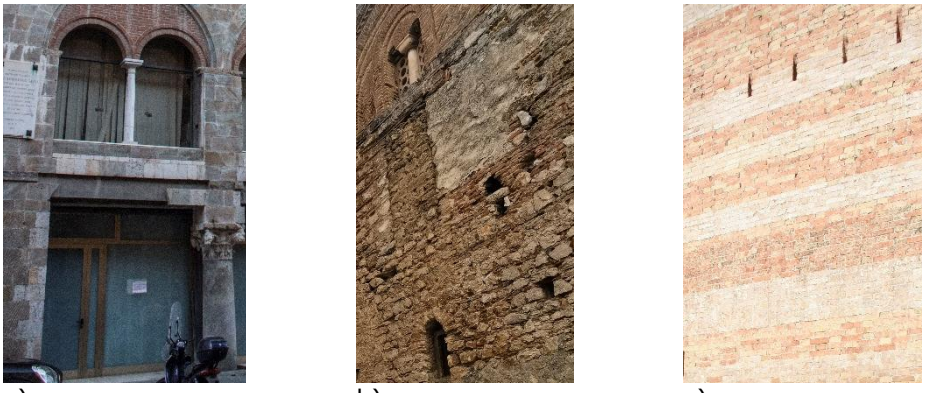


a) b) c)

Fig. 2.4 Contemporary masonry buildings designed by the author

2.3 Masonry Block Types

Diverse varieties of masonry blocks, including stone blocks, clay bricks, and concrete blocks, have been used in a variety of purposes throughout history and some continue to be used today (Fig. 2.5). Blocks made of stone, such as limestone, granite, and sandstone, have been used for construction ever since ancient times due to their durability and aesthetic appeal. They have been used in the construction of significant monumental structures [34] that are still standing to this day. In addition to this, they provide a wide range of aesthetic looks, ranging from the straightforwardness of traditional clay bricks to the unusual shapes and colours of contemporary variations [35]. Concrete blocks on the other hand, which were developed in the 20th century, ultimately reveal to have some advantages from a structural point of view due to the homogeneity of the material and adaptable geometry [36].



a) b) c)

Fig. 2.5 Masonry structures – a) stone masonry; b) limestone masonry; c) clay brick masonry

Studies focusing on the mechanical properties and structural performance of various masonry blocks (Fig. 2.6) show that stone blocks offer a good load-bearing capacity while being difficult to manipulate and require the assistance of professional labourers, which makes them suitable for monumental construction projects [37]. Clay bricks on the other hand are favourable in both historic and contemporary buildings because of their adaptability and simplicity of handling. Despite not having a high compressive strength, they are advantageous in various types of constructions [38]. Ultimately concrete blocks have a higher compressive strength and are homogenous but are heavier and have less aesthetic appeal than stone or brick, which makes them more often used in the case of structures which must be cost-effective [26].

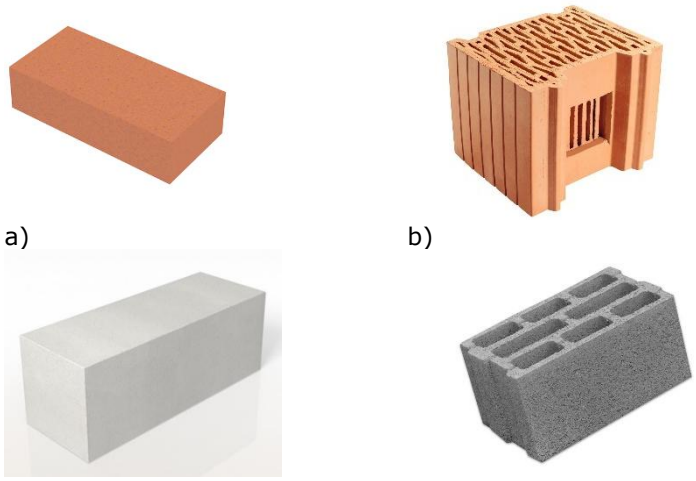


Fig. 2.6 Masonry blocks – a) clay bricks [39]; b) contemporary multi-cellular clay block [40]; Autoclaved aerated concrete [41] c) Concrete block [42]

Contemporary manufacturing methods have led to the production of masonry blocks with different types of advantages like lightness, fire-resistance and thermal efficiency [43], all connected to simplified construction techniques which is ultimately leading to a significant reduction of building costs [44] (Table 2-1).

Table 2-1 Physical-mechanical properties of masonry blocks

Masonry block type	Dimensions [mm]	Density [kg/m3]	Thermal conductivity [W/mK]	Compressive strength [N/mm^2]
Clay brick [39]	240x115x63	1530	0.435	30
Multi-cellular Clay Block [40]	250x300x238	850	0.142	10
Autoclaved aerated concrete [41]	250x599x199	580	0.148	5.10
Concrete block [42]	400x 250x195	1035	1.11	7

2.4 Mortar and Masonry Bond

The strength and stability of masonry walls are mainly influenced by various bonding patterns, including English, Flemish, and running bonds – stretcher bond and header bond (Fig. 2.7). Effective bonding allows for a better load transfer and crack

BUPT

distribution. Studies show that running bonds provide both excellent stability and a decreased resistance to lateral loads. The Flemish bond provides a more uniform weight distribution and enhances aesthetics by inverting the headers and stretchers. The best structural stability is provided by the English bond, which consists of rows of alternating stretchers and headers [45].

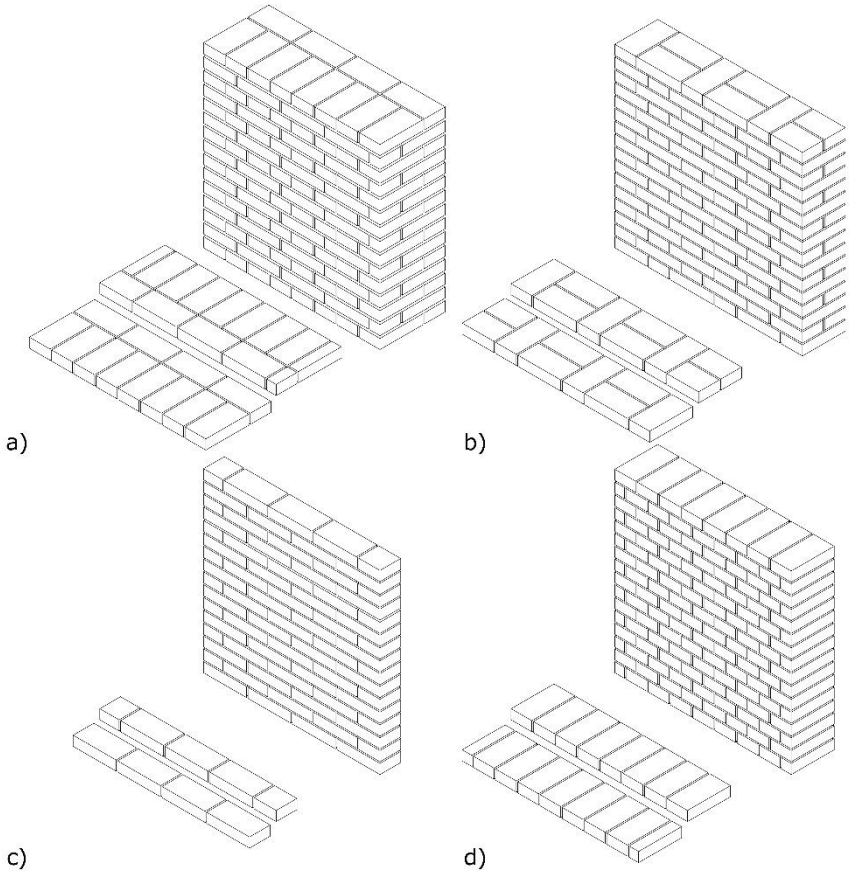


Fig. 2.7 Masonry bond patterns – a) English; b) Flemish; Running bonds – c) Stretcher bond; d) Header bond

Besides the bond, another important component of masonry structure is the mortar which is used as a binding agent that holds the masonry pieces together (Table 2-2). It also disperses weight and allows for little movements within the structure. The type of mortar that is used has an impact on the wall's ability to withstand stresses, weathering, and thermal expansion and contraction [46]. Three different types of mortars are used: composite mortars, cement mortars, and lime mortars. Lime mortar is a traditional mortar that is well-suited for historical restorations due to its flexibility and breathability [47]. Cement mortar is a construction material that is extensively used in contemporary construction because it has a better strength and a faster setting time than traditional mortar. Even though it offers a good binding, it does not possess the flexibility of lime mortar [48]. Composite mortars on the other

hand are mortars that are made from lime, cement, and several additional additives. These mortars are used to improve certain features, like as durability and thermal insulation of a building [49].

Table 2-2 Physical-mechanical properties of mortar

Mortar type	Thermal conductivity [W/mK]	Compressive strength [N/mm^2]
Lime mortar [50]	0.82	5
Cement mortar [51]	0.80	5
Composite mortar (cement-lime) [52]	0.87	5

Replicating the mortar properties of the original structure is often challenging when renovating historical buildings. Important considerations include breathability, aesthetic alignment, and compatibility with current materials [53]. This issue remains a challenge for the interventionist and should be judged for each case-study.

2.5 Wall Thickness

Historically important masonry buildings often have walls that are between one and two meters thick for two primary reasons: so that they are stable and that they provide thermal insulation. Contemporary masonry structures are often thinner, than the historical ones, due to the presence of reinforced concrete elements included to ensure a better structural behaviour [54] reaching down to 95 mm in the case of load-bearing cavity walls in areas with low seismicity [55]. However, thicker walls might be more vulnerable to earthquake stresses due to their increased mass. Reinforcement methods must therefore achieve a balance between these parameters to improve the general performance of the exterior load-bearing walls. Thinner and more flexible reinforced walls provide a decrease in total weight and an improvement in flexibility to enhanced seismic performance [56].

Generally, the strengthening of historic masonry structures involves solutions applied on the inner and outer side of a load-bearing wall. There are various strengthening methods that could include the addition of steel rods or meshes to the walls to increase their tensile strength and applying various materials to the wall's exterior side to increase the load bearing capacity without drastically changing the wall's appearance [57].

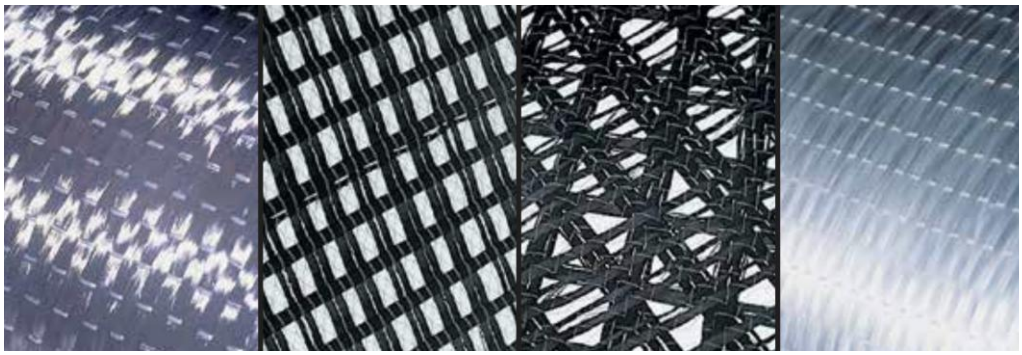
2.6 Evolution of Composite Materials Used for Masonry Walls Reinforcement

Concrete jackets with embedded steel mesh have been used since the early 20th century to strengthen and stabilize masonry structures, particularly in seismic zones. This method provides a robust external shell that improves load distribution and resistance to lateral forces [58]. Effective in improving the compressive and shear strength of masonry walls, concrete jackets are widely used in retrofitting historical buildings to enhance their seismic resilience. They can be applied internally or externally, depending on the structure’s requirements [59].

Fibre reinforced polymers (FRP) include composites such as carbon, glass, and aramid fibres (Fig. 2.8), providing high tensile strength, lightweight, and corrosion resistance. They are flexible and can be applied in various forms, such as sheets,

BUPT

strips, or rods [60]. Commonly used for external reinforcement, FRP strips and sheets are bonded to masonry surfaces to improve tensile and flexural strength. Successful applications include retrofitting bridges, walls, and heritage buildings. For example, FRP has been used to reinforce historical buildings in seismic zones, enhancing their ability to withstand earthquakes [61].



a) b) c) d)

Fig. 2.8 FRP fabrics – a) uni-directional carbon fibres; b) bi-directional carbon fibres; c) quadri-directional carbon fibres; d) uni-directional glass fibres [62]

Fibre reinforced cementitious matrix (FRCM) combines fibre reinforcements, such as carbon or glass, with a cementitious matrix, offering improved bonding and compatibility with masonry substrates (Fig. 2.9). This composite material provides enhanced durability and resistance to environmental degradation. Studies show significant improvements in shear and flexural performance, with FRCM providing an effective alternative to traditional FRP systems. FRCM systems have been successfully applied in the retrofitting of historical and modern masonry structures, offering a balanced combination of strength and compatibility [63].

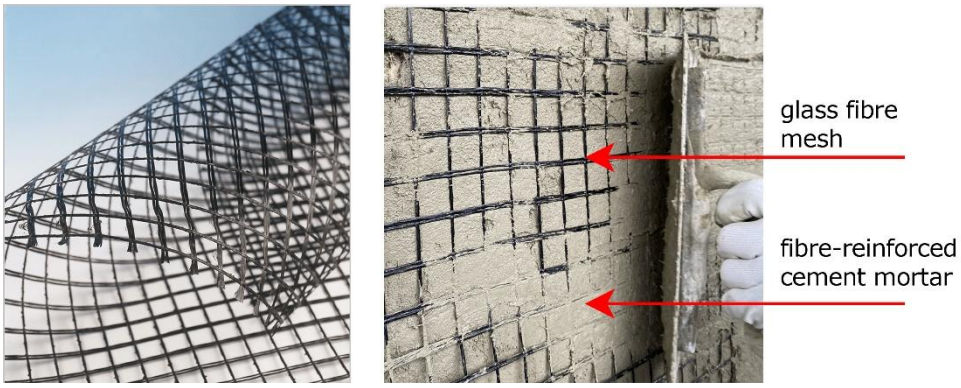


Fig. 2.9 FRCM strengthening solution using glass fibre mesh and fibre reinforced cement mortar [64]

Textile reinforced mortar (TRM) incorporates high-strength textiles, such as glass, basalt, or even steel fibres within a mortar matrix, enhancing the ductility and strength of masonry walls (Fig. 2.10). This method is particularly suitable for reinforcing complex geometries and curved surfaces. TRM offers better compatibility

and ease of application compared to FRP and FRCM, making it suitable for both historical and modern structures. Its flexibility and adaptability make it an ideal choice for preserving the aesthetic integrity of historical buildings while providing structural reinforcement [65].

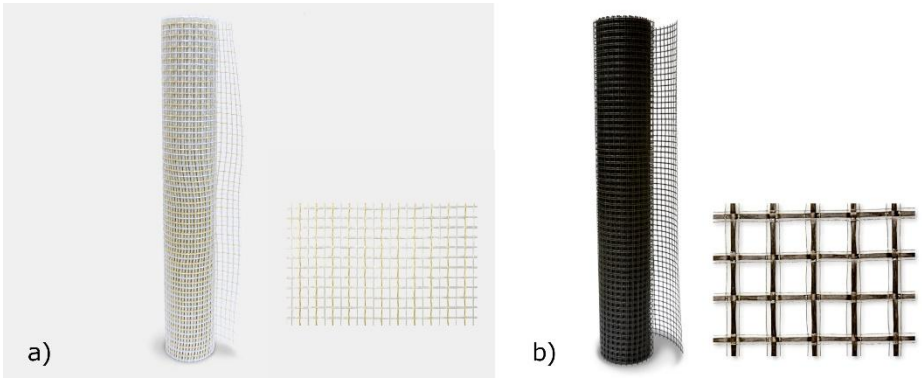


Fig. 2.10 Textile reinforced mortar (TRM) strengthening solutions – a) Bi-axial mesh of alkali-resistant glass and aramid fibre [66]; b) Bi-axial mesh of basalt fibre [67]

Composite reinforced mortar (CRM) integrates fibres and additives within the mortar, improving its mechanical properties and durability (Fig. 2.11). This composite material is used to reinforce masonry walls, providing enhanced resistance to cracking and environmental degradation. CRM has been used in various retrofitting projects, showing improvements in structural integrity and durability. Experimental results indicate that CRM systems can significantly enhance the load-bearing capacity of masonry walls [68].

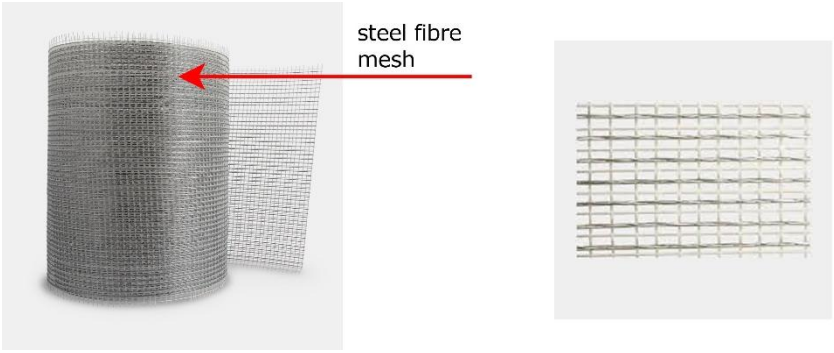


Fig. 2.11 Composite reinforced mortar (CRM) composed of a lime-based mortar matrix and a steel fibre mesh [69]

Steel fibre reinforced polymers (SFRP) combine steel fibres with a polymer matrix, providing enhanced toughness and load distribution capabilities. This composite material is used to reinforce masonry structures against seismic and dynamic loads. SFRP offers high tensile strength and durability, making it suitable for

BUPT

reinforcing critical structural elements. Its application in retrofitting historical buildings has demonstrated significant improvements in structural performance without compromising the architectural heritage [70].

Cross-laminated timber (CLT) panels offer high strength-to-weight ratios and are used for internal reinforcement, improving seismic performance while preserving exterior aesthetics. This innovative material is gaining popularity for its sustainability and ease of installation. CLT panels provide sustainable and reversible reinforcement solutions but may require careful consideration of connections and load paths. Their use in seismic retrofitting has shown promising results in improving the resilience of masonry structures [59].

Innovations in composite materials include nano-engineered materials that enhance strength, durability, and resistance to environmental factors, and smart materials that can self-heal or change properties in response to environmental conditions, offering advanced solutions for masonry reinforcement [61].

Contemporary strategies for masonry reinforcement include a combination of surface treatments, internal reinforcements, and the use of advanced composites to improve structural performance. These strategies are tailored to address specific challenges, such as seismic resilience, load-bearing capacity, and environmental durability [71]. FRP, for example, offers high strength and lightweight but can be expensive and sensitive to UV exposure. It is ideal for external reinforcement but requires careful application and protection from environmental factors [72]. FRCM and TRM provide excellent compatibility with masonry and ease of application but may have lower tensile strength compared to FRP, making them suitable for historical structures where aesthetic preservation is crucial [73]. CLT panels are sustainable and effective for seismic retrofitting but require careful consideration of installation techniques. They provide a balance of strength, sustainability, and ease of installation [74].

Single-side reinforcement can be effective in improving performance while minimizing disruption to interior spaces. Challenges include ensuring adequate bond and load transfer, as well as addressing any potential aesthetic impacts on historical structures. Examples of successful single-side reinforcement projects demonstrate its viability in both historical and modern contexts. Projects have shown that single-side reinforcement can significantly enhance structural performance without compromising the integrity or appearance of the building [75].

2.7 Strategies for Numerical Analysis of Proposed Solutions

Procedures used to assess the shear strength of historic masonry structures include shear testing, diagonal compression testing and numerical simulations. All these assessment methods are used to understand the influence of different strengthening solutions [76]. During laboratory tests, an important component in understanding the seismic behaviour of a structure is the analysis of the diagonal tensile strength of a wall specimen. To be able to perform these laboratory tests, a series of different standards, like EN 1052-3 [77] or ASTM E519/E519M-20 [1] are providing relevant guidelines. Besides these, there are also other standards which focus on determining the in-plane shear strength of masonry walls but from different points of view, like BS EN 1052-4:2000 [78], which addresses the shear strength of horizontal bed joints and can be performed on masonry wallets but also on couplets and triplets [79].

BUPT

Starting from the results obtained during the laboratory testing, numerical analysis can subsequently be used in order to better understand the behaviour of masonry wall under seismic loads. Considering the complexity of heritage structures a series of modelling strategies can be employed with different levels of complexity:

- Macro-modelling, where the analysed structure is modelled as a homogeneous element, becoming therefore a strategy which can easily be used in the case of large-scale structures [80]
- Simplified micro-modelling, where the brick masonry elements are modelled as elements, but the mortar is only considered as a interface between the brick elements, making the analysis more accurate without and high modelling effort [30], [65]
- Detailed micro-modelling, where all the composing elements are modelled leading the highest level of accuracy but high effort in the modelling process [65]

At the same time, in the case of seismic behaviour analysis, different types of analysis can be performed depending on the type of results relevant to be analysed subsequently:

- Static Linear Analysis - This method implies a static analysis of the structure, considering the mass of the load-bearing materials from each floor of the building and the seismic response spectrum for the considered location [10]. The software subsequently determines the horizontal seismic load and applies it to each floor. Being a linear static analysis, the structural materials are kept in the linear elastic range and is offering limited information about the behaviour of the structure and cannot be used to identify failure mechanisms.
- Dynamic Linear Analysis – this method implies the analysis of the load bearing structure under dynamic seismic loads but consider that the materials are kept in the linear elastic range.
- Static Nonlinear Analysis – obtained by applying also a load equal to the mass of the load-bearing elements, in a positive and negative direction perpendicular to the analysed wall, but this time the non-linearity of the structure and material is also taken into consideration. In this case the analysis can be used to also determine the failure mechanisms developed in the structure.
- Dynamic Nonlinear Analysis – Ultimately, this method is considering both the dynamic seismic load and the non-linear behaviour of the structure, leading to a comprehensive analysis of its deformation and developed failure mechanisms.

In order to be able to perform these analyses, various computer software using discrete element modelling (DEM) or finite element analysis (FEA) are frequently employed [81]. ANSYS, ABAQUS, DIANA, and other well-known platforms offer tools for simulating complex structures [82]. Case studies (Fig. 2.12) demonstrate how FEA and DEM can be successfully applied to model both modern and old masonry structures [29], [70], [83].

BUPT

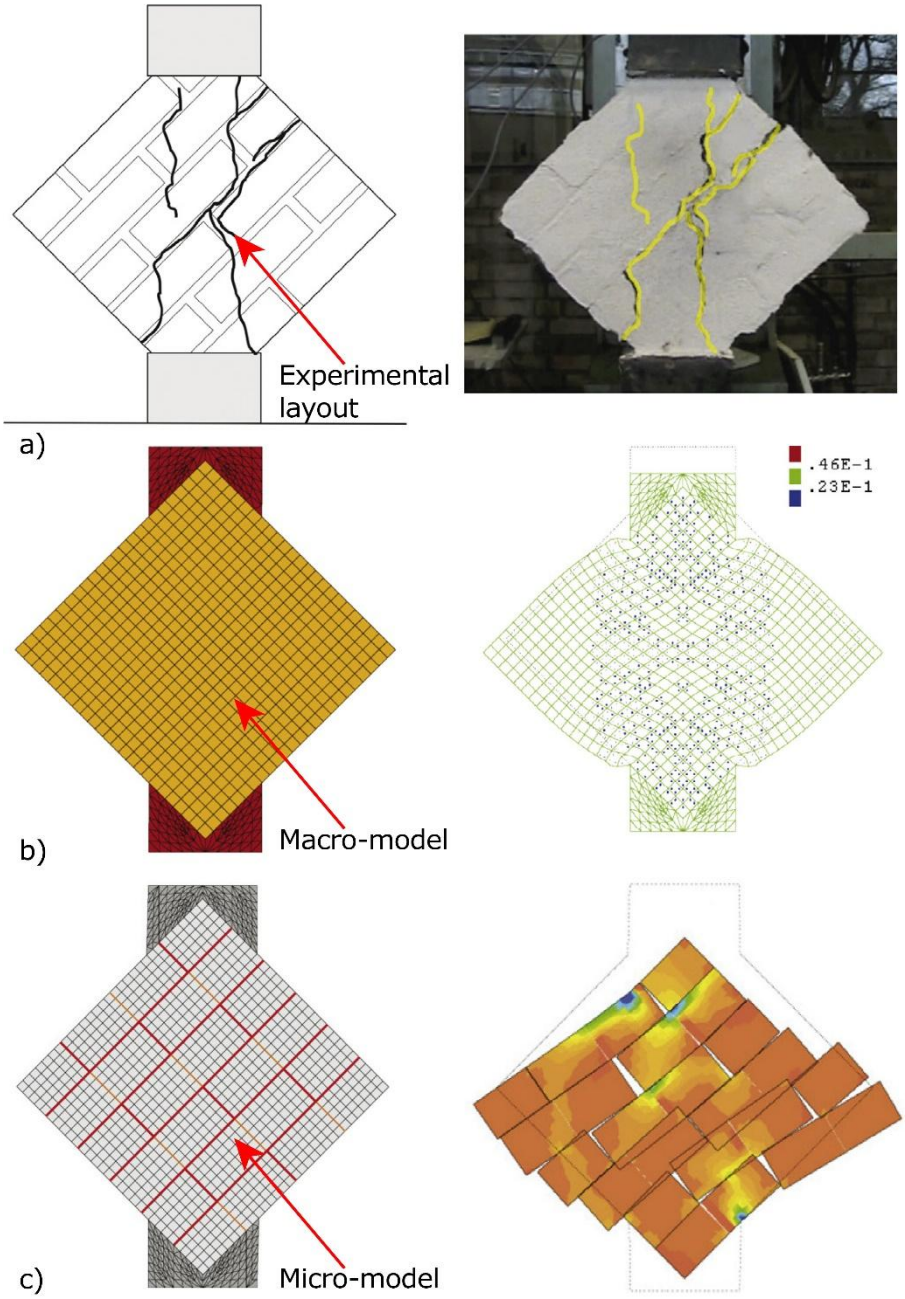


Fig. 2.12 Comparative results obtained for a masonry wallet subjected to diagonal compression during a) laboratory testing; b) micro-modelling; c) macro-modelling (performed in the DIANA software) [29]

2.8 Combining Seismic Retrofit with Thermal Retrofit Opportunities

When seismic and thermal retrofitting are combined, the structural performance and energy efficiency of the building are both improved, which results in a full set of benefits for the structural sustainability. Not only does this integration guarantee that the structural behaviour of a building is improved but it also ensures that they are energy-efficient, which contributes to a reduction in operational expenses [58]. One of biggest challenges in coordinating these two retrofit solutions is to ensure that the new materials are compatible with existent ones while also considering the initial costs and the long-term payback [84].

A material which can effectively be used to improve both the seismic and thermal performance of a building are insulated fibre-reinforced polymers (FRP). These materials can be used to approach retrofit in a holistic way by using the tensile strength of fibre-reinforced polymer combined with its thermal insulation qualities, therefore influencing the seismic and thermal performance of the building [85]. This solution can help approach building retrofitting in a holistic way. Significant improvements in seismic performance and energy efficiency shown by this project indicated the effectiveness of the integrated retrofitting strategies [55].

Other solutions involve structurally insulated panels (SIPs) which are used in integrated panel systems. These panels provide simultaneous benefits of providing structural reinforcement and thermal insulation, representing a single solution that may fulfil a variety of different retrofitting requirements [68].

Mesh reinforcement materials are a optimal solution which can be used to perform integrated thermal and seismic retrofit suitable for historic buildings. Studies performed by the author [86], in the case of integrated retrofit solutions suitable for heritage structures with valuable ornaments on the outside, show that due to the reduced thickness of the seismic mesh reinforcement, the strengthening layer can easily be applied beneath the insulating layer, leading to a reduced loss of usable space on the inside, while increasing the load bearing capacity of the masonry wall. At the same time, due to the application of the strengthening solution on the inside, de valuable ornaments can be preserved. Despite these advantages, there are only few studies which approach the effects of single-sided mesh reinforcements or these types of integrated retrofit solutions.

In the future, it is envisioned that integrated retrofitting will include the use of smart building technologies like smart sensors and control systems to optimise structural and thermal performance in real time. Furthermore, eco-friendly materials with seismic and thermal benefits will be produced, helping to advance sustainable building practices [4].

2.9 Conclusion

The study provides insights on the development and effectiveness of a wide range of reinforcing materials and techniques, emphasising the need of providing solutions suitable for historic masonry buildings. Modern strengthening solutions, such as FRCM, TRM, and CLT panels, significantly improve structural performance while being compatible with both historical and contemporary masonry constructions. They show that comprehensive solutions for enhancing building resilience and energy efficiency can be developed by combining seismic and thermal retrofitting methods [33].

BUPT

To provide full retrofitting solutions, future research should focus on the development of innovative materials, the optimisation of reinforcing solutions, and the development of interdisciplinary solutions. Among the particular areas that demand more research are the long-term performance and durability of contemporary reinforcement materials, the optimisation of single side strengthening methods, the creation of affordable and scalable solutions for combined seismic and thermal retrofitting, and the improvement of numerical modelling tools for more realistic simulation of reinforced masonry behaviour [87].

BUPT

3 EXPERIMENTAL INVESTIGATION ON MASONRY SPECIMENS

3.1 Analysis of Load-Bearing Masonry Structures

The masonry buildings subjected to seismic forces must cope with forces induced by the lateral and vertical accelerations of the ground. The out of plane collapse of the masonry walls is the greatest threat to their integrity, but if this is controlled by the presence of transversal walls (Fig. 3.1) and good connections to floor and roof structures, the in-plane shear failures become the greatest threat [88]. This can be the case especially on the façade walls where the presence of window and door openings limits the width of the masonry elements.

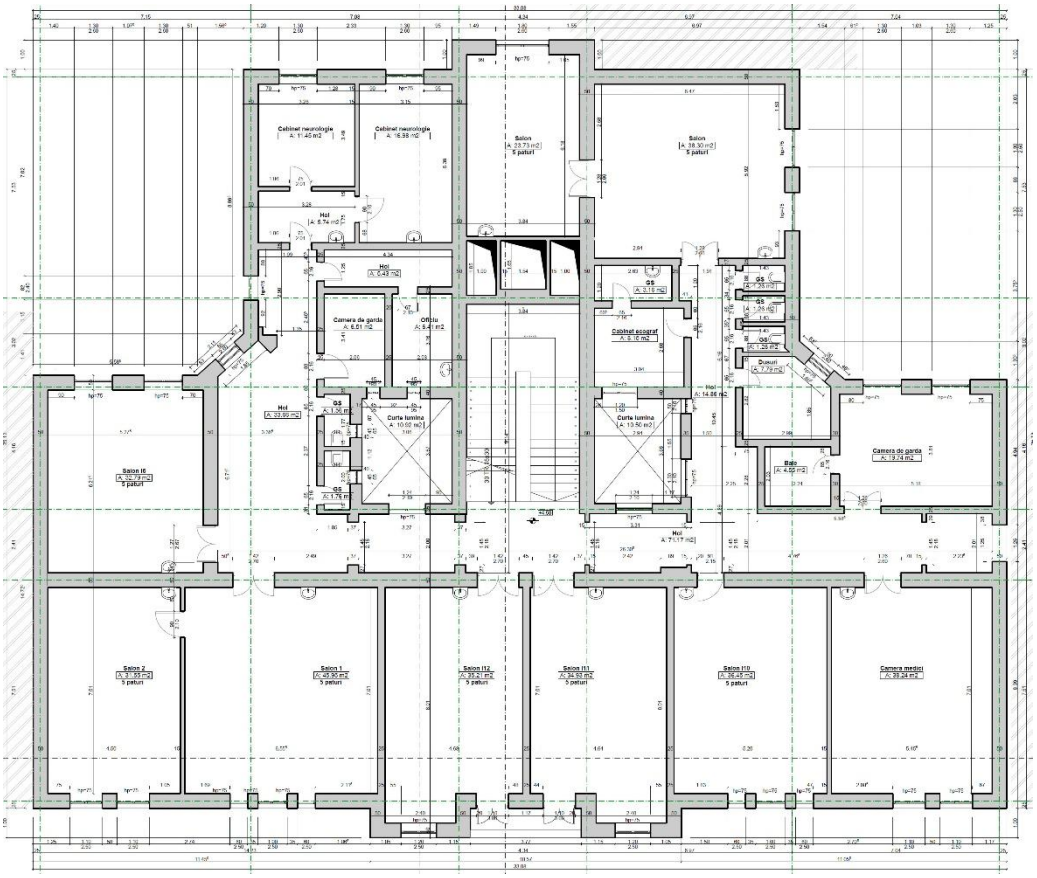


Fig. 3.1 Typical floor plan with bracing walls (CFR hospital Timisoara)

For in-plane damage, various failure mechanisms can occur depending on the wall dimensions and proportions, the vertical load exerted, connections to adjacent elements, and the strength of the masonry units and mortar.

BUPT

The typical failure modes of masonry walls subjected to shear forces are visible in Fig. 3.2. If the vertical force is relatively low, rocking damage is predominant, potentially leading to toe crushing at the wall panel corners.

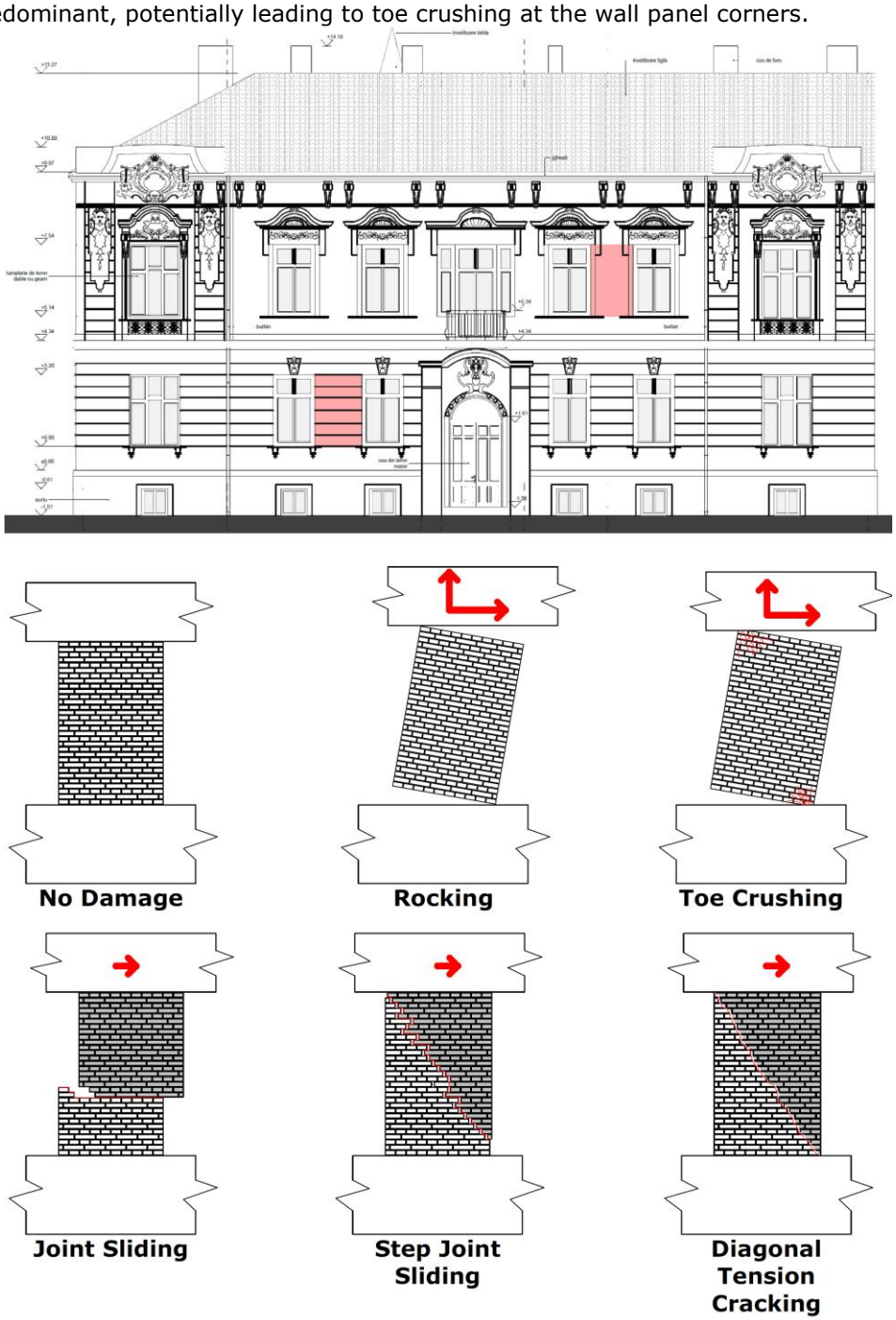


Fig. 3.2 Typical failure modes of masonry wallets [88][89]

Conversely, if the vertical load is significant, shear failure is possible. Depending on the relative strengths of the mortar and masonry units, shear sliding along a horizontal joint or diagonal tension cracking might occur. This can result in a stepped crack line through the mortar bed and head joints or a diagonal crack through both mortar and bricks, the latter being considered a brittle failure. The cracking corresponds to the maximum force, followed by a sudden drop in the unit's capacity to carry horizontal loads[88]. According to Dizhur *et al.* [88] checking for diagonal tension characteristic is very important because of the different outcomes caused by either the joint sliding more ductile behaviour or the diagonal tension brittle cracking that might be followed by immediate failure of the structure.

The present study investigates the diagonal tension cracking as this failure mechanism presents a real danger leading to sudden brittle collapse. In the context mentioned in the first chapter, the subject of study concerns the heritage buildings of Timișoara city and its surroundings within the historic context. This zone is scattered with many buildings that use similar construction techniques dated from the 19th century to the beginning of the 20th century. Based on this structural typology, the shear strength of masonry wallets with a 45cm thickness, as observed during on site studies in upper floor exterior load-bearing walls was analysed. The wallets were built using traditional building techniques with historic bricks and lime-based mortar, and subsequently subjected to diagonal compression tests.

3.2 Considerations For Choosing the Case-Study

The study starts from characteristic brick masonry structures from the western part of Romania built until the beginning of the 20th century.

According to extensive studies performed between 2015-2021 [90], a series of common characteristics were identified regarding used structural systems and importance of ornamental elements. The study showed that all the investigated buildings were built using clay brick masonry with lime-based mortar, with thicknesses ranging from 80-90 cm at the underground level and ground floor and decreasing down to 30-45 cm at the top level in the case of exterior walls, maintaining the linearity of external surface. In most of the cases, another load-bearing wall is placed in the middle of the building parallel to the other exterior walls. The study also shows that the walls placed transversal to the street exterior walls are generally non-bearing, with thinner thicknesses reaching up to 15 cm, in some cases being even poorly connected to the exterior walls. These walls have a rather functional purpose, dividing the building into different spaces.

Based on the analysis of the brick pattern visible in the case of buildings with damaged exterior plaster or buildings which are currently being restored (Fig. 3.3), a clear use of English bond can be observed with one line of stretchers and one subsequent line of headers.

Horizontally, two different structural systems were identified in all cases, with brick vaults placed at the under-ground level and in some cases at the ground level and timber slabs in the case of all upper floors. All buildings have a complex timber roof structure placed above the last floor, with different structural systems based on the knowledge of the construction period.

BUPT



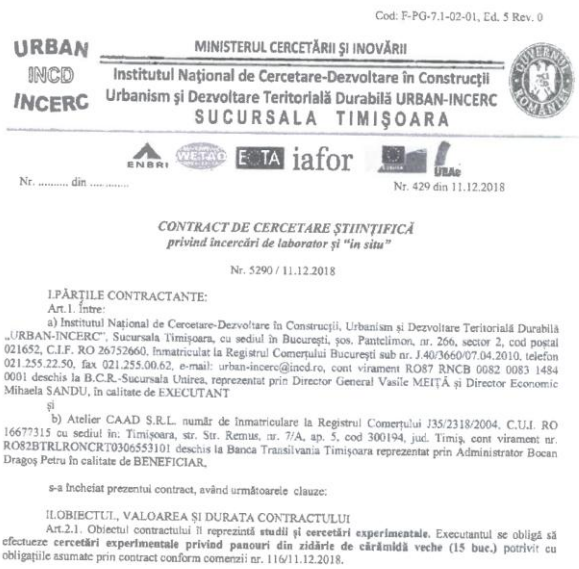
Fig. 3.3 Existing masonry bond on typical historic building (suspended work site, Emanoil Ungureanu street, no. 17 Timisoara)

3.3 Presentation of the Testing Programme

Due to the importance of in plane shear strength of masonry walls as stressed by existing research [91][25][92], as the in-plane failures of URM lead to brittle failures of the masonry elements, the evaluation of shear strength was considered of maximum importance and considered in this study. As a basis for testing, the ASTM International standard E519/519M-15 was selected as the results can be compared to a large pool of similar work.

The experimental tests were performed in a dedicated laboratory of the INCD URBAN-INCERC (National Institute of Research and Development in Construction, Urbanism and Sustainable Development) facility which presented the most potential for support. (Fig. 3.4).

BUPT



Cod: F-PG-7.1-02-01, Ed. 5 Rev. 0

URBAN INCD INCERC

MINISTERUL CERCETĂRII ŞI INOVĂRII
Institutul Naţional de Cercetare-Dezvoltare în Construcţii Urbanism şi Dezvoltare Teritorială Durabilă URBAN-INCERC
SUCURSALA TIMIŞOARA

Nr. ..... din ..... Nr. 429 din 11.12.2018

CONTRACT DE CERCETARE ŞTIINŢIFICĂ
privind încercări de laborator şi "in situ"

Nr. 5290 / 11.12.2018

I.PĂRŢILE CONTRACTANTE:
Art.1. Între:
a) Institutul Naţional de Cercetare-Dezvoltare în Construcţii, Urbanism şi Dezvoltare Teritorială Durabilă „URBAN-INCERC", Sucursala Timişoara, cu sediul în Bucureşti, şos. Pantelimon, nr. 266, sector 2, cod poştal 021652, C.I.F. RO 26752660, înmatriculat la Registrul Comerţului Bucureşti sub nr. J.40/3660/07.04.2010, telefon 021.255.22.50, fax 021.255.00.62, e-mail: urban-incerc@incd.ro, cont virament RO87 RNCB 0082 0083 1484 0001 deschis la B.C.R.-Sucursala Unirea, reprezentat prin Director General Vasile MEIŢĂ şi Director Economic Mihaela SANDU, în calitate de EXECUTANT
şi
b) Atelier CAAD S.R.L. număr de înmatriculare la Registrul Comerţului J35/2318/2004, C.U.I. RO 16677315 cu sediul în: Timişoara, str. Str. Remus, nr. 7/A, ap. 5, cod 300194, jud. Timiş, cont virament nr. RO82BTRLRONCRT0306553101 deschis la Banca Transilvania Timişoara reprezentat prin Administrator Bocan Dragoş Petru în calitate de BENEFICIAR,

s-a încheiat prezentul contract, având următoarele clauze:

II.OBIECTUL, VALOAREA ŞI DURATA CONTRACTULUI
Art.2.1. Obiectul contractului îl reprezintă **studii şi cercetări experimentale.** Executantul se obligă să efectueze **cercetări experimentale privind panouri din zidărie de cărămidă veche (15 buc.)** potrivit cu obligaţiile asumate prin contract conform comenzii nr. 116/11.12.2018.

Fig. 3.4 URBAN-INCERC Contract for performing the experimental shear-strength tests on wallets

Fifteen masonry specimens were built according to the standard dimension, of 1200x1200 mm in-plane dimension. The thickness of the specimens was selected to be similar with the historic masonry walls present on the first floors of many existing buildings from the studied era (Fig. 3.3). Thus, a 1½ brick thickness was used, built in an English bond pattern, resulting in a total thickness of 450 mm, which is generally thicker than most of the reported tests in the literature.

To reproduce the original workmanship and considering the testing conditions of specimens as prescribed in the standard, a special conceived pallet was designed to allow for lifting and transportation of the specimens (Fig. 3.5). It had a removable part that could be taken away to make room for the loading shoe. The pallet supported the masonry in the position (Fig. 3.6).



Fig. 3.5 Pallets for construction of specimens



Fig. 3.6 Specimens constructed horizontally on pallets

The masonry specimens were erected on the wooden pallets placed on a solid surface. The identified 1 ½ brick English bond was used (Fig. 3.7). All joints including vertical ones were filled with mortar. The bed of mortar was 12 to 15 mm and it accommodated for the irregularities in the brick thickness.

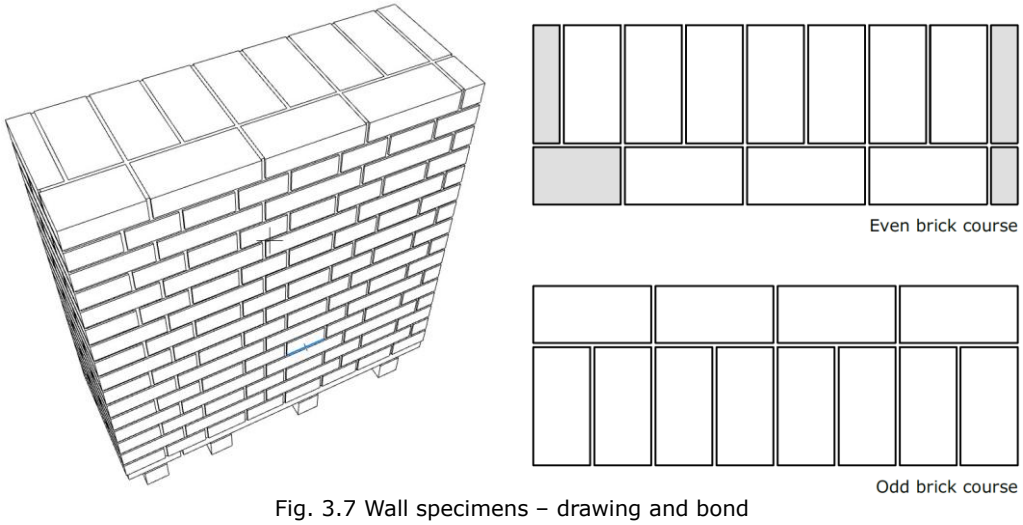


Fig. 3.7 Wall specimens – drawing and bond

The finished specimens were kept for 10 months, thus considering the mortar ageing. The specimens were divided in 4 groups, each containing three specimens (Fig. 3.8). Other three specimens were initially left as a reserve.

The first group of three specimens, the original unreinforced masonry used to establish a basis of results and used as reference, was covered in simple lime sand plaster considering the historic information. The water content used to prepare de plaster proved out to have been wrongly calculated as the plaster developed a variety of cracks. During testing, the main role of the surface plaster is to allow the visibility of the cracks that were developing. Due to the observed cracks the original plaster

was scrapped down and a new plastering layer made of commercially available lime-gypsum plaster was used. The new stretched plaster is similar in composition with the internal plasters of the original masonry period and has a sufficiently low-tension strength to show the cracks of the supporting masonry on the surface.



Fig. 3.8 Unreinforced wall specimens

Other two sets of specimens were strengthened (Fig. 3.10). One set of specimens of three testing specimens, was strengthened on both sides for comparison, while the other set, of additional three testing specimens were strengthened on only one side to simulate the intervention on one side without disturbing the apartment owners or destroying decoration.

For the specimens strengthened on both sides the strengthening layer was composed of Geocalce F Antisismico [93] mortar, with a thickness of 10–15 mm. On both sides, two perpendicular reinforcement layers of 300 mm-wide Geosteel G600 [69] were applied to a layer of fresh mortar and were immediately covered by another layer of the same mortar (Fig. 3.9).

BUPT

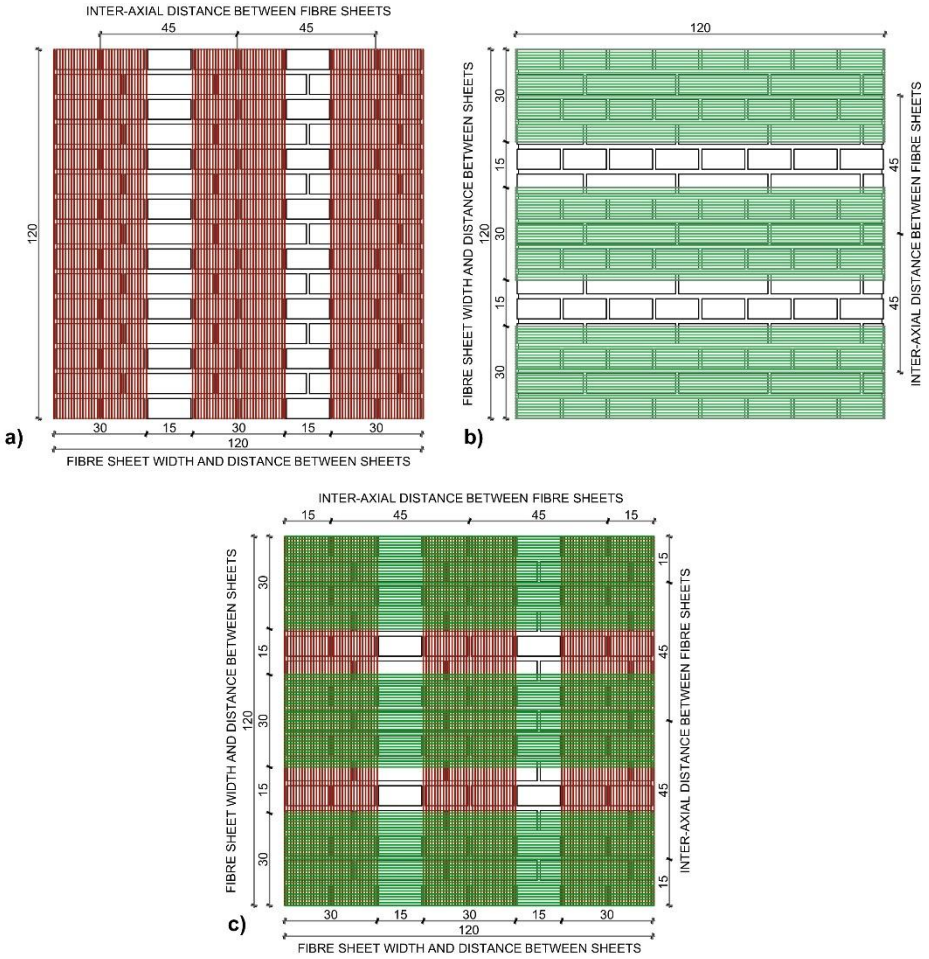


Fig. 3.9 Application of reinforcing sheets – a) first layer of reinforcement, b) second layer of reinforcements c) final reinforcement layout

The second set received a strengthening consisting of two perpendicular layers of Geosteel G1200 [94], applied as three 300 mm-wide strips in each direction along the 1200 mm width of the specimen. This reinforcement was applied only on one side. The same Geocalce F Antisismico mortar was used as the matrix for the reinforcement. The non-reinforced side was finished with a sand-lime plaster. This setup was intended to mimic situations where one side cannot be altered, as discussed in chapter 2.

Since Geosteel G1200 has twice the steel cord section per centimetre of strip width, both sets of specimens were reinforced with the same number and section of cords. The key difference lies in the placement of the steel cords.



Fig. 3.10 Application of reinforcing sheets

The fourth group consisting of the six remaining specimens were reserved for future testing. One of them made the subject of a horizontal barrier against capillary water insertion test, others were used in tests regarding strengthening using aluminium profiles.

In order to be able to track the testing results the 3 specimen groups were given reference designations, NA for the unreinforced URM specimens, A2 for the specimens reinforced on both sides and A1 for the specimens reinforced on one side. These designations were then preceded by the actual number of the test from the first to the last, in chronological order.

Table 3-1 Testing specimens and the considered strengthening solution

Specimen group	Specimen	Mortar (face 1)	Strengthening (side 1)	Mortar (side 2)	Strengthening (face 2)
NA	1NA	Lime based mortar	-	Lime based mortar	-
A2	2A2 3A2	Geo calce F Antisismico	Geosteel G600	GeoCalce F Antisismico	Geosteel G600
A1	4A1 5A1 6A1	Lime based mortar	-	Geo calce F Antisismico	Geosteel G1200

3.4 Testing Set-up and Loading Protocol

3.4.1 Testing Set-up and Interpretation of Results

The masonry wall specimens were tested under uniaxial diagonal compression loads to determine the in-plane shear behaviour of the original un-strengthened and subsequently strengthened specimens. The test setup was designed according to the ASTM E519/E519M standard, which defines the standardised test method for diagonal tension (inducing shear) in masonry assemblages [25], [95].

Because the wall specimens were built in their natural position - horizontal and the test loading should be aligned with the diagonal of the specimens, a transport jig was developed (Fig. 3.11). It was designed to be assembled around the specimens

BUPT

like a cage, then raised with the crane. Multiple hook points cut in the side profiles provided stability and, being close enough to the centre of gravity, allowed the specimen to be rotated in the test position (Fig. 3.12).

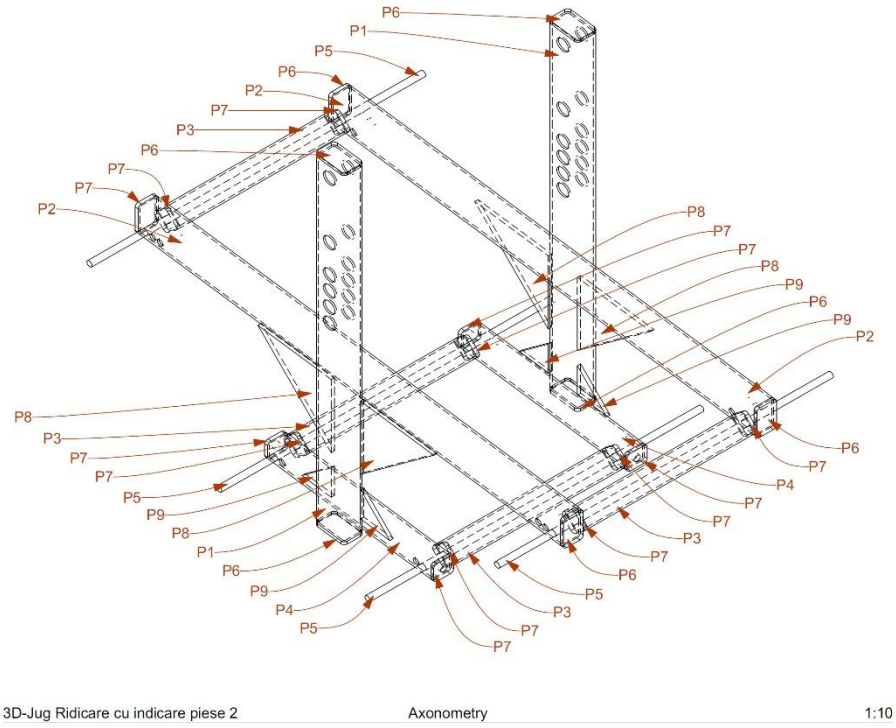


Fig. 3.11 Design of transportation jig



Fig. 3.12 Transportation and rotation using the jig

To subject the specimens to diagonal compression, the ASTM E519/E519M – a 15-loading shoe design was adapted to fit the width of the masonry and plaster [1]. Since its design is modular, there was no challenge in adapting its size to the required with of the masonry wallet. Two similar steel loading shoes were manufactured, each for either diagonal end of the specimen (Fig. 3.13). The lower shoe was fixed to the rigid floor of the laboratory and was used for every performed test. The upper shoe was used for every test and fixed to each specimen using fast setting mortar, which could be loaded after 5 minutes. Still, at least 24 hours were allocated before each test, between the mounting of the upper shoe and testing.

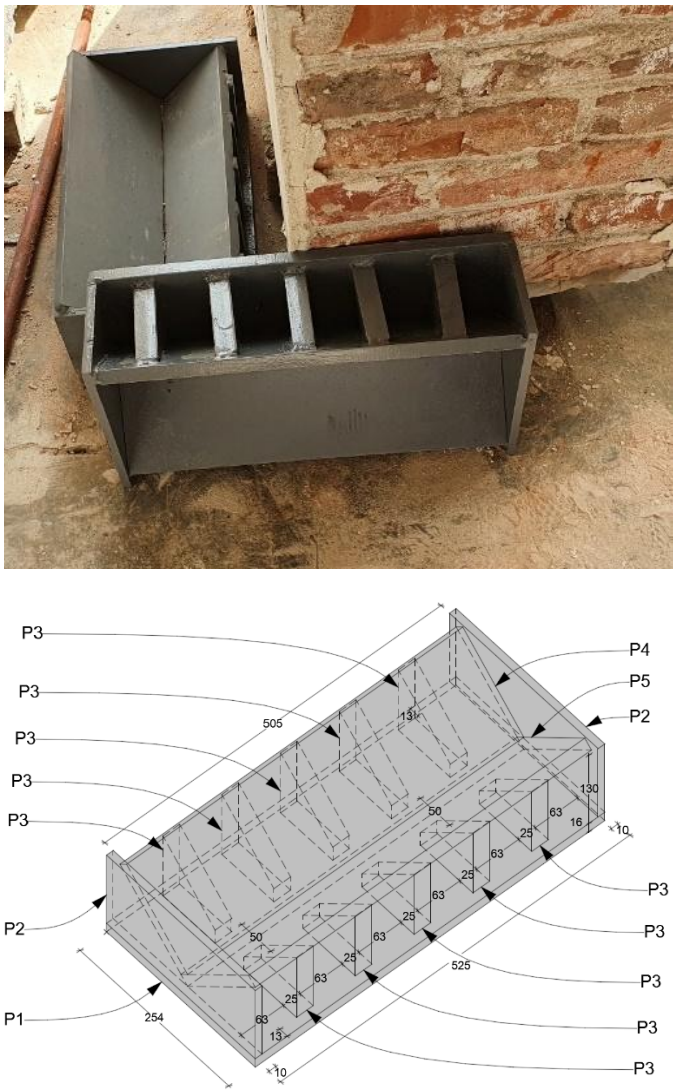


Fig. 3.13 Loading shoe design

BUPT

On both sides, each diagonal was monitored using transducers (Ahlborn FWA100TR displacement tracers) that could measure both expansion and contraction. The mechanical stroke of the transducers was 105mm and their independent linearity value was +/- 0.075%. The measurement devices were fixed on bolts anchored in the masonry substrate in drilled holes filled with epoxy mortar (Fig. 3.15).



a) b)

Fig. 3.14 Displacement Tracer [96]; mounting solution

The transducers were loosely secured to the stand using sling tape to be kept safe in case of specimen collapse. A hydraulic actuator was used to load the specimens along the vertical diagonal acting on the top shoe. The actuator pushed vertically against the steel cantilever of the stand (Fig. 3.15, Fig. 3.16).



Fig. 3.15 Specimen placement with loading cell (hydraulic actuator)

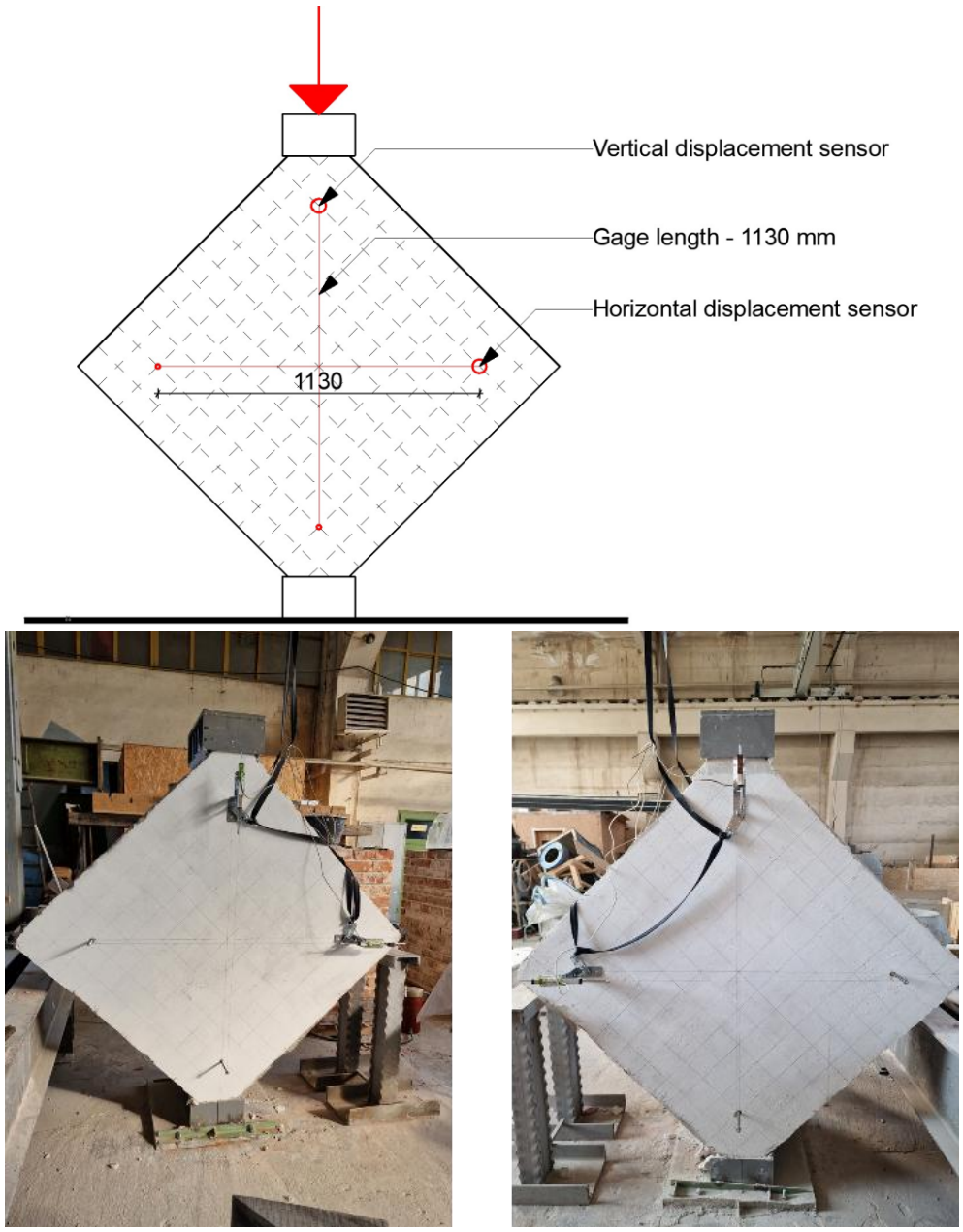


Fig. 3.16 Layout according to "Standard Test Method for Diagonal Tension (Shear) in Masonry Assemblages – ASTM E519/E519M – 15" [97]

The displacement tracers were connected to an Ahlborn Almemo 5690-2 data acquisition system that informatically monitor the computer deformation and piston (hydraulic jack) pressure data each 2-3 s. The data was sent and stocked on computer files.

As the age of specimens when tested is important especially when dealing with lime mortar [95], a sufficient time was left between construction and testing of at least 6 months. In practice because of the testing campaign overlap with the COVID-19 pandemic and restrictions, the time intervals were larger than planned. Thus, the masonry specimens were built in July 2019, the rendering and reinforcing materials were applied in May-June 2020 and the testing campaign started in August 2022 and ended with the last specimen tested in January 2023. The specimens were kept inside the testing laboratory hall in partially controlled temperature, above freezing during the resting period.

According to the used standard [1] the shear stress is calculated with the equation:

$$s_s = \frac{0.707}{A_n} P \tag{3.1}$$

Where A_n is the net area of the specimen, P is the diagonally applied load.

The net area of the specimen is computed using its geometrical dimensions:

$$A_n = \left(\frac{w+h}{2}\right) tn \tag{3.2}$$

The dimensions of the sample are w, h, t (width, height, and thickness), n being the percent of the specimen area that is solid expressed as a decimal. For the samples that were built this takes the value of 1.

The shear strain calculation is based on the variations of the vertical and horizontal diagonals (Δx, Δy), where Δx is the shortening in the direction parallel to the loading and Δy the extension in the direction perpendicular to loading, which makes both value absolute, and the gage length in the direction parallel to the loading force (g). The formula is:

$$\gamma = \frac{\Delta x + \Delta y}{g} \tag{3.3}$$

The modulus of rigidity, G is calculated on the above values as it follows:

$$G = \frac{s_s}{\gamma} \tag{3.4}$$

3.4.2 Loading Protocol

As described in the selected diagonal test standard, ASTM E519 [25] [98] the force application speed was progressively increased up to half the expected maximum load then it was regulated to target a 1-2 minutes time to reach the maximum design load. In practice this could not be done during all tests, as the load was in many situations stopped for close inspection of the specimen or the maximum expected load could not be properly evaluated.

BUPT

3.5 Material Properties

3.5.1 Brick

To get more accurate results, attention was paid to the historic accuracy of the specimens regarding to materials used and to the workmanship, as considered in other researches (Mezrea *et al.*) [98] .

The brick used in the specimens was recovered from a demolition site of a utilitarian construction (animals stable), near Timisoara, in Sacosu Turcesc (Fig. 3.17). The building was erected in 1910, at the end of the studied period. The type of fired bricks and their dimensions are in line with the material used in Timișoara city centre. The recovered bricks were subsequently transported to the laboratory where they were cleaned by removing any particles that were not strongly adhering to their surface (Fig. 3.18).



Fig. 3.17 Brick recovery site

The recovered bricks are solid clay masonry units, fired, but not sintered, considered as porous bricks. Their dimensions are standardised, but small variations were measured due to the manufacturing and firing process. The standard dimensions are 290x140x65 mm (L x W x H), together with the mortar joints leading to a masonry module of 300x150x80 mm. These dimensions are different than what became standard in a later time in the same geographical area of 240x125x83 cm (Fig. 3.19).



Fig. 3.18 Brick transported to lab site

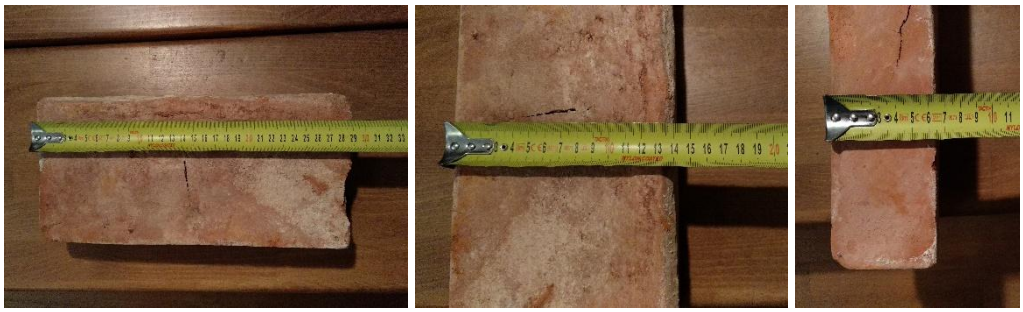


Fig. 3.19 Brick dimensions

The brick was tested for compression strength by the URBAN-INCERC lab. The test consisted in compressing 3 specimens composed of a stack of 2 brick halves and 3 layers of high resistance mortar. The results for the compression strength were 8.47, 11.3 and 9.56 Mpa (Table 3-2).

Table 3-2 Brick compression tests (scan from report of URBAN-INCERC Timisoara)

	L1 [mm]	L2 [mm]	Forța [daN]	f [N/mm2]	
B1	148 150 148	147 146 138	18080	8.47	
B2	144 143 144	146 149 144	23750	11.30	
B3	144 147 141	140 139 142	19310	9.56	

The densities of brick specimens were calculated (Table 3-3). The average density of the clay brick was 1539.25kg/m^3.

Table 3-3 Brick density

Specimen Code	L [mm]	l [mm]	H [mm]	Mass [kg]	Density[kg/m3]
C1	295	145	70	4.69	1566.335
C2	300	145	72	4.77	1522.988
C3	290	145	75	4.93	1563.218
C4	300	140	80	4.83	1437.500
C5	280	135	70	4.25	1606.198
				Average Density	**1539.248**

3.5.2 Lime-based Mortar

The used mortar had to be reconstructed. For this purpose one of the building manuals of the time, the Lothar Abel's "Allgemeiner Bauratgeber - Ein Hand- und Hilfsbuch für Bauherren, Architekten, Baunternehmer, Baumeister, Bautechniker, Bauhanweker, Landwirte und Rechnungsbeamte" [17] which gives the mixing proportions for the lime mortars. The absence of predictable lime putty was a hurdle, but the reference mentioned the usage of hydrated lime, and the extra water quantity used in order to improve the workability.

The mortar used had the 1:3:1.25 (hydrated lime, sand, water) proportions by volume. It aimed to reproduce the historic lime mortar found around the year 1900 in the usual Timisoara's masonry. The recipe was extrapolated from the information in the "Allgemeiner Bauratgeber" [17]. The resulted mortar had good workability. The binder used, branded Supercalco M, was produced by Carmeuse and is a CL80-S hydrated lime. The sand was delivered in sacks and was composed of grains measuring 0.1-1 mm. Mixing was done using 25 litres of water for each 20 kg of hydrated lime.

The densities of mortar specimens were calculated (Table 3-4). The average density of the masonry mortar was 1946.31 kg/m^3.

Table 3-4 Masonry mortar density

Volume for 40x40x160mm [mm3]	Mold mass [g]	Wet mass (with mold) [g]	Wet mass [g]	Dry mass (with mold) >28 days[g]	Dry mass >28 days [g]	Specimen mass [g]	Density [g/mm3]	Density [kg/m3]
256000	9584.6	11244.20	1659.60	11012.60	1428.00	476.00	0.001859375	1859.38
		11244.20	1659.60	11012.60	1428.00	476.00	0.001859375	1859.38
		11244.20	1659.60	11012.60	1428.00	476.00	0.001859375	1859.38
		11187.20	1602.60	10949.20	1364.60	454.87	0.001776823	1776.82
		11187.20	1602.60	10949.20	1364.60	454.87	0.001776823	1776.82
		11187.20	1602.60	10949.20	1364.60	454.87	0.001776823	1776.82
		11514.40	1929.80	11276.30	1691.70	563.90	0.002202734	2202.73
		11514.40	1929.80	11276.30	1691.70	563.90	0.002202734	2202.73
		11514.40	1929.80	11276.30	1691.70	563.90	0.002202734	2202.73
							Average Density	**1946.31**

BUPT

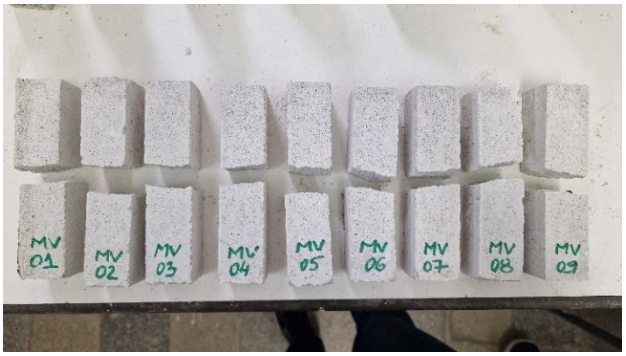




Fig. 3.20 Mortar specimens during testing

Mortar standard samples were tested for bending and compression strength (Fig. 3.20). In total nine samples were tested, that were first broken in bending tests, then one of each half was tested for deriving compression strength. The results are listed in the Table 3-5.

Table 3-5 Mortar testing results

Specimen	Bending max. load [kN]	Bending load [N*m]	Bending stress [N/mm²]	Bending pace rate	Compression max. load [kN]	Compression area 40x40mm [mm²]	Compression load [N/mm²]	Compression stress [N/mm²]	Pace rate [kN/s]
MV1	2.04	51.00	4.792	0.05	1.09	1600	0.68	0.681	2.4
					1.08		0.68	0.677	2.4
MV2	1.91	47.75	4.488	0.05	1.05		0.66	0.654	2.4
					1.14		0.71	0.713	2.4
MV3	2.14	53.50	5.007	0.05	1.27		0.79	0.792	2.4
					1.22		0.76	0.763	2.4
MV4	2.55	63.75	5.985	0.05	1.09		0.68	0.682	2.4
					1.15		0.72	0.718	2.4
MV5	2.42	60.50	5.664	0.05	1.07		0.67	0.666	2.4
					1.14		0.71	0.715	2.4
MV6	2.37	59.25	5.564	0.05	1.17		0.73	0.731	2.4
					1.2		0.75	0.75	2.4
MV7	2.37	59.25	5.556	0.05	1.01		0.63	0.631	2.4
					1.09		0.68	0.681	2.4
MV8	2.42	60.50	5.664	0.05	1.21		0.76	0.758	2.4
					1.08		0.68	0.678	2.4
MV9	2.46	61.50	5.775	0.05	1.16		0.73	0.724	2.4
					1.11		0.69	0.694	2.4
Average bending stress [N/mm²]			**5.388**		**Average compression stress [N/mm²]**			**0.706**	

3.5.3 Masonry

For the masonry assemblies the characteristic strengths were calculated according to the Eurocode 6 guidelines.

The characteristic compressive strength of masonry, fk can be calculated according to the formula:

$$f_k = K f_b^{0,7} f_m^{0,3} \tag{3.5}$$

For solid clay brick K=0.55

The value for compressive strength of the masonry units, f_b, was considered of 8MPa, conservatively reduced from sample resistance of8.47MPa to 11.30MPa

The value of the compression strength of the mortar was taken from the testing results average of 5.39MPa.

The compressive strength for the masonry resulted:

$$f_k = 3.90MPa \tag{3.6}$$

Based on the densities of brick and mortar the density for masonry resulted as:

$$\rho = 1636.17\ k_g / m^3 \tag{3.7}$$

These characteristic values were used later in numerical simulations that were compared to the test results. Other values, like shear strength, elastic modulus and shear modulus were derived from the unreinforced masonry (URM) test results.

3.5.4 Strengthening Materials

The used strengthening materials were chosen from the Italian producer Kerakoll Spa, that has specialized products lines for intervention on historic buildings.

For the reinforcing matrix the specially designed Kerakoll Geocalce F Antisismico was used [93]. It is a NHL M15 class lime mortar compatible with a large array of reinforcement materials (Fig. 3.21), including the steel fibre sheets as mentioned below. It is widely accepted as a solution for covering historical masonry built with lime-based mortar as it has a good chemical compatibility and water vapour permeability.

BUPT



Fig. 3.21 Mortar used as matrix

The Kerakoll unidirectional steel fibres sheets were used as reinforcement, because of their larger compatibility envelope including the tested specimens. The width of one sheet is 300 mm, and it is highly deformable, being built from steel 0.538 mm^2 micro-cords each made of 5 wires. One cord has a breaking load of 1500 N. The cords are fixed to a fibreglass mesh to be held in sheet form for better workability and easier installation.

Aiming to observe the effect of one-sided strengthening, roughly the same steel reinforcement section was applied for both strengthened specimen sets (A1 and A2). As the layout of the fibres was going to be the same this was done using two products. The Geosteel G600 (Fig. 3.22) has 1.57 cords per cm and the Geosteel G1200 (Fig. 3.23) 3.14 cords per cm [69] [94]. The tensile breaking load for 15 cm width of the G600 is 35 kN and for G1200 is 70 kN. Hence, G600 was used for double-sided strengthening specimens while G1200 was used for the specimens strengthened on one side.



Fig. 3.22 Reinforcement used for double-sided strengthening specimens



Fig. 3.23 Reinforcement used for single-sided strengthening

The main properties of the materials used for strengthening can be found below (Table 3-6).

Table 3-6 Reinforcing materials properties [93] [69] [94]

Name	Role	Mass	Static Modulus of Elasticity, Normal Modulus of the Sheet	Compressive Strength / Flexural Tensile strength (at 28 days)	Tensile strength of the sheet/Equivalent Thickness	Break Warp (Elongation) of the Sheet	Adhesion on clay brick	Reaction to fire
Geocalce F Antisismico	Plaster Matrix	1.58 kg/m^3	9 GPa	15 Mpa / 5MPa	-	-	1 MPa	A1
Geosteel G600	Reinforcement 300mm wide	650 g/m^2	190 GPa	-	3000MPa/ 0.084mm	2%	-	D-s2, d0
Geosteel G1200	Reinforcement 300mm wide	1200 g/m^2	190 GPa	-	3000MPa/ 0.169mm	2%	-	D-s2, d0

BUPT

3.6 Testing Results

After the laboratory test were concluded, the obtained results were analysed and subsequently compared to fully understand the effectiveness of the considered strengthening solutions. The results were analysed in terms of force-deformation curves, force-drift characteristic curve, shear stress-strain curves and ultimately ductility and energy dissipation. Finally, the failure mechanisms of each specimen were analysed.

3.6.1 Unreinforced Specimen 1NA

3.6.1.1 Force-Deformation Curves

Below it can be observed the force - compression deformation response curves (Fig. 3.24, Fig. 3.25, Fig. 3.26, Fig. 3.27).

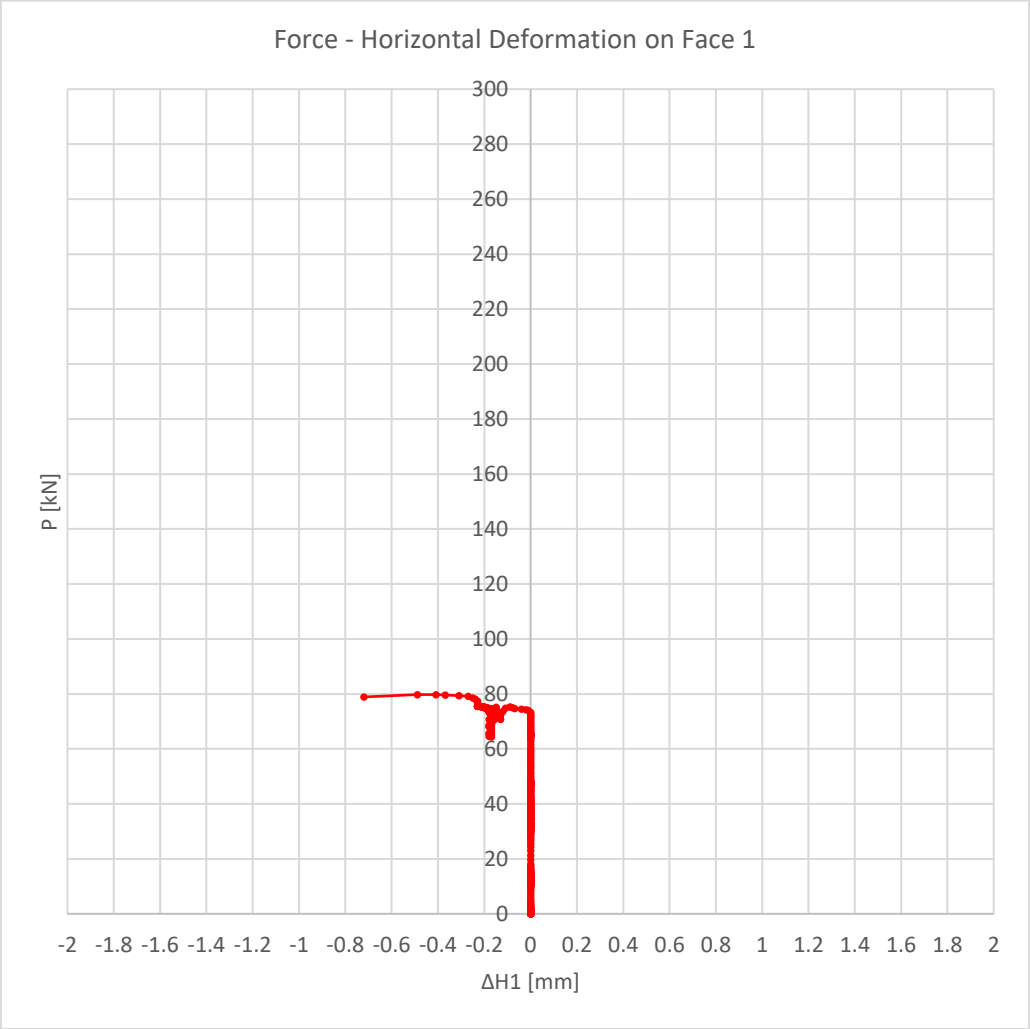


Fig. 3.24 Force by horizontal deformation on face 1 chart of 1NA specimen

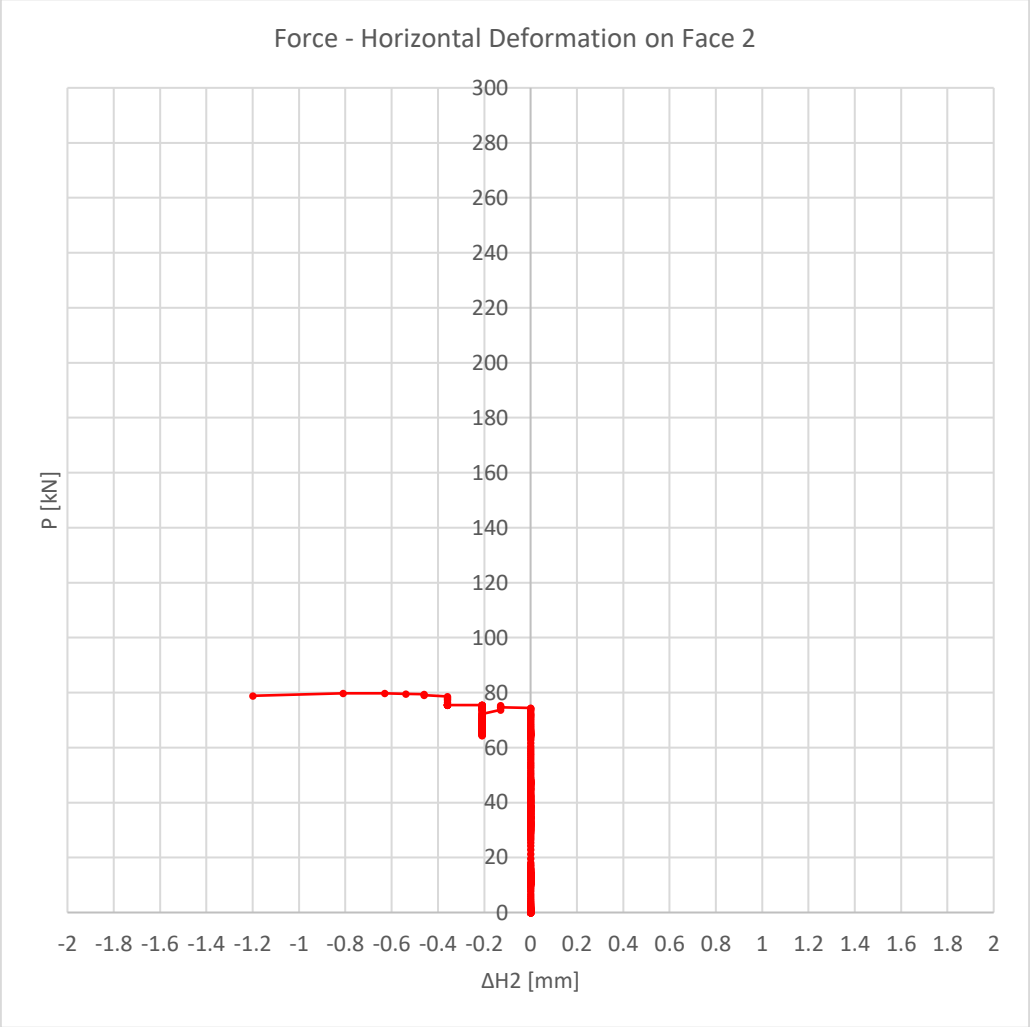


Fig. 3.25 Force by horizontal deformation on face 2 chart of 1NA specimen

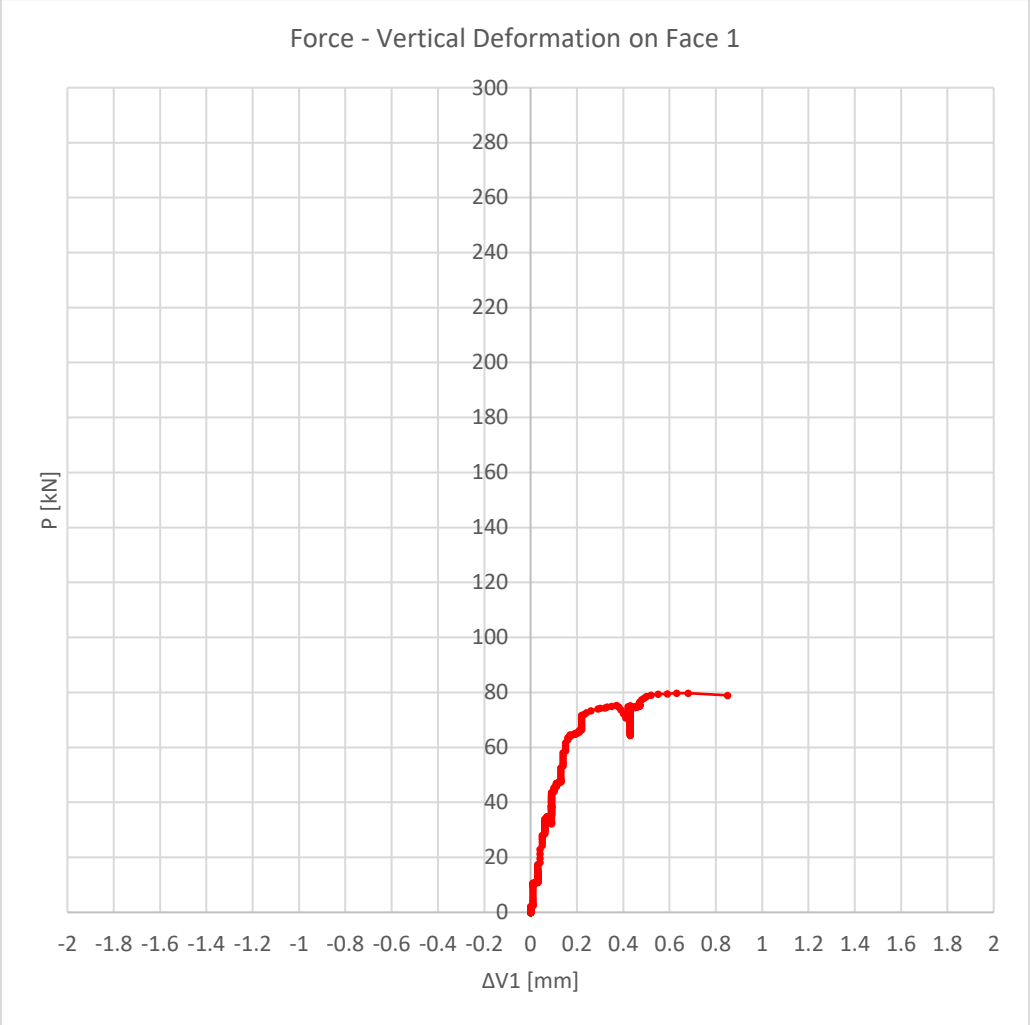


Fig. 3.26 Force by vertical deformation on face 1 chart of 1NA specimen

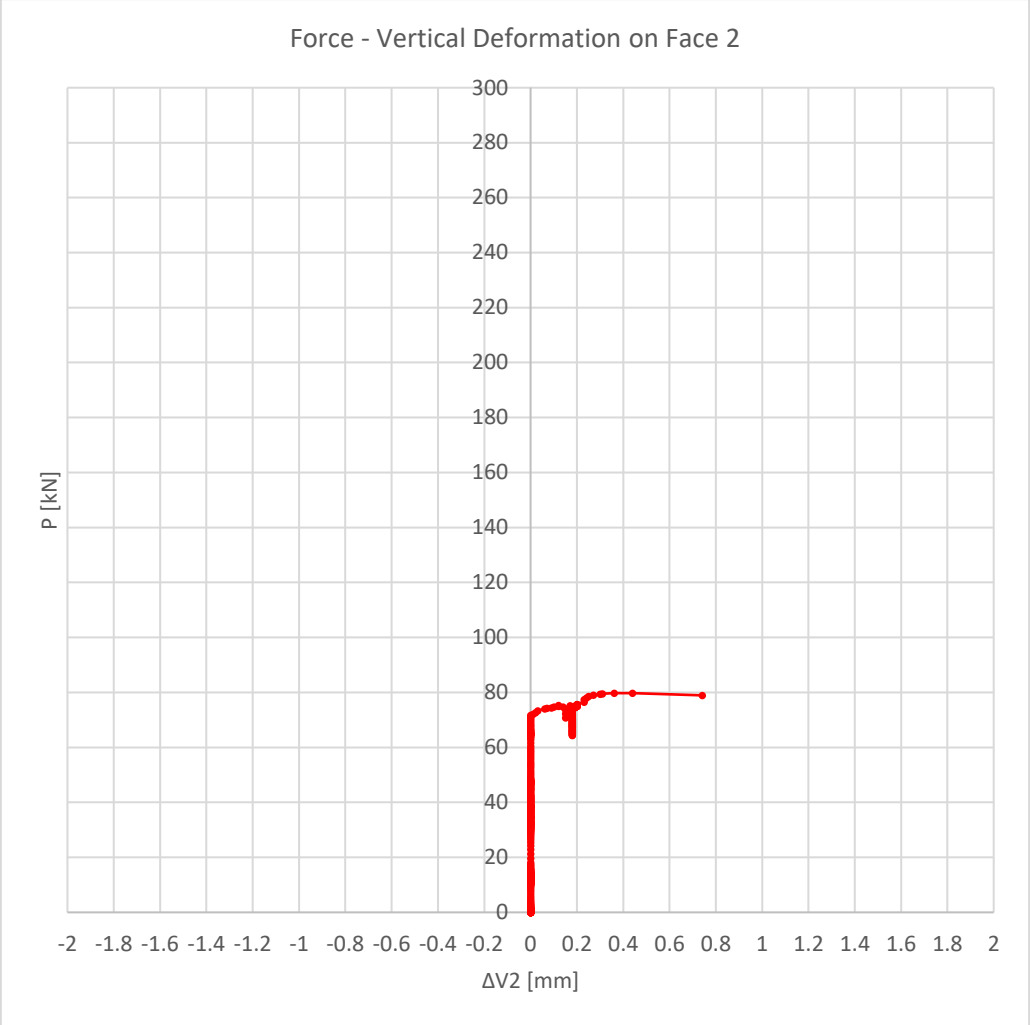


Fig. 3.27 Force by vertical deformation on face 2 chart of 1NA specimen

As could be observed in the previous figures, the deformations recorded during the laboratory tests are quite similar in directions, reaching a displacement of up to 0.7 mm horizontally and 0.85 mm vertically which highlights the rigidity of the considered wallets. At around 80 kN, the sample experienced a brittle failure despite the low displacements.

The drift percent value was calculated as per Dizhur *et al.* [91], Ismail et al [89] and Soleymani at al. formula [99], and the shear stress-drift curve was plotted. The validity of the formula was checked using geometric particular cases. The average value was computed from the values recorded on the two sides.

$$\delta = \frac{\Delta S + \Delta V}{2g} (tan\,\alpha + cot\,\alpha) \tag{3.8}$$

BUPT

$$\delta = \frac{\left(\frac{\Delta S_1 + \Delta S_2}{2} + \frac{\Delta V_1 + \Delta V_2}{2}\right)}{2g}(\tan\alpha + \cot\alpha) \quad (3.9)$$

Where ΔS is the deformation on the horizontal axis (perpendicular to the piston force) as the specimen is tested; ΔV is the deformation along the vertical axis (along the piston force); $\Delta S_1 and\ \Delta S_2$ are the horizontal deformations on face 1 and 2; $\Delta V_1 and\ \Delta V_2$ are the vertical deformations on face 1 and face 2; g – is the gauge original distance, the deformation measurement length and α – is the angle of the diagonal-45° (∏/4 radians). The results showing the drift percent-loading force relationship are plotted below (Fig. 3.28):

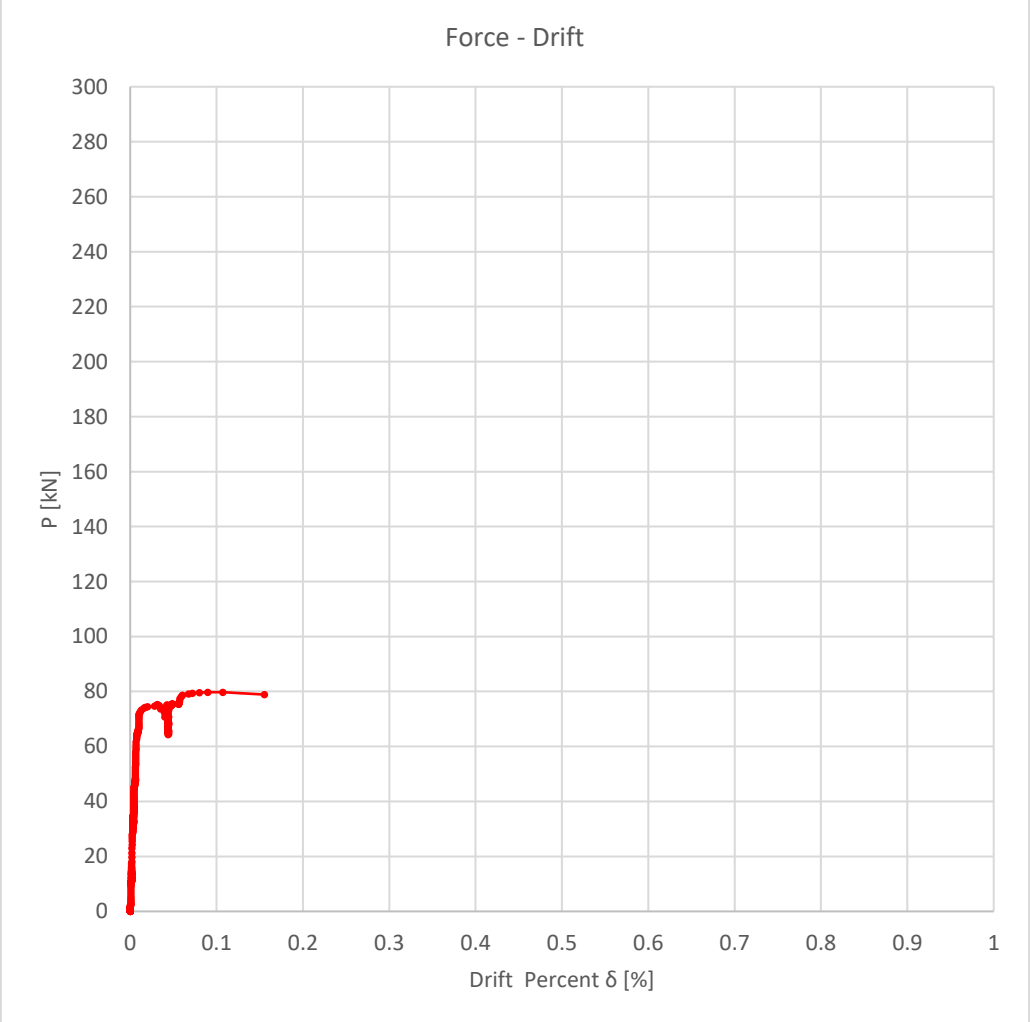


Fig. 3.28 Force-drift percent response curve for 1NA URM specimen

3.6.1.2 **Shear Stress Strain Curves**

The stress-strain chart is plot in Fig. 3.29. The behaviour of the specimen could be characterised to have an elastic-plastic behaviour, loosing elasticity at 0.1 Mpa. The maximum shear strain attained 1600 micro-strains.

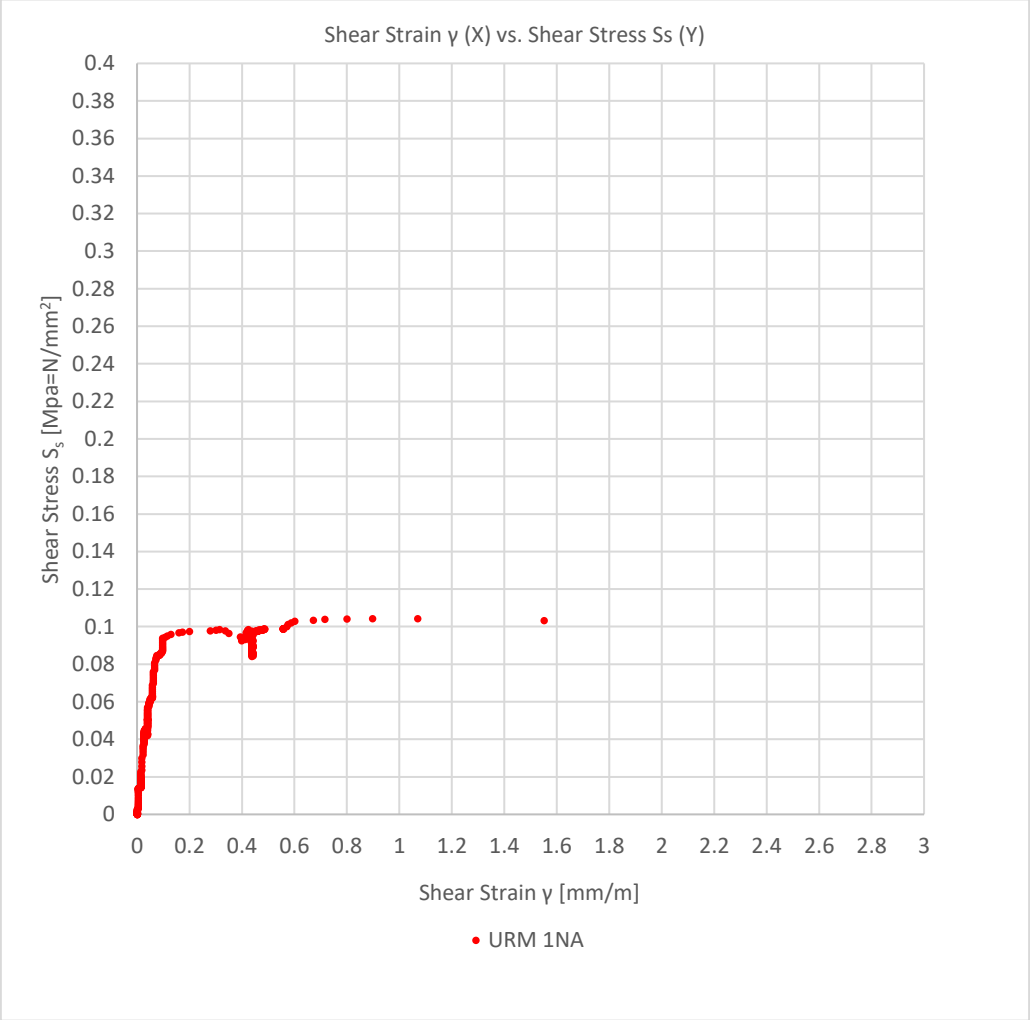


Fig. 3.29 Shear stress-shear strain chart for 1NA URM specimen

3.6.1.3 **Ductility and Energy Dissipation**

The behaviour of the unreinforced specimen confirmed the brittle nature of the diagonal tension cracking type of failure. The specimen passed from a geometrically recognisable state to a pile of rubble in 2s, as visible on the recorded film (Fig. 3.30; Fig. 3.31), similar to the research offered by Turkmen *et al.* [55] .

BUPT



Fig. 3.30 1NA Specimen before collapse -2s



Fig. 3.31 1NA Specimen after collapse

Due to the dangerous nature of this specimen collapse it was decided that the laboratory would not test other unreinforced masonry specimens.

3.6.2 Double-sided Strengthened Specimen

Two of the double-sided strengthening specimens were tested – specimens 2A2 and respectively 3A2. For specimen 2A2, due to two loading breaks and discharges made to assess specimen damage and cracking, there were made effectively 3 cycles of loading (Fig. 3.32). For the reporting charts, only the first cycle was considered.

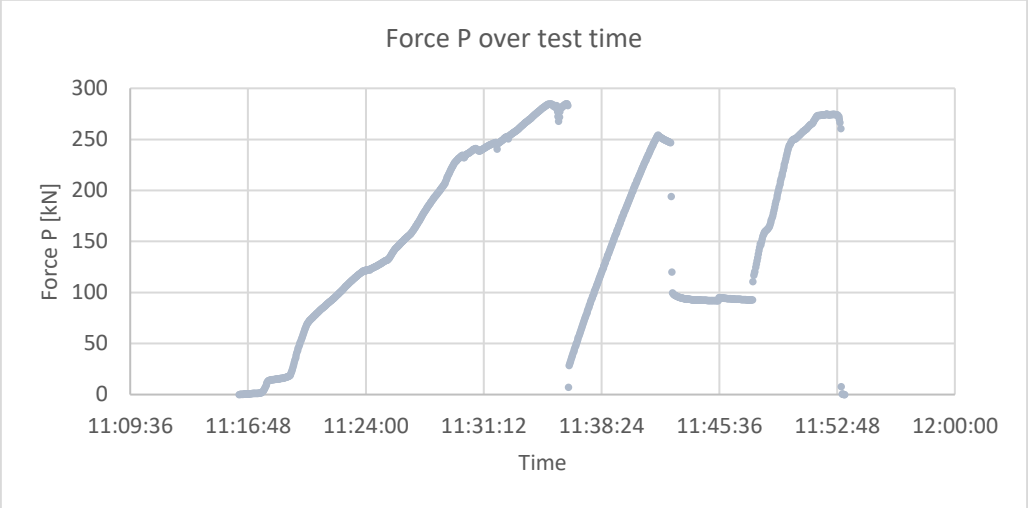


Fig. 3.32 Applied force in the 3A2 test intervals – breaks due to damage assessment

3.6.2.1 Force-Deformation Curves

The compression deformations show differences on each side possibly due to eccentricities in the test bed, elastic top beam of the stand (Fig. 3.33; Fig. 3.34; Fig. 3.35; Fig. 3.36). The main difference from the unreinforced masonry 1NA specimen is that after the plastic deformation began to occur the force continued to gradually rise in a strain-hardening phenomenon. Compared to 1NA, the maximum load applied to the masonry wallets reached up to 280 kN, presenting a 3.5 increase. The same was also observed in the case of the recorded deformations in horizontal and vertical direction, both specimens presenting ductility, unlike the URM 1NA specimen.

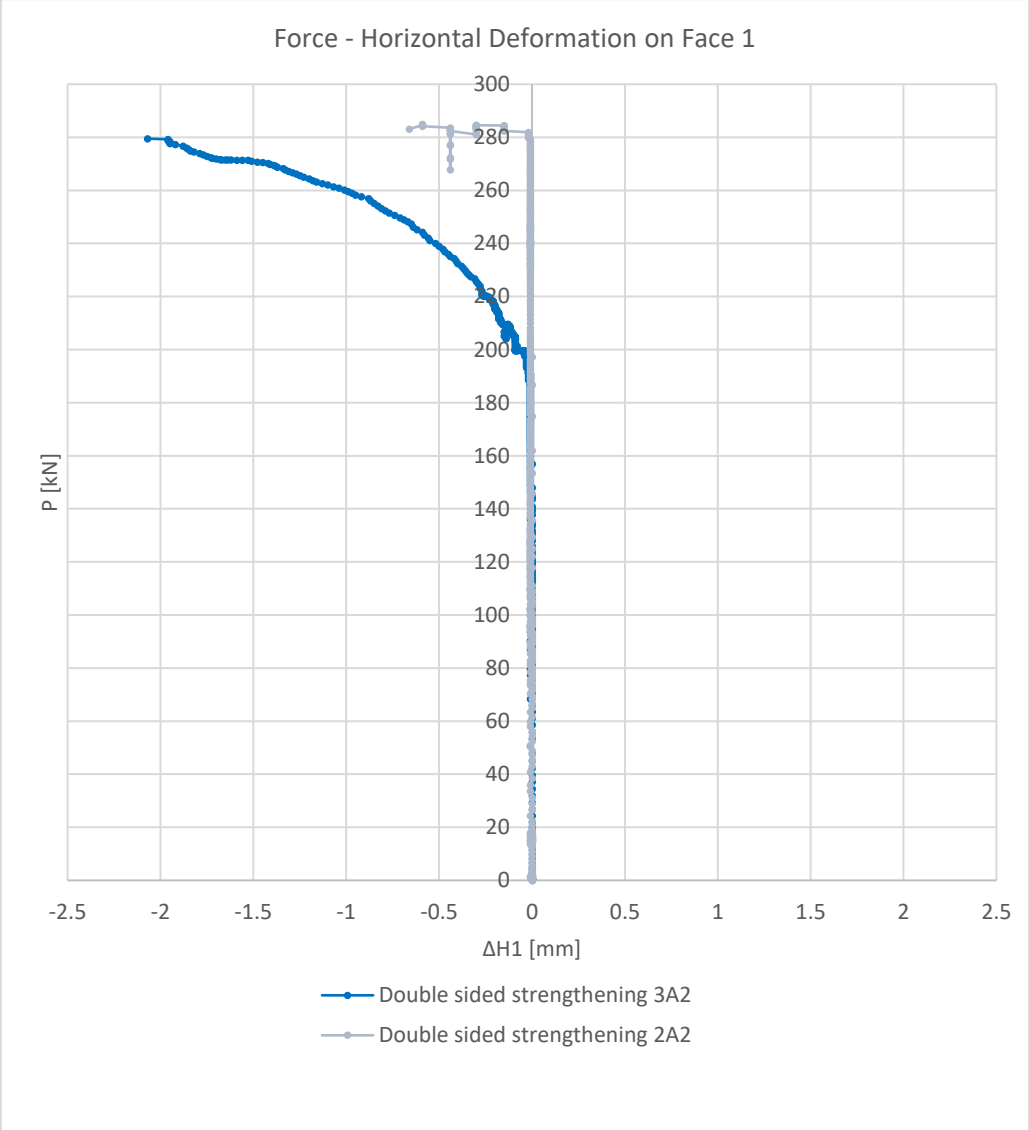


Fig. 3.33 Force by horizontal deformation on face 1 charts of 2 of 2A2 and 3A2 specimens

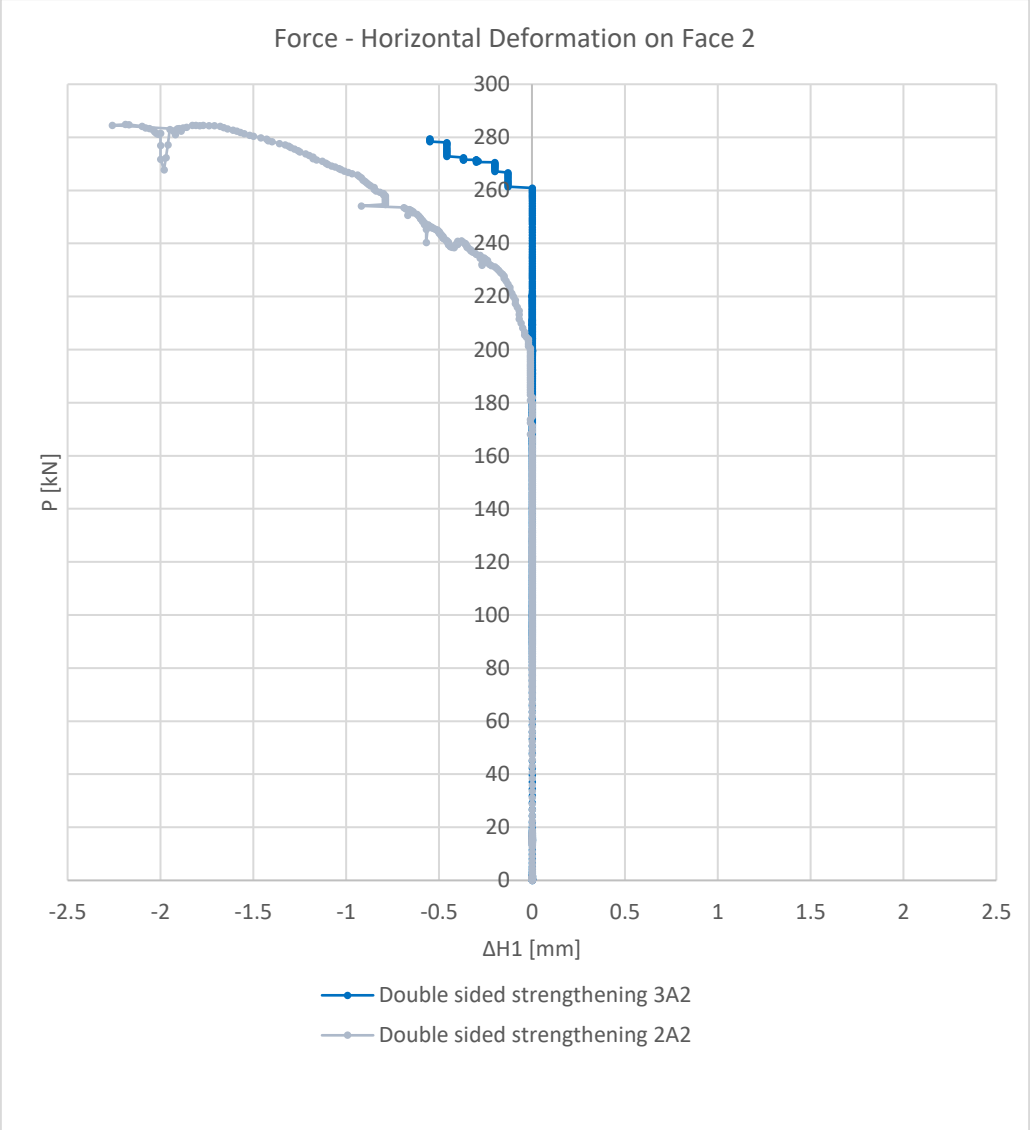


Fig. 3.34 Force by horizontal deformation on face 2 charts of 2A2 3A2 specimens

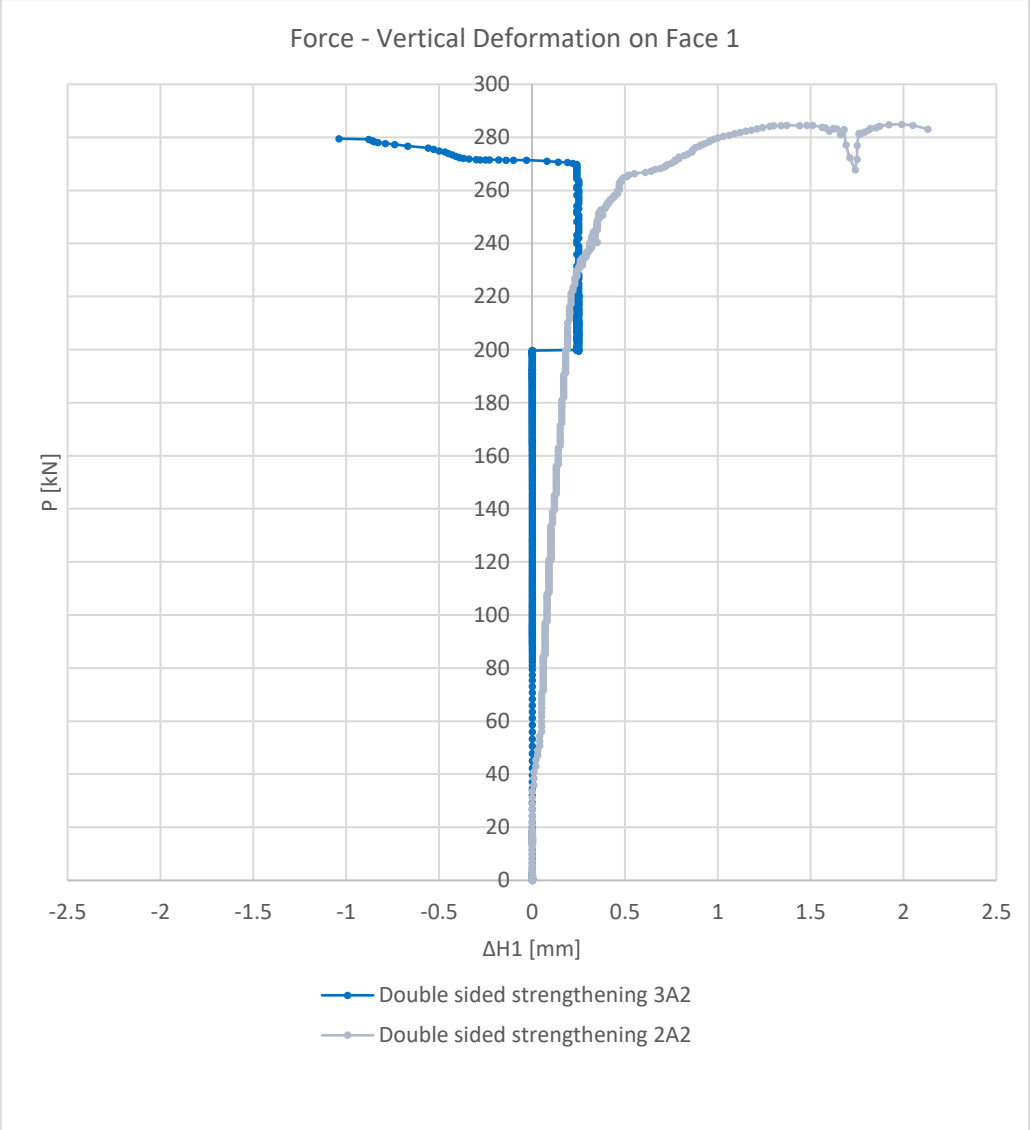


Fig. 3.35 Force by vertical deformation on face 1 charts of 2A2 and 3A2 specimens

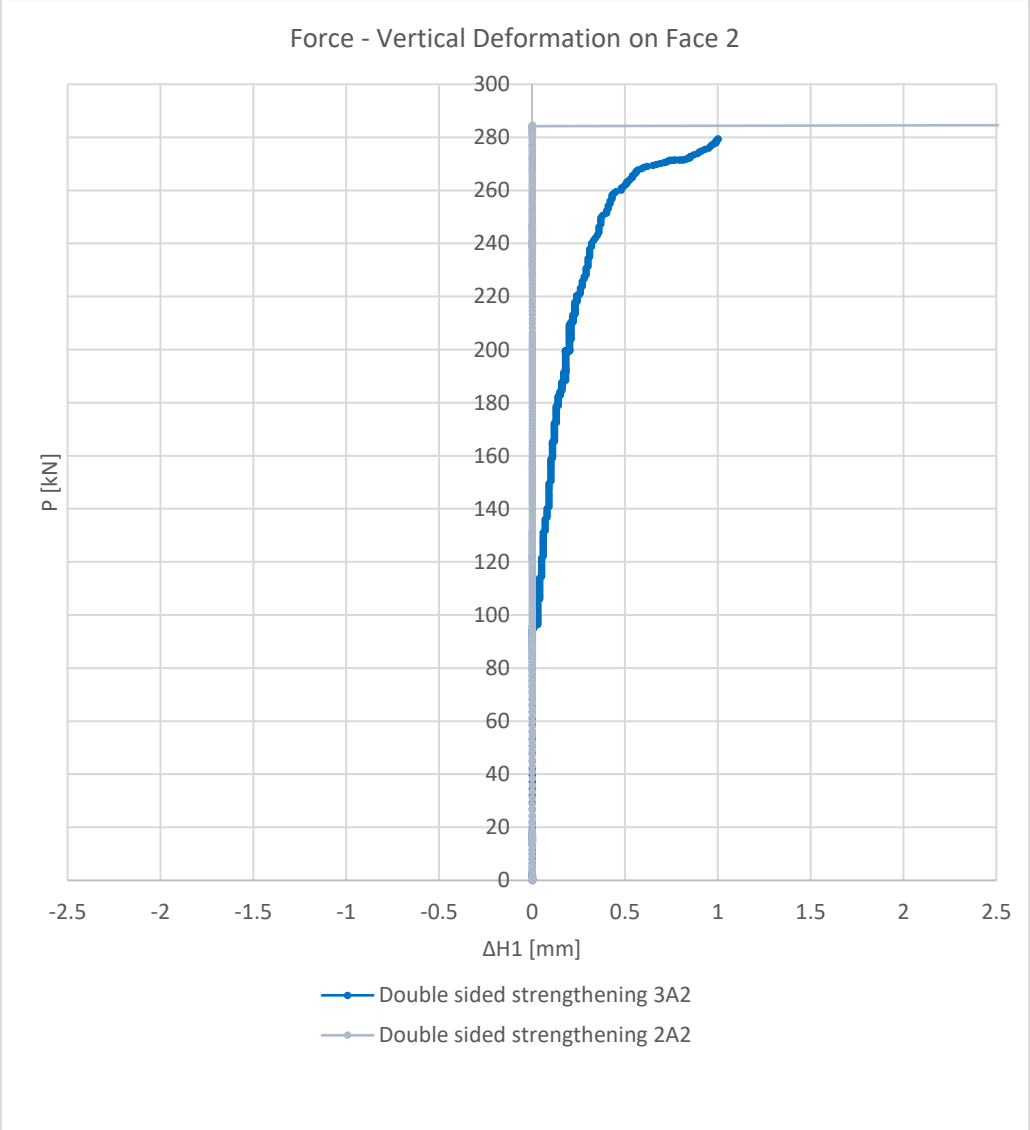


Fig. 3.36 Force by vertical deformation on face 2 charts of 2A2 and 3A2 specimens

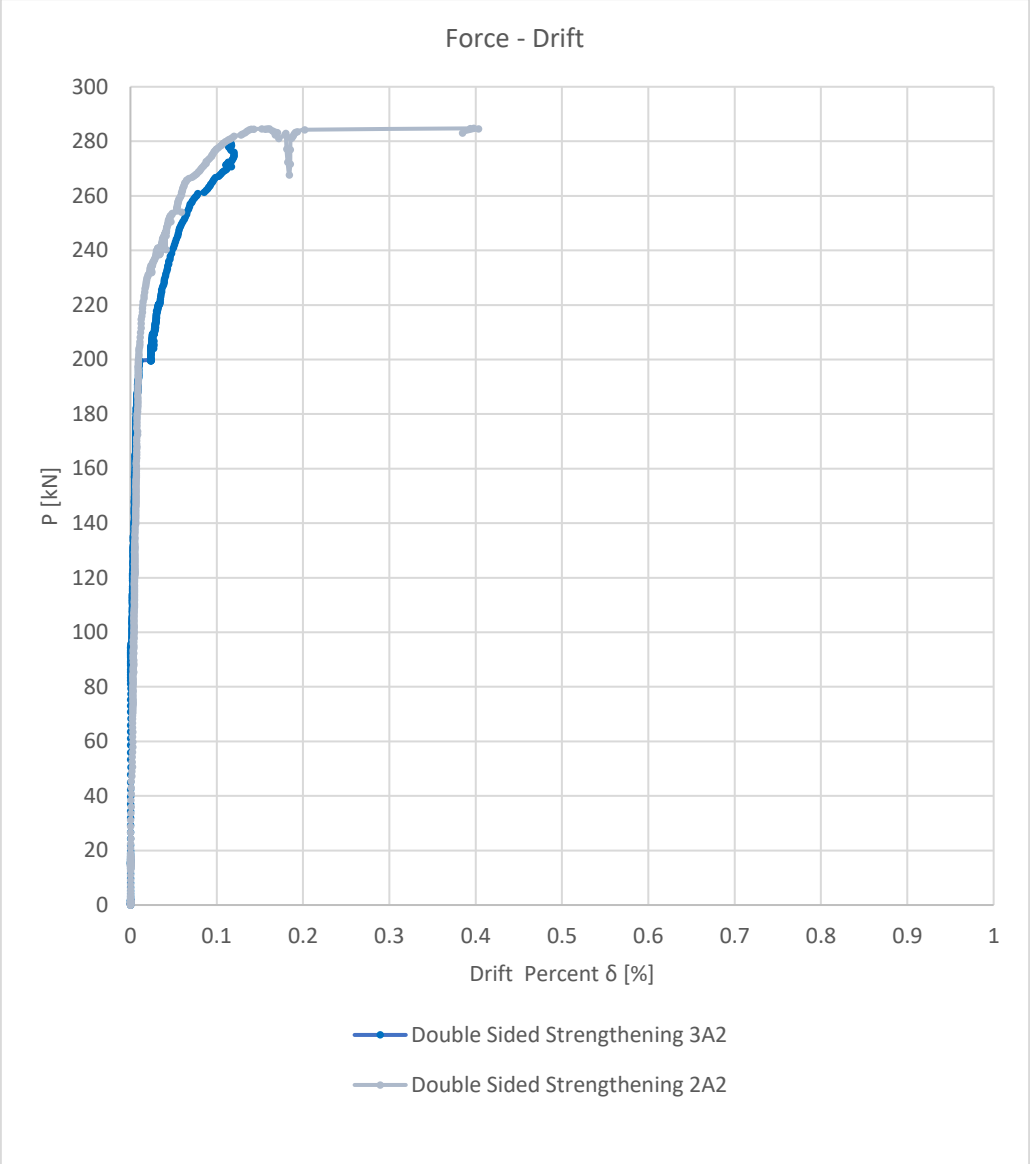


Fig. 3.37 Force-drift percent chart for 2A2 and 3A2 symmetrically strengthened specimens

Unlike the URM specimen, the force-drift chart shows that after the elastic phase the specimen could take a significant load increase of about 80 kN.

3.6.2.2 **Shear Stress Strain Curves**

The stress-strain characteristic response curve also shows ductile behaviour of the specimen and the fact that under reinforcing consolidation, the reinforced masonry can take further stress after cracking (Fig. 3.38).

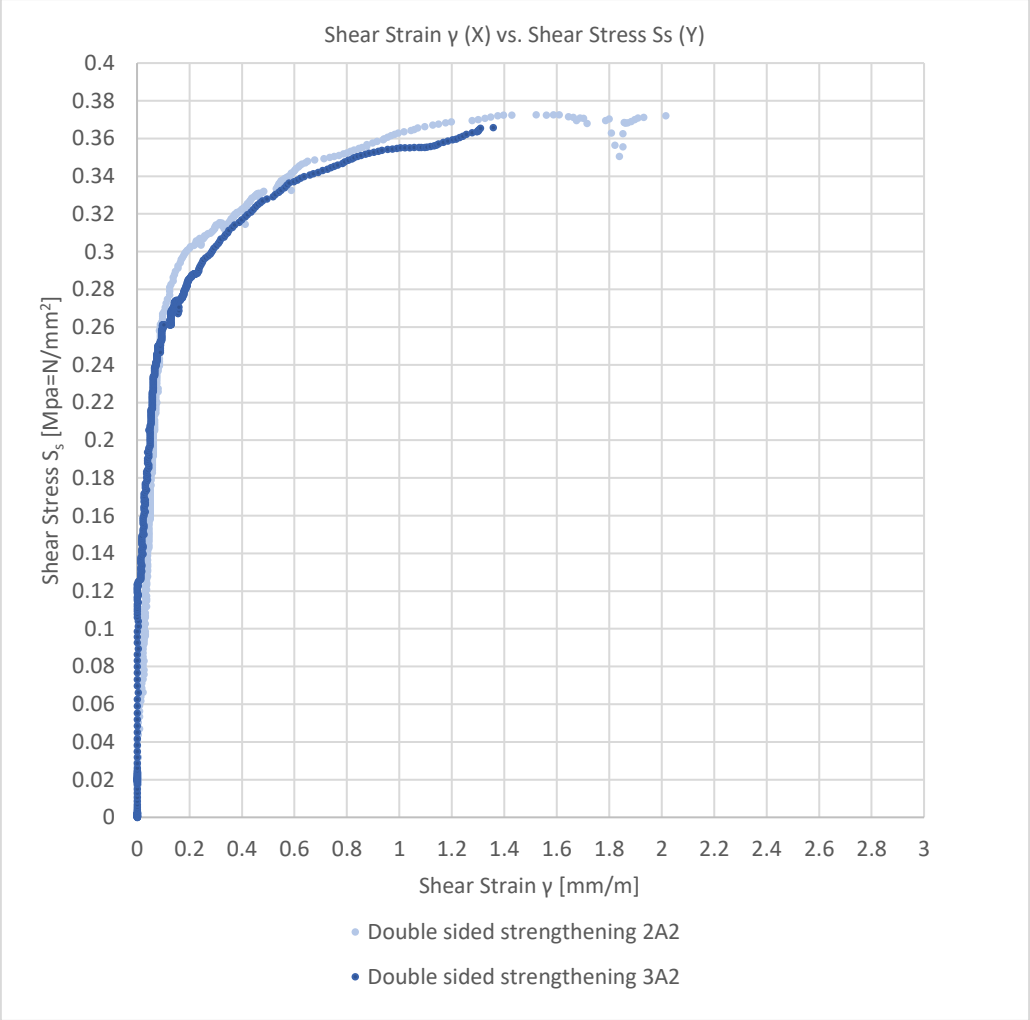


Fig. 3.38 Shear stress-shear strain chart for 2A2 and 3A2 symmetrically strengthened specimens

When comparing the shear behaviour of the unreinforced masonry specimen with the double-sided strengthened specimens it could be observed that there is a significant increase of the ductility of the wallets, the drift increasing from 0.155 in the case of 1NA up to 0.493 in the case of 2A2 and 3A2. The same can be observed in the case of the position of the cracking point where the shear stress is presenting a 176 % increase in the case of the strengthened specimens.

3.6.2.3 Ductility and Energy Dissipation

The 2A2 and 3A2 specimens tested show considerable ductility (as shown later in chapter on Table 3-7 Comparison of key data) . Even partially damaged, the specimens prove a significant increase in shear resistance. The load discharging and subsequent reloading due to observations done on the 3A2 specimen show that even damaged reloaded masonry reinforced on both sides can take similar loads as during the first loading process (Fig. 3.32). The ductility and energy dissipation is connected to several damage mechanisms that could be observed in the masonry mass. The lack of damage at the reinforcement level shows that the strengthening can be further optimised (reduced) to obtain energy dissipation also through yielding of the reinforcement. These tests prove that the double -reinforced well documented solution is valid.

After the conclusive results obtained from the 2A2 and 3A2 specimens the third specimen with double reinforcement was not tested anymore.

3.6.3 Single-sided Strengthened Specimen

The focus of the testing resided on the 4A1, 5A1 and 6A1 specimens. They belong to the group of specimens strengthened on one side. Their damage during testing did not lead to complete collapse. The damage was visible on the unreinforced side, while the reinforced one had no distinguishable cracks. The cracks were more distributed probably due to traction exerted on the masonry units by the steel mesh resisting elongation horizontally on the reinforced side.

3.6.3.1 Force-Deformation Curves

During the 5A1 test the horizontal displacement tracer on face 1 gave anomalous readings and was disregarded. Using the recorded film of the test, distance information was extrapolated analysing it frame by frame. Scatter deformation readings measured on video frames for 5A1 specimen, by considering pixel sizes and measurement pointers placements (Fig. 3.39). Due to this measurement error the horizontal deformation is not shown on some charts. Reinforced side readings exhibited compression (Fig. 3.41), due to the offset of the displacement tracers from the masonry surface and it's out of plane deformation. A similar deformation was noted by researchers on other occasions that tested single-sided strengthened specimens as observed by Turkmen *et al.* [55]. However, for other two specimens, the displacement tracers correctly recorded the deformations.

The specimens did not collapse, but the tests were stopped due to large deformations that overpassed the top piston stroke. In these conditions the loading was stopped before real failure.

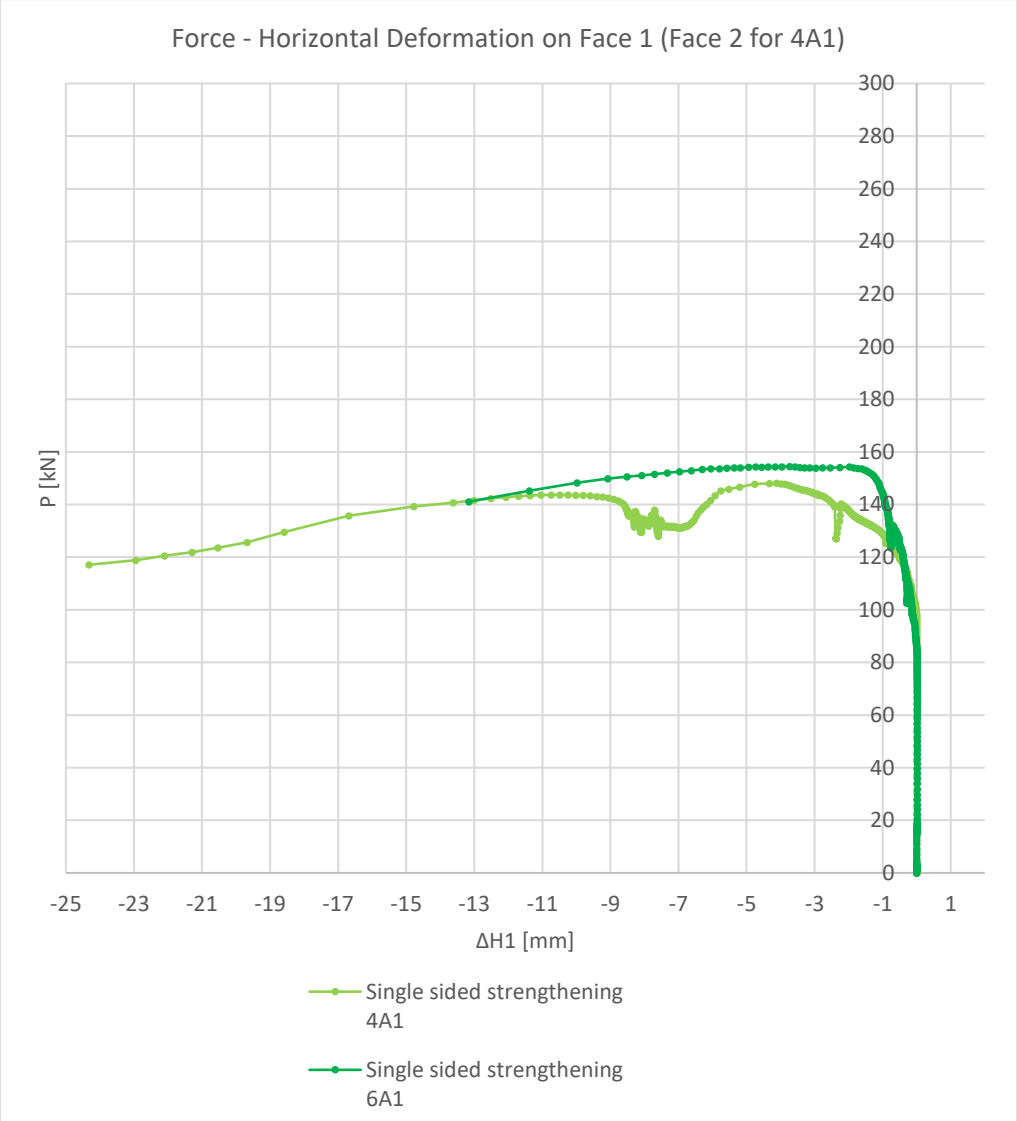


Fig. 3.39 Force by horizontal deformation on the non-reinforced face 1 (face 2 for 4A1 specimen) charts of 4A1 and 6A1 specimens

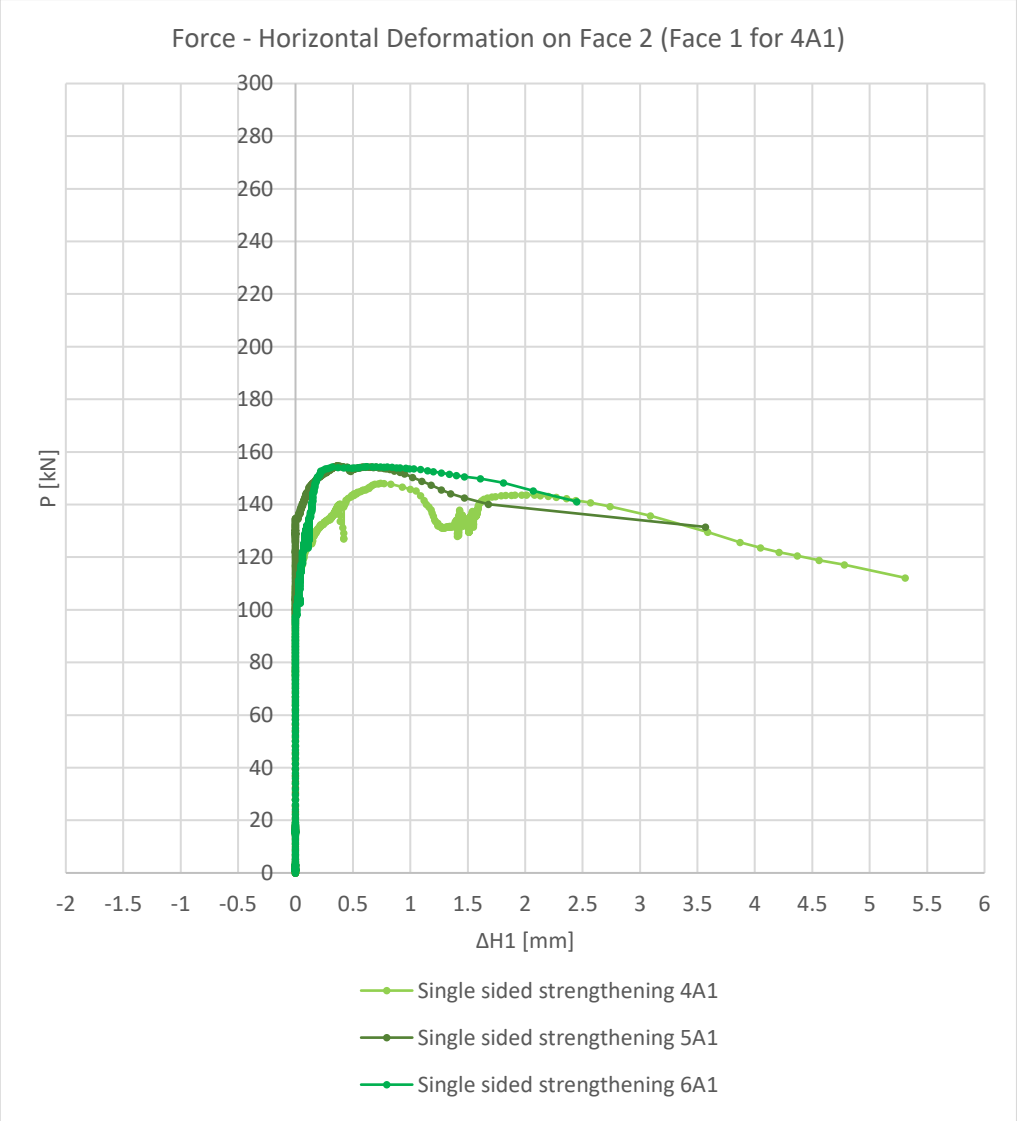


Fig. 3.40 Force by horizontal deformation on the reinforced face 2 (face 1 for 4A1) charts of 4A1, 5A1, 6A1 specimens – compression shown

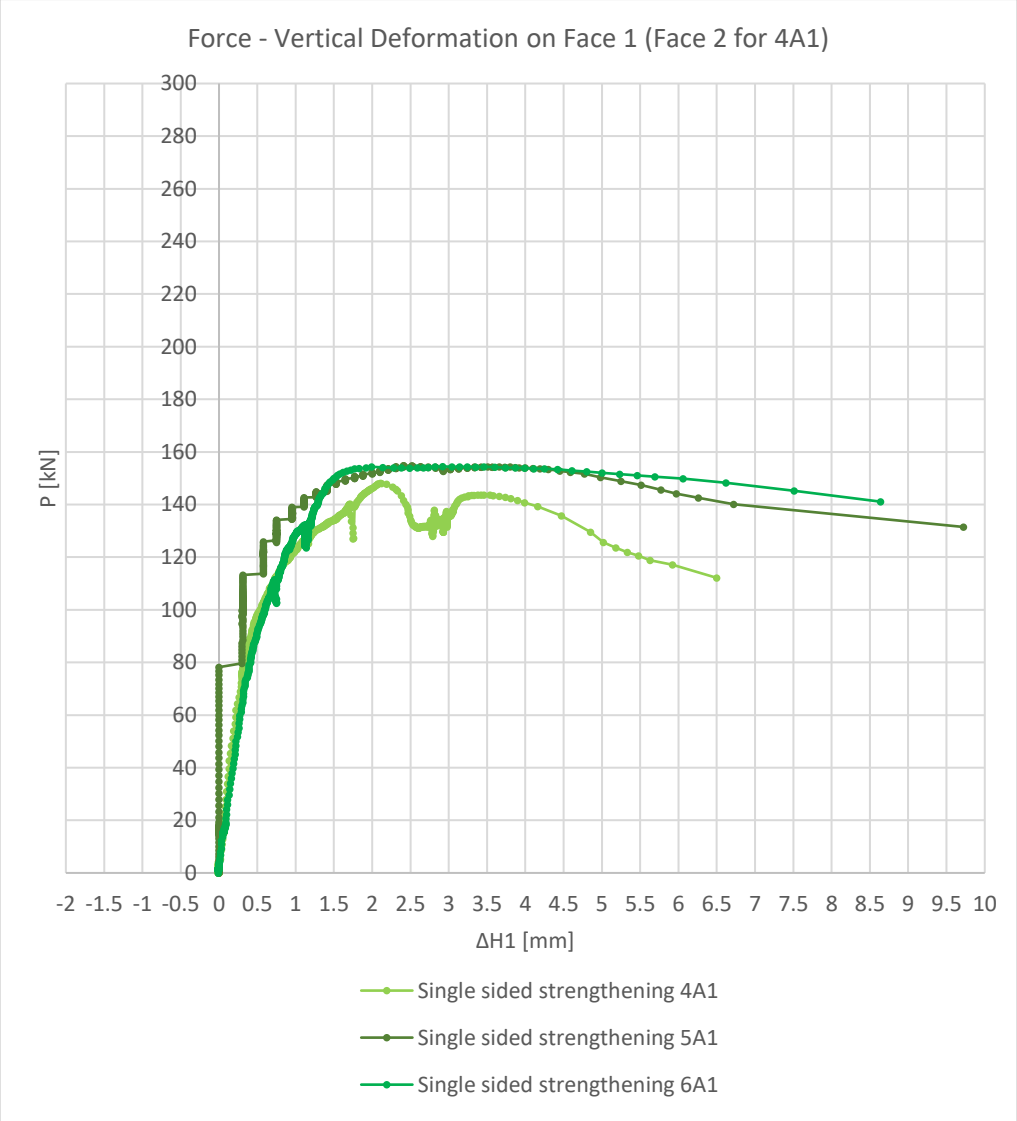


Fig. 3.41 Force by vertical deformation on the non-reinforced face 1 (face 2 for 4A1) charts of 4A1, 5A1 and 6A1 specimens

Considering the chart below (Fig. 3.42) an effect attributed to the steel fibre reinforcement can be seen. As soon as the hydraulic pressure was released the steel elastic fibres pulled back the specimen. Negative deformations were recorded due to damage that allowed for a larger deformation on the return.

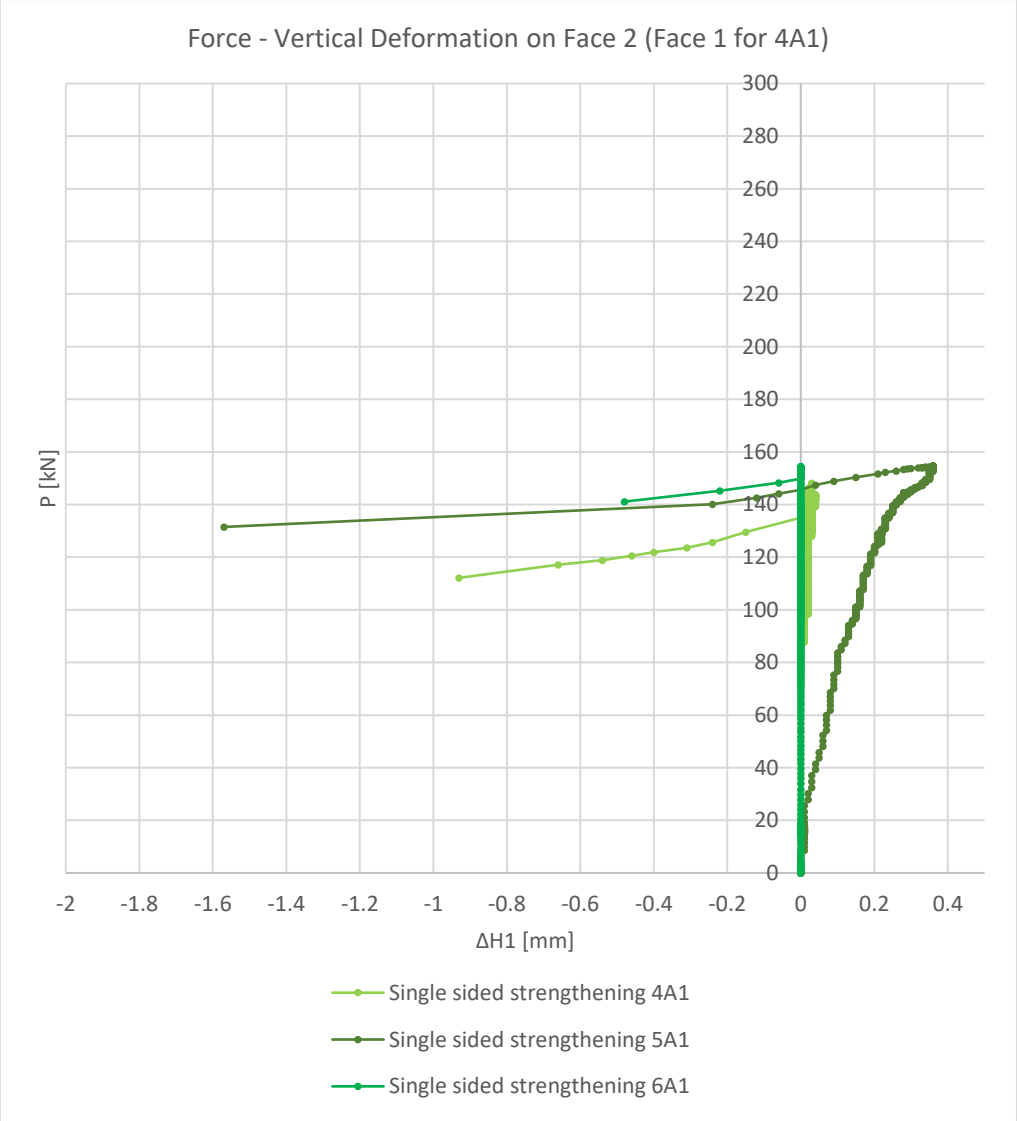


Fig. 3.42 Force by vertical deformation on the reinforced face 2 (face 1 for 4A1) charts of 4A1, 5A1 and 6A1 specimens

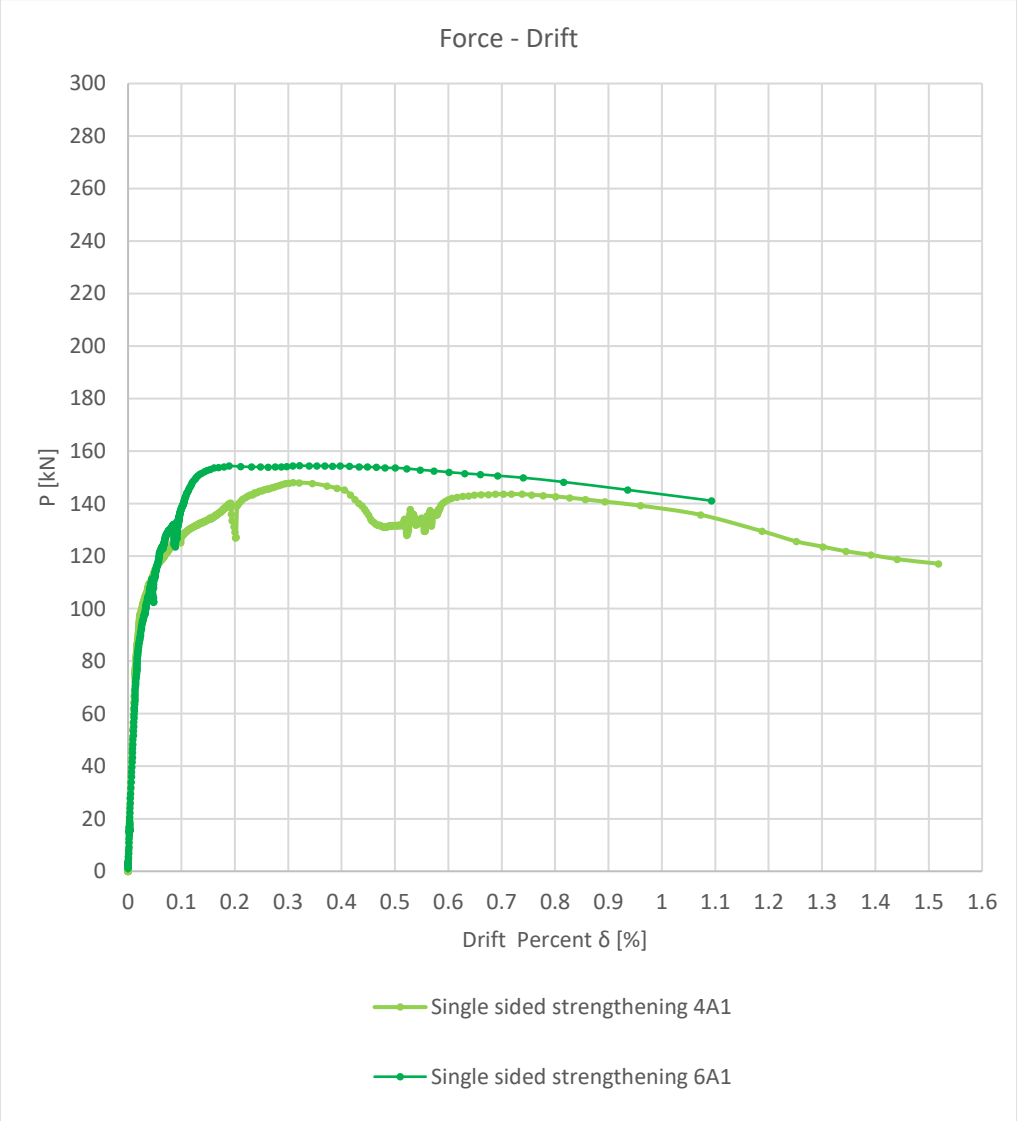


Fig. 3.43 Force-drift percent chart for 4A1 and 6A1 one-sided strengthened specimens

3.6.3.2 **Shear Stress – Shear Strain Curves**

Fig. 3.44 show the characteristic Shear Stress – Shear Strain response curves for specimens 4A1, 5A1 and respectively 6A1. For the specimen 5A1 scatter is also visible in the stress-strain chart. Thus, the results for this specimen are considered as non-concluding and ignored in further interpretations.

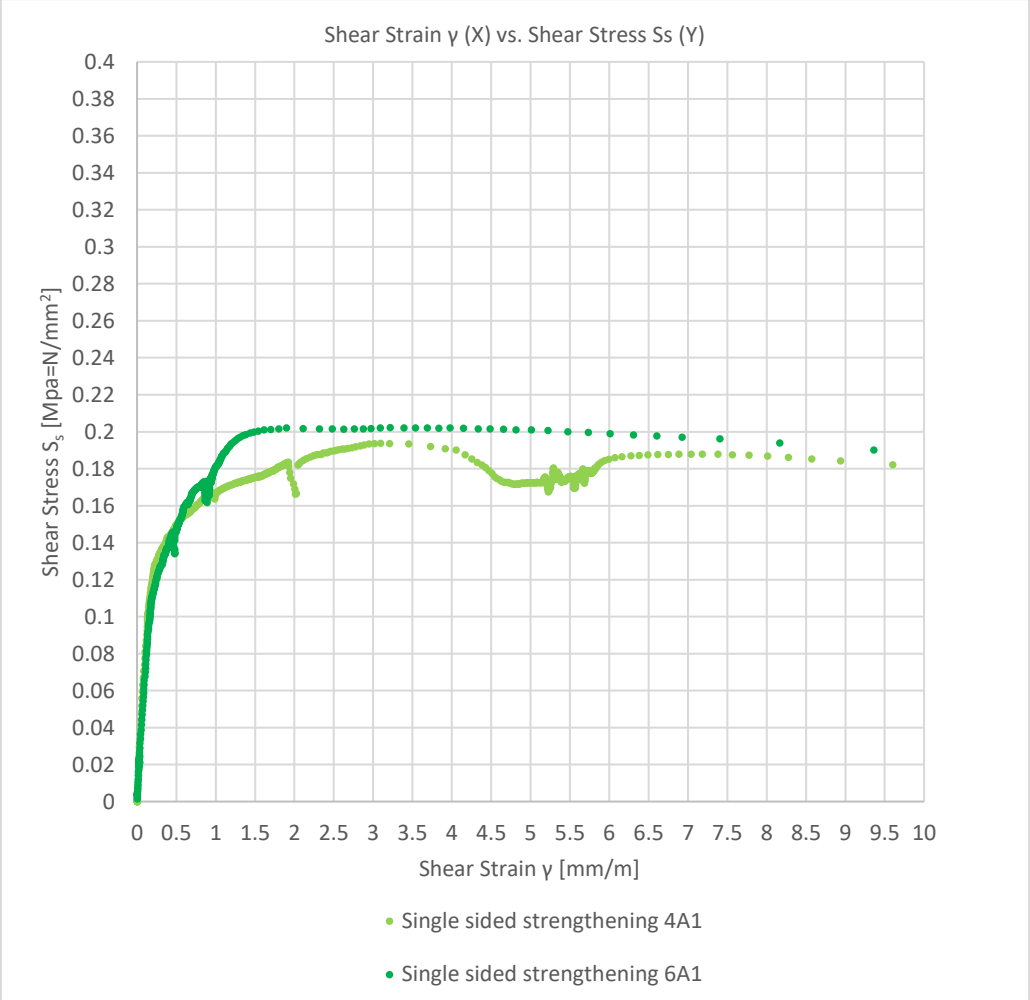


Fig. 3.44 Shear stress-shear strain chart for 4A1 and 6A1 one-sided strengthened specimens

When comparing the shear behaviour of the unreinforced masonry specimen with the single-sided strengthened specimens it could be observed that there is a significant increase of the ductility of the wallets due to the presence of the steel reinforcements, the drift increasing from 0.155% in the case of 1NA up to 1.093% in the case of 4A1 and 6A1. The same can be observed in the case of the position of the cracking point where the shear stress is presenting a 52 % increase in the case of the strengthened specimens.

3.6.3.3 **Ductility and Energy Dissipation**

Similarly to the specimens reinforced on two sides, 2A2 and 3A2, the 4A1, 5A1 and the 6A1 specimens exhibited pseudo-ductility and damage localised in the masonry mass (detailed in the Table 3-7 Comparison of key data). The presence of the steel reinforcement led to strain-hardening in the post-elastic range and to an important ductility of the system. The shear-input energy was absorbed in this process by the steel cords leading to a late failure situation.

3.6.3.4 **Corrections**

As mentioned before, because the strengthening is only on one side, a measurable out of plane deformation was present at the end of the 4A1, 5A1 and 6A1 tests. The eccentricity can be seen in the results of deformations and in the cracks that were developed only on the non-strengthened side.

Because the displacement tracers are anchored to the specimen on 10 cm long rods perpendicular to the surface there was concern that the unilateral deformation as seen in Fig. 3.45 would alter the calculated strain due to the geometric offset that occurs.



Fig. 3.45 Deformation on the horizontal diagonal plane

Considering this deformation on an almost circular shape, a method to correct the deformation values was devised as in the below figure Fig. 3.46.

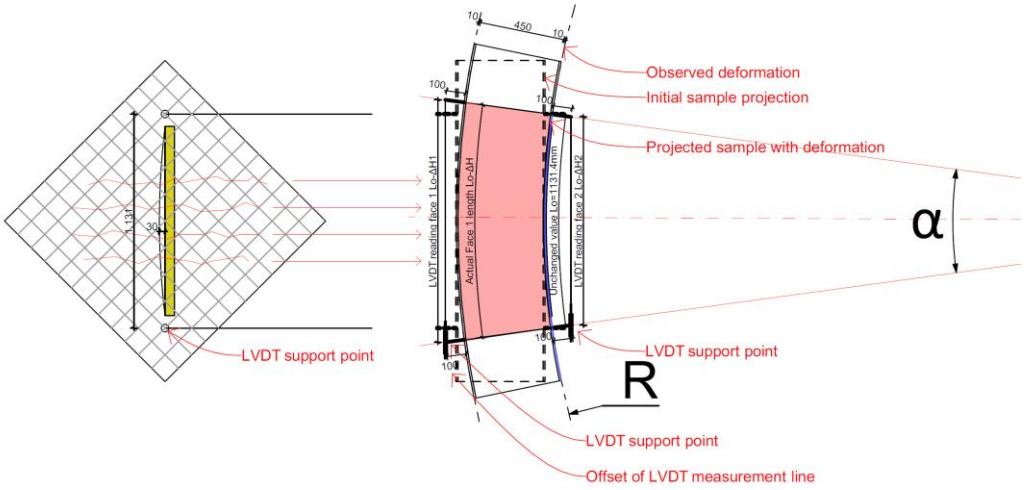


Fig. 3.46 Analysis of deformation implications

From the measured geometry a formula was devised for the affected horizontal deformation on the non-reinforced side (ΔH). The horizontal deformation on the non-reinforced side displacement tracer was denoted as (ΔH_1). The horizontal deformation recorded by the reinforced side displacement tracer was denoted as (ΔH_2). The initial distance between the displacement tracers' supports is (L_0=1131.4 mm). This remained the same on the reinforced side throughout the test, although it was not anymore, a straight line but become a circular curve. No cracks we present on this side. The virtual radius of the circle that the deformation curve was approximated to be on was called (R). The curvature angle made regarding the circle centre by the LVD support rods was denoted as (α). Considering the formulae for chords length and the arc length on the unreinforced side a corrected formula for the horizontal deformation on the un-strengthened side ΔH was obtained. The angle α was considered in radians in the calculation.

$$L_0 - \Delta H_1 = 2(R + 570)\, sin\frac{\alpha}{2} \tag{3.10}$$

$$L_0 - \Delta H_2 = 2(R - 100)\, sin\frac{\alpha}{2} \tag{3.11}$$

$$L_0 = R\alpha \tag{3.12}$$

$$L_0 - \Delta H = (R + 470)\alpha \tag{3.13}$$

Dividing the first two equations (3.10); (3.11) and substituting the radius obtained from the last equation (3.13), in the division the correction for the horizontal deformation on the non-reinforced side was obtained.

$$\Delta H = \frac{(\Delta H_1 - \Delta H_2)531758}{570(L_0 - \Delta H_2) - 100(L_0 - \Delta H_1)} \tag{3.14}$$

Introducing this compensation into the data sets while proving to be about 2mm for the maximum force, reflected only to about 0.0034 mm/m at the shear strain level and 0.00006 GPa at the corresponding shear modulus. This is not important in the ultimate results. The procedure used by other authors, that use the average between the deformation readings on the two sides compensate well even this kind of deformations. As averaging between the readings on the two sides was used also in the calculations done previously in the chapter it is considered that the geometric error induced is minimal (Fig. 3.47).

R	S	T	U
Vertical Displacement on Face 2, ΔV_2 (LVDT4) [mm]		Shear Strain γ - Average of faces ASTM E519 [mm/m]	Shear Modulus G (S_v/γ)/1000 [GPa]
0	mm	2.969771964	0.067947838
0	mm	3.089093159	0.065429201
0	mm	3.212833657	0.062960171
0	mm	3.389605798	0.059628438
0	mm	3.535442814	0.057168765

Fig. 3.47 Shear strain and shear modulus corrected values for specimen 6A1

For specimen 5A1 an error in the reading of the horizontal displacement tracer from the unreinforced side corrupted the ΔH_1 deformation data as seen on Fig. 3.48. The other readings were unaffected. A method was put in place to recover deformation data from video frames recorded on that side. To this end, frames were extracted at every 10 seconds of the video recording made during testing. They were scaled to 1:1 dimension in Archicad software. A measurement was made for each frame between well visible markings (Fig. 3.49). The pixel size, evaluated based on the specimen grid, is 2.02 mm and in consequence the considered uncertainty was considered +/- 1 mm. This reflects on the deformation values below 2 mm, the larger ones that were taken after the cracking occurred can be considered as valid.

BUPT

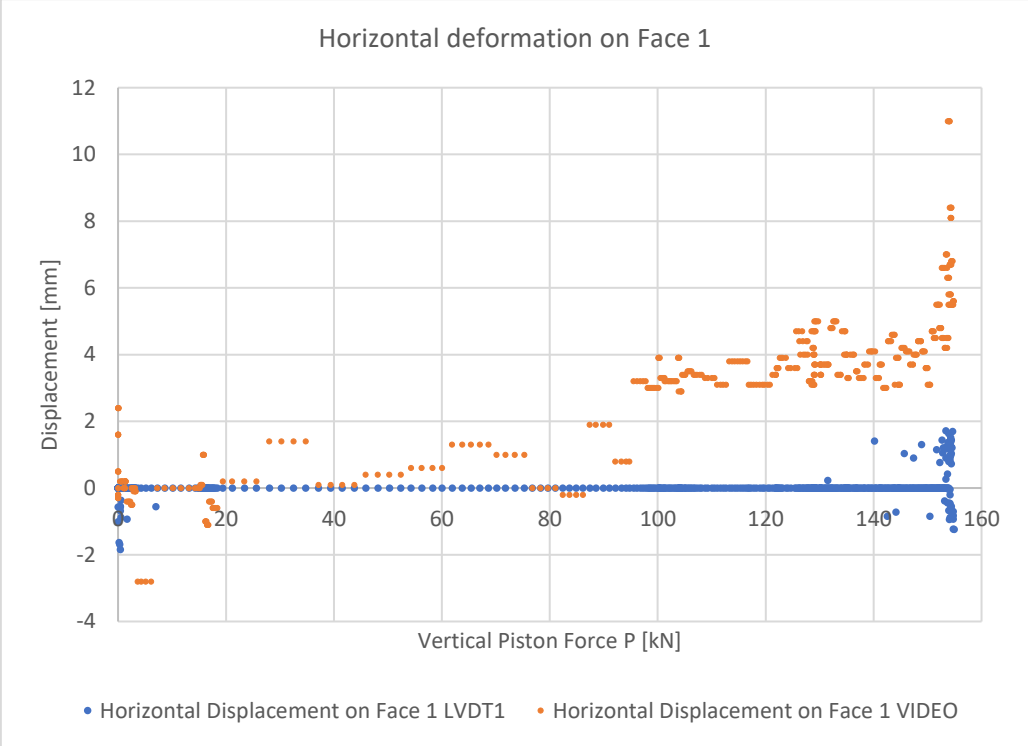


Fig. 3.48 Readings from the faulty data and video analysis



Fig. 3.49 Example of image measurement

The data that could be exploited from 5A1 test with precision consists of force, vertical deformations on both faces, and horizontal deformation on face 2 (reinforced

side). As the data for the horizontal deformation on face 1 obtained from the displacement tracer 1 is not usable, the data extracted from the video frame is usable after the moment of cracking, with an error of +/-1 mm.

3.6.4 Failure Modes

The 1NA specimen cracked along the loading diagonal, exhibiting diagonal tension cracking that went through the masonry units. A small drift of 1.24 mm (0.155 %) was recorded before the sudden brittle collapse. The crack passed through masonry units and joints having a clear (not stepped) path on face 1. On face 2 joint sliding was recorded, possibly leading to the slightly (~30 %) larger deformation on this side. The decrease in downforce seen on the load/deformation charts can also be attributed to this partial joint slide. The visible cross-section side of the wall remained unaffected by any damage before the final second (Fig. 3.50).

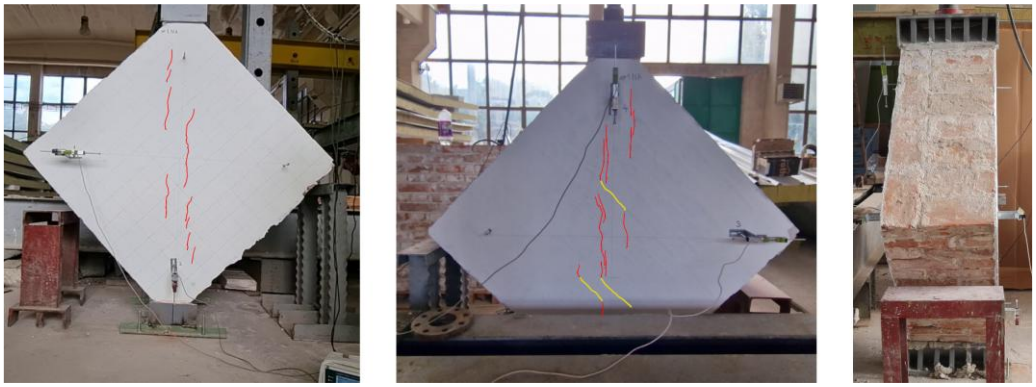
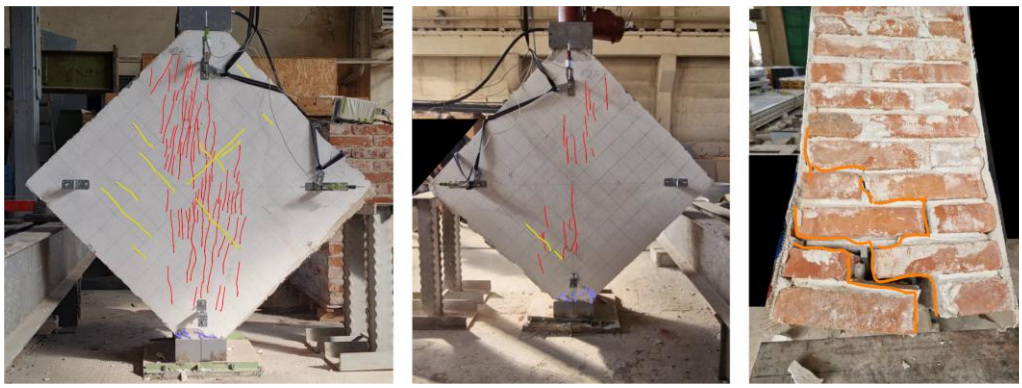


Fig. 3.50 1NA specimen failure due to diagonal tension cracking; Red – diagonal tension cracking; Yellow – Shear joint sliding

The 2A2 test specimen had more extensive damage due to the 3 load cycles it was subjected to because of the intermediary damage inspections. There were recorded small cracking due to diagonal tension, but its distribution is wider while the masonry has been held together by the surface reinforcement. The joint sliding is more extensive, but well contained by the reinforced plaster. There was recorded the masonry crushing especially around the inferior loading shoe, possibly because of the added weight of the specimen compared to the upper loading shoe. The main damage is surprisingly not perpendicular to the masonry plane but contained in it. The traction of the face reinforcements resisting the Poisson effect led to the joints of the far sides to separate and slide, effectively delaminating the masonry. The bond strength of the mortar plaster to the masonry units was strong as delamination from the bricks is very localized and has taken away the top layer of masonry units' surface. One side of the specimen sustained more damage than the other, probably because of eccentricities in the load and the stand deformation. This is also visible in the deformation readings that are approximatively double on face 1 (Fig. 3.51).

BUPT



a) b) c)

Fig. 3.51 Failure mode of the 2A2 specimen; Red – diagonal tension cracking; Yellow – Shear joint sliding; Purple – crushing; Orange – joint sliding delamination

The 3A2 specimen was subjected to a gradually increasing load. The damage is much less apparent on the faces of the specimen. Face 1 (Fig. 3.52a) has damage localized in the centre plane consisting of diagonal tension cracks and joint sliding. Everything was held in place by the surface reinforcement. Face 2 (Fig. 3.52b) has almost no apparent damage (Fig. 3.52).



Fig. 3.52 Failure modes of the 3A2 specimen; Red – diagonal tension cracking; Yellow – Shear joint sliding; Purple – crushing; Orange – joint sliding delamination

From the two tests performed on specimens strengthened on both sides, the 2A2 specimen was chosen to be presented here with the damage history along the loading test. Only the first loading cycle is presented below to keep a similar reference data form all tests. The 3A2 specimen suffered similar damage.

Subsequently the failure modes of the single sided strengthened specimens were analysed (Fig. 3.53, Fig. 3.54, Fig. 3.55). From the three tests done on one-sided reinforced specimens, the 4A1 specimen was selected to be presented herein to describe the sequence of events during loading (see Annex A). This selection was chosen as it presents the most complete data, and the loading was complete enough to see a diminishing of the exerted force due to damage. The side for illustrating the events was the unreinforced side (Face 1), as the reinforced side (Face 2) didn't exhibit any visible cracks during testing. However, during the final part of the test the reinforced side exhibited a curvature visible from the side edge due to the

considerable lengthening of the horizontal diagonal of the unreinforced side. Cracking in the plane of the specimen, similar to the double-side reinforced specimens was not observed.

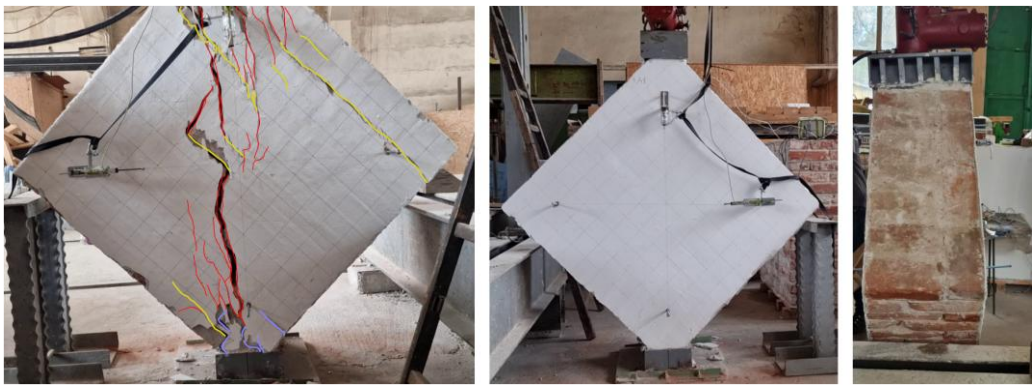


Fig. 3.53 Failure mode of 4A1 specimen; Red – diagonal tension cracking; Yellow – Shear joint sliding; Purple – crushing



Fig. 3.54 Failure mode of 5A1 specimen; Red – diagonal tension cracking; Yellow – Shear joint sliding; Purple – crushing



Fig. 3.55 Failure mode of 6A1 specimen; Red – diagonal tension cracking; Yellow – Shear joint sliding; Purple – crushing

An extensive presentation of the observed and computed data for all the performed laboratory tests can be observed in Annex A.

3.7 Discussion of Testing Results and Comparison

A thorough analysis was done on the drift – shear stress results plots. The points where cracking occurs were drawn using the intersection of the initial rigidity line representing the elastic range of the graphs and the tangent to the plot zone where 10% of slope is reached. These points give a cracking shear stress and a corresponding cracking drift. The "cracking" notion is used because in the case of the tested specimens, the plastic deformations started due to development of cracks in the masonry mass.

On the same plots points of maximum shear stress and their drift were identified and analysed for further comparison. Also, maximum drifts corresponding to collapse for the 1NA specimen and extensive deformation for specimens 2A2 (strengthened on two sides), and respectively 4A1 and 6A1 (strengthened on one side) were identified. This extensive deformation meant that further testing had to be stopped in absence of total collapse. The interpreted values obtained were considered maximum drifts (δu), and together with the cracking drifts (δb) were used to obtain pseudo-ductility values as similarly described by other researchers like Ismail et al. [89], Turkmen et al. [92] and Micelli et al. [100]

The combined graphs comparison is visible below in Fig. 3.56:

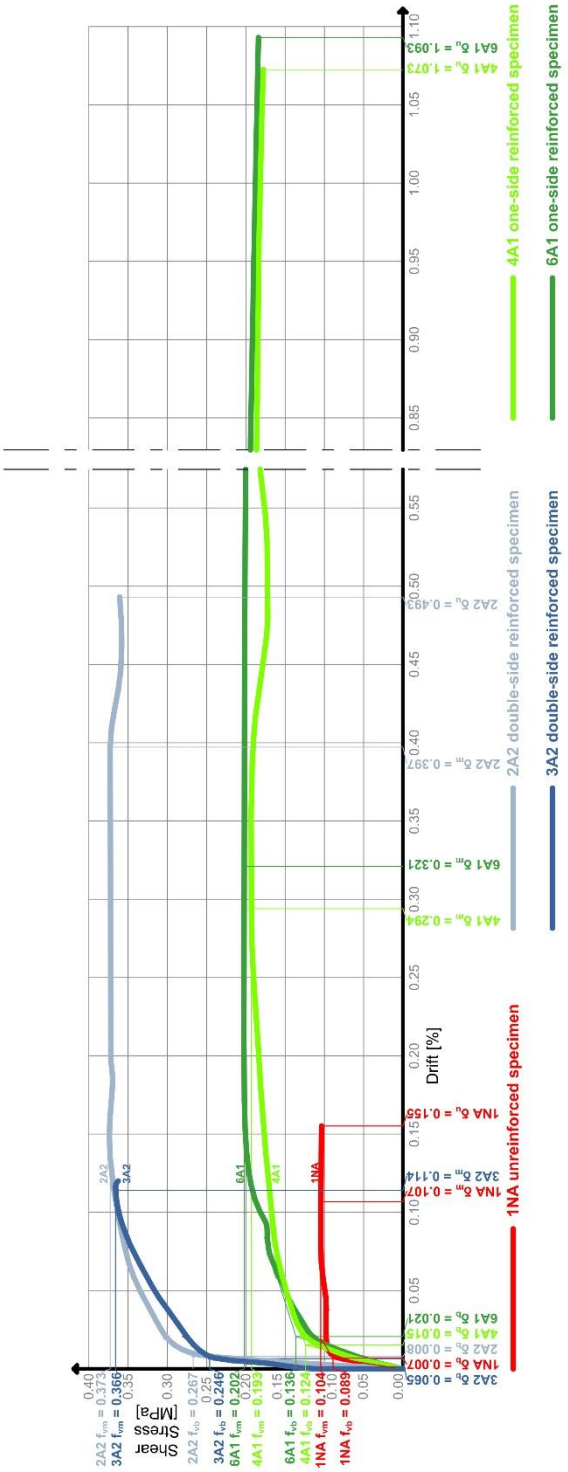


Fig. 3.56 Drift-Shear Stress Graphs

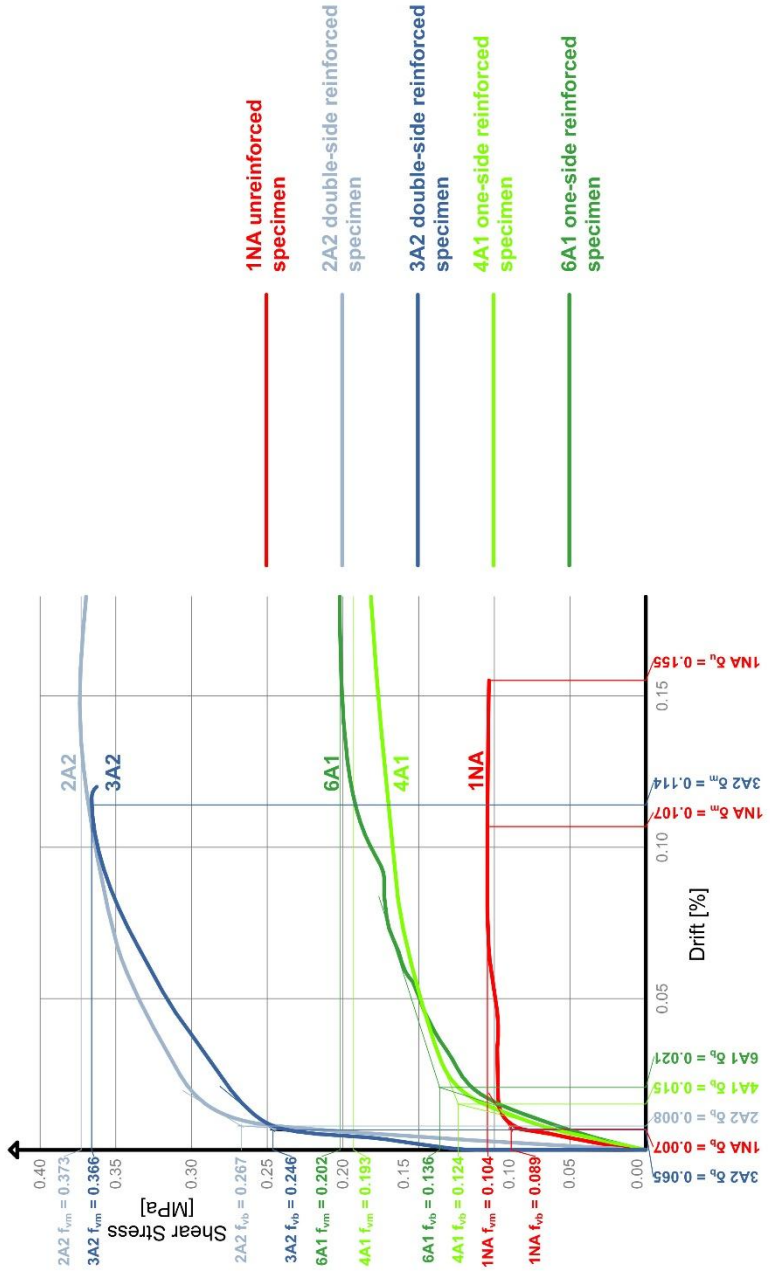


Fig. 3.57 Drift-Shear Stress Graphs - Enlarged First Part

The results from this analysis and the test data can be seen in the following comparison table (Table 3-7):

Table 3-7 Comparison of key data

Specimen	1NA	2A2	3A2	4A1	5A1	6A1
Shear Modulus G [GPa]	1.507	3.885	3.980	0.852	Inconclusive	0.781
Max. Shear Force V_{max} [kN]	56.383	201.406	197.606	104.459	109.496	109.232
Max. Shear Strength f_{vm} [Mpa]	0.104	0.373	0.366	0.193	0.203	0.202
Cracking Shear Strength f_{vb} [Mpa]	0.089	0.267	0.246	0.124	Inconclusive	0.136
Design Shear Force CNR-DT 200 R1/2013 (ITA) GeoForce One [kN]	43.643	100.687	100.687	65.042	65.042	65.042
Design Shear Strength f_{vd} [Mpa]	0.081	0.186	0.186	0.120	0.120	0.120
Drift at Cracking Shear Strength δ_b [%]	0.007	0.008	0.007	0.015	Inconclusive	0.021
Drift at Max. Shear Strength δ_m [%]	0.107	0.397	0.114	0.294	Inconclusive	0.321
Max. Drift at Considered Failure δ_u [%]	0.155	0.493	Inconclusive	1.073	Inconclusive	1.093
Pseudo-ductility ratio $D=\delta_u/\delta_b$	22.143	61.625	Inconclusive	71.533	Inconclusive	53.317
Notes	Baseline		Late elastic zone (54-61% for G evaluation), stopped before considered failure		Displacement errors	

The basis shear strength of the 1NA URM specimen was the one determined experimentally from the unreinforced test. Based on this value and on the other properties of the reinforced masonry samples shear strength simulations have been made using the Geoforce One software from Kerakoll SpA that uses the Italian guide CNR-DT 200 R1/2013.

The simulated shear strength obtained using Geoforce One FEM software from Kerakoll S.P.A., for the specimens reinforced on both sides is 70-75 % of the tested one, and 88-96 % for the ones strengthened on one side, maintaining the safety of the computed shear strength regarding the cracking shear strengths calculated according to the results of the experimental results.

The shear modulus increases 2.6 times for the specimens strengthened on two sides 2A2 and 3A2 in comparison to the basic specimen 1NA. However, the shear modulus for the 4A1 and 6A1 specimens drops to approximatively half of the URM one. This is also confirmed by the macro-modelling FEM simulation presented in the next chapter. For now, there is one possible explanation for this phenomenon, that the one-sided application of the reinforcement moves the stiffness towards its side making the wall section work only partially on the reinforced side. This could be further amplified by the way the wall bends out of plane, pulling de corners of the unreinforced side away from the loading shoes. The reinforcement works as confinement of one side while the other side proves a larger deformation.

Nevertheless, the maximum shear strength of these samples is 140-152 % to that of the 1NA specimen.

The analysed specimens present a hardening section, exhibiting a larger shear strength at considerable higher drift than the cracking point drift. This is most probably due to using steel reinforcement and to change in the load redistribution in the element. The double-sided strengthened specimens show hardening section representing 49 % of the linear part while the single sided ones reach up to 55% of the linear part. The unreinforced specimen shows only a 17 % hardening section compared to the linear section. Compared to the 1NA specimen, the double side specimens show an 8-fold increase of the hardening section and the single sided specimen a 5 fold increase.

The pseudo-ductility increases to 277 % for the 2A2 and 3A2 samples and 240-323 % for the 4A1 and 6A1.

These phenomena can also be observed on the shear strain-stress plots below (Fig. 3.58).

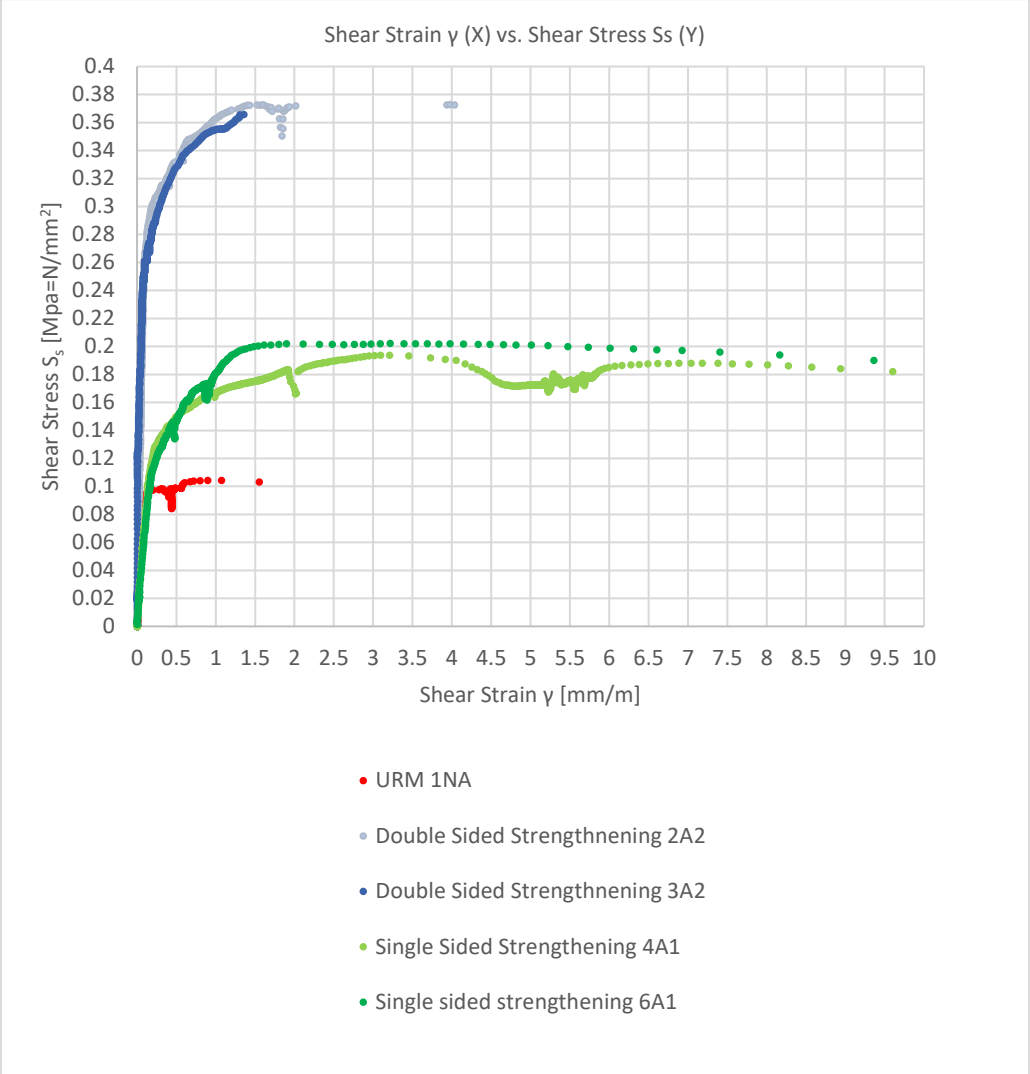


Fig. 3.58 Shear strain-stress diagrams for all relevant tested specimens

3.8 Conclusions of the Experimental Study

Considering the principal concept expounded in this study, the single-side intervention on the historical masonry walls is proposed. From the three sets of tests, the solution that uses one-sided strengthening show the following improvements regarding the original (non-reinforced) masonry:

- Considerably changes the behaviour of the masonry from brittle to a pseudo-ductile masonry-reinforcement assembly
- Extends the elastic behaviour of the masonry by 39-52 % for one-side strengthening, 176-200 % for two-sided strengthening (Fig. 3.58)
- Increases the pseudo-ductility by at least 140%. The ultimate drift [87] figure was not obtained due to practical setup and safety reasons

regarding the test stand. The specimens strengthened on two sides had shown similar increase in drift capacity.

The strengthening on two-sides is clearly superior to the one-sided one, but the benefits of the last, as described in the previous paragraph are clear.

In the context where due to certain limitations and goals it is not possible to strengthen both sides of a masonry, the strengthening on one side can yield tangible results in getting the buildings safe and limiting the damage due to expected seismic activity. Therefore, it becomes apparent that depending on the scale of the structural retrofit and the state of conservation of the historic masonry structure, single sided or double-sided reinforcement solutions can be employed.

More than this, the study highlights a series of equations and calculation methods (as per ASTM E519/E519M-15 [1])which can be used to evaluate the effect of the used reinforcement methods on test specimens, which prove out to be conclusive in the laboratory tests.

4 FINITE ELEMENT INVESTIGATIONS

4.1 FE Modelling of Wallet Specimens

Based on the experimental results obtained from the diagonal compression tests, from separate tests done on the constitutive materials (bricks and lime mortar) and from information provided by material suppliers, a numerical computer simulation was performed in collaboration with Endo Research Group, from Shinshu University, Japan, led by Prof. Dr. Yohei Endo.

The model comprised a Finite Element Model of the test specimen subjected to similar forces. The model had the same dimension and orientation regarding external forces as the physical specimens on the test stand (Fig. 4.1).

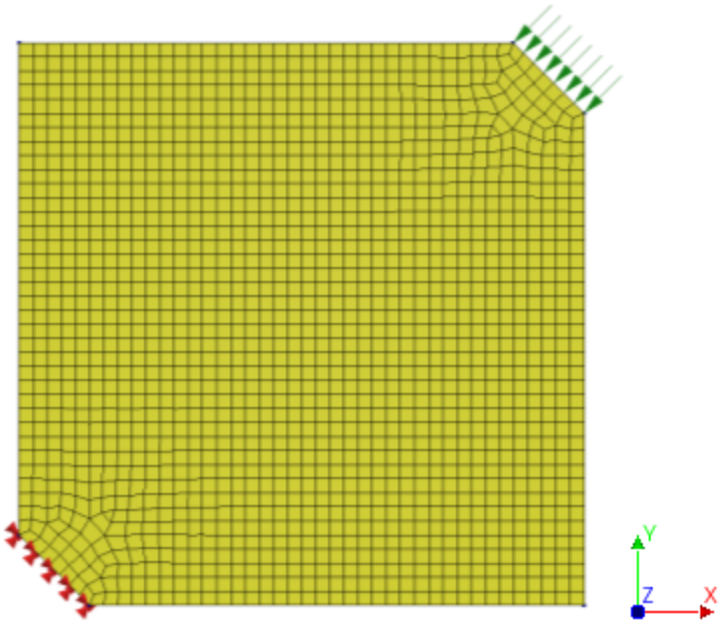


Fig. 4.1 Numerical model

4.1.1 Macro-Modelling Approach

For the macro-modelling the DIANA software was used. A homogeneous model with anisotropy was considered, adopting different constitutive laws in direction parallel to the bed joints versus the direction of the head joints. An extension of the smeared crack model was used as the description of the material constitutive laws were shifted from an isotropic stress-strain relation to an orthotropic one upon crack occurrence [28].

Tensile cracking and compressive crushing were designated to occur along the bed and head joints, while shear failure was considered only along the bed joints. The tensile behaviour was assumed to be identical in both the bed and head joint directions. The stress-strain response in was characterized by linear softening with secant unloading (Fig. 4.2). For shear, failure was modelled using the Coulomb friction model along the bed joints, with the stress-strain curve exhibiting linear softening

BUPT

until cohesion was reduced to zero (Fig. 4.3). The angle of diagonal stepwise cracks (θ) was set at 0.6 radians, based on the observed angles of diagonal cracks in the experiments. In compression, the stress-strain relationship featured parabolic pre-peak softening, linear post-peak softening, and a subsequent horizontal plateau (Fig. 4.4). The unloading stiffness was equal to the initial stiffness.

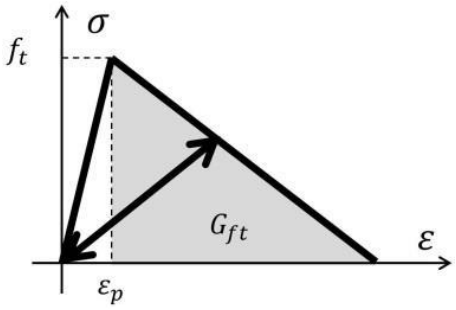


Fig. 4.2 Tension

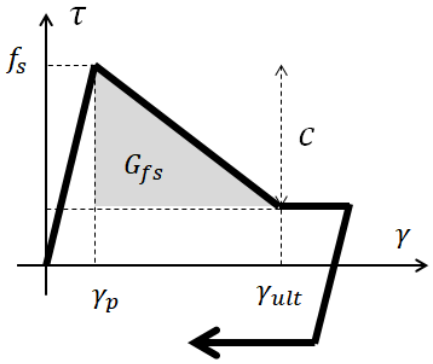


Fig. 4.3 Shear

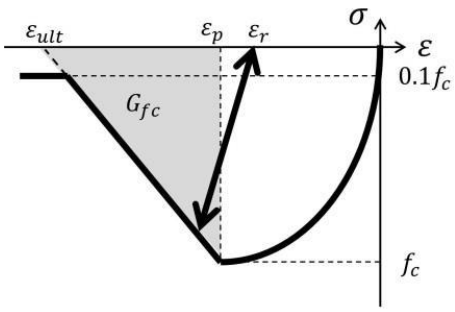


Fig. 4.4 Compression

4.1.2 Input Data and Procedure

The model included 1647 nodes and 1570 four-node quadrilateral shell elements. The lower left corner was fixed in all three translational directions, as illustrated in Fig. 4.1. Diagonal loads were applied to the upper right corner. For the

one-side strengthened model, an eccentric load (e = 0.18 m) was applied to account for the wall's deformed shape resulting from the difference in rigidity induced by the strengthened side. This was modelled after studying the one-side strengthened specimens testing results. Table 4-1 details the material parameters for the URM, double-sided and one-sided strengthened models. The density for all three models was 1,800 kg/m³. The values for the URM model characteristics were based on material laboratory tests performed on masonry elements, while the double-sided reinforcement material characteristics were selected according to the manufacturer's specifications [93][69]. The one-sided reinforced model parameters were averaged between the URM and double-sided models, except for cohesion, which was higher in the one-sided model. This adjustment was made to account for the out-of-plane deformation observed in the one-side strengthened wall after testing, suggesting that the load was primarily resisted by the strengthened side, thus necessitating an increase in cohesion. The specifications of the reinforcement manufacturer were also considered for the one-sided strengthening model [94].

Table 4-1 Material properties used in the macro-scale model

	Stiffness		Tension		Shear			Compression	
FE Model	E [N/mm^2]	G [N/mm^2]	f_t [MPa]	G_{ft} [N/m]	c [MPa]	Θ [rad]	G_{fs} [N/m]	f_c [MPa]	G_{fc} [N/m]
URM (no reinforcement)	500	200	0.07	15	0.1	0.6	75	8	1000
Double-side reinforcement	1000	400	0.27	60	0.36	0.6	300	10	1250
One-side reinforcement	750	300	0.17	37.5	0.3	0.6	187.5	9	1125

4.1.3 Numerical Results

The three models led to shear stress – shear strain responses that closely matched the experimental results (Fig. 4.5). When analysing the differences between the laboratory tests results and the numerical results, it can be observed that in the case of the unreinforced masonry wallet the differences are under 5 %. The same (under 5 % differences) can be observed in the case of the double-sided reinforced samples, in the elastic and plastic area, with difference reaching up to 15 % in the pre-peak softening area. In the case of the single sided reinforced samples a very good match can also be observed for the cracking shear force, but an acceptable match, with a difference of maximum 15 % was obtained in the elastic and plastic portion.

However, the double-side strengthened model did not exhibit pre-peak softening and rather showing an elastic-plastic behaviour, likely because the macro-scale models treated masonry as a homogeneous material [28][29]. Consequently, the tensile strength used in the macro-scale analysis was that of the masonry itself. The crack patterns and their progression were like those observed in the experiment (Fig. 4.6). Initially, damage appeared at the corners of the wall and extended as deformation increased. At the ultimate state, shear damage was distributed across the wall in locations similar to the experiment. The one-side strengthened model displayed an out-of-plane deformation of 2.1 cm, like the one observed experimentally (Fig. 3.45).

The model with one-side strengthening has shown a 50% increase in shear strength compared to the URM. At the end of the elastic behaviour, the experimental

BUPT

values are similar to those resulted from the numerical analysis. After that the experimental values are slightly higher.

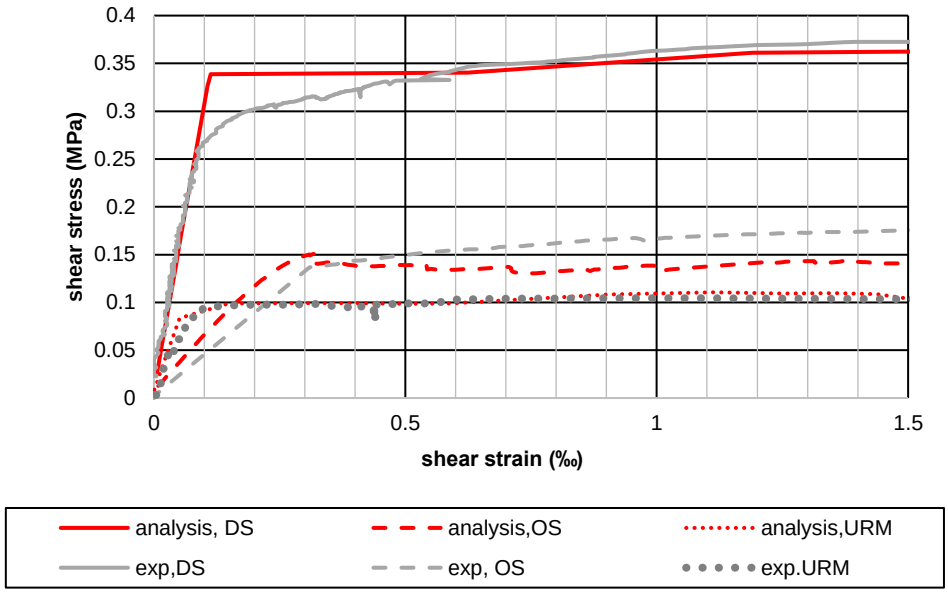


Fig. 4.5 Simulation Results

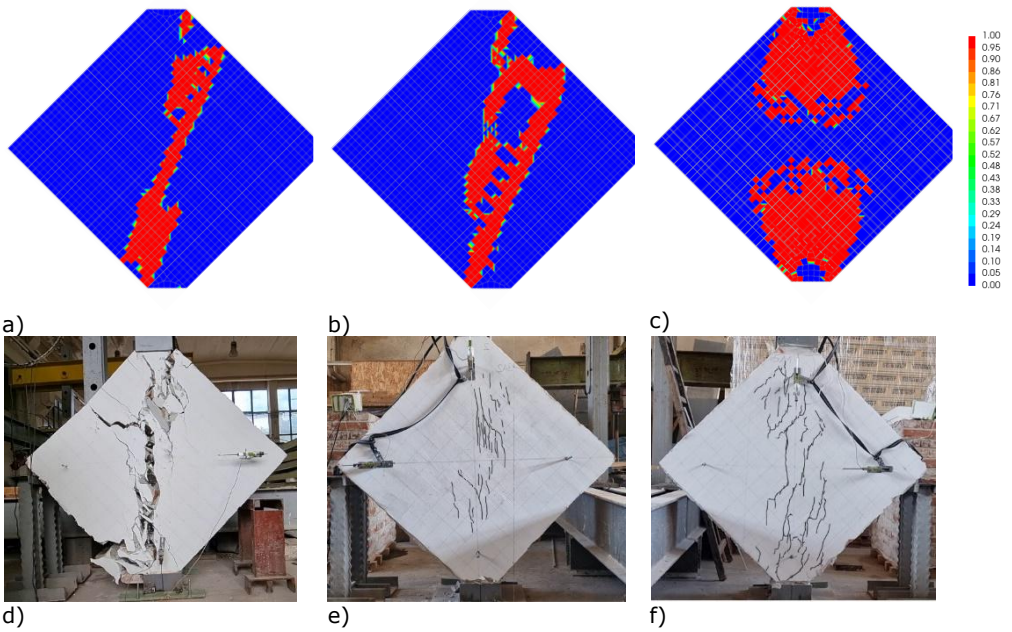


Fig. 4.6 Damage location in simulated model and laboratory tested specimen (numerical simulation - a) unreinforced masonry model; b) double-sided reinforced model; c) single-sided reinforced model; laboratory test - d) unreinforced masonry specimen; e) double-sided reinforced specimen; f) single-sided reinforced specimen)

4.2 Structural FE Model

In order to evaluate the strengthening effects at a building scale, a complementary FE analysis was performed. Because of the focus on masonry strengthening the 3Muri software from S.T.A. DATA was selected for modelling a small building. This dedicated software can simulate the seismic loading and for this reason is used generally in seismic areas where masonry structures are being retrofitted.

4.2.1 Calibration at Specimen Scale

In order to calibrate the FEM parameters used for materials, a simulation was considered to validate 3Muri program response at the scale of tested specimens. To this end, a dedicated assembly was modelled having a 120 cm level height (Fig. 4.7), having similar geometric values to the tested specimens (presented in chapter 3). The model comprised two identical 120x120x45 cm wallet specimens anchored at the base and vertically loaded by a perfectly rigid floor plate on top, interlocking the wallets. The FE models were conceived in three scenarios: the URM, DS, and OS, as in the case of tested specimens. For each scenario the loads exerted by the floor plate were fixed to that of the maximum tested equivalent force in the laboratory.

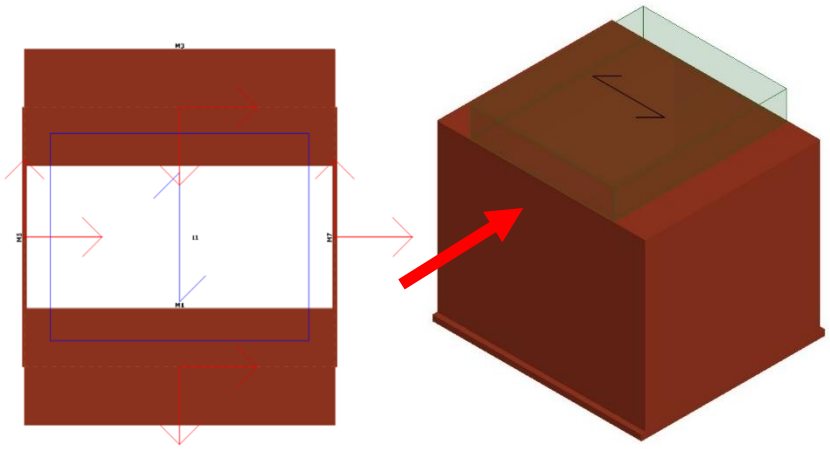


Fig. 4.7 2D and 3D Projection of virtual specimen test assembly

Following several iterations, the parameters for the unreinforced masonry were set for the final used values, only with small differences to those found in the previous chapter (Fig. 4.8):

- Modulus of elasticity: 4000 MPa
- shear modulus: 1590 N/mm^2, adjusted from 1507 N/mm^2 to match the experimental response on elastic range;
- Poisson's ratio: 0.25;
- The law of response: Mohr-Coulomb

BUPT

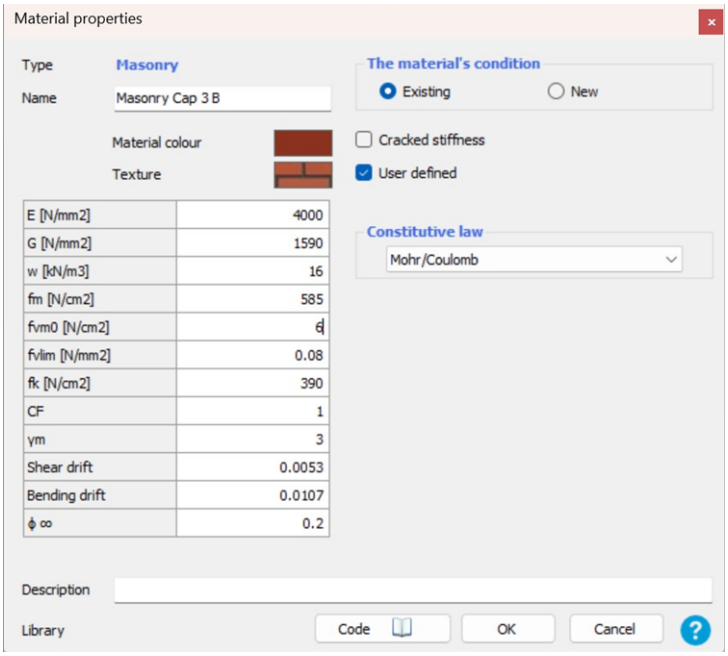


Fig. 4.8 Calibrated URM parameters

Using the calibrated unreinforced masonry data and known library values (Fig. 4.9) for the bidirectional used reinforcement, further pushover simulations were performed for the DS (reinforced on both sides) and OS (reinforced on one side) specimens. The DS reinforcement is usually used in this software environment as it is known and tested. For the OS specimen a less efficacious anchoring method was considered to partially account for the eccentricity observed during the experimental tests.

	Pier
Layout	Discontinue
bf [mm]	300
Step[cm]	45
tf [mm]	0.084
Layers number	1
Effect typology	Shear
Application	Double side
Bending anchor	Efficacious
ηa	0.80
Ef [N/mm2]	195,200.00
ε fk [%]	1.50000
ε fd [%]	0.31990
f fdd [N/mm2]	416.3

	Pier
Layout	Discontinue
bf [mm]	300
Step[cm]	45
tf [mm]	0.169
Layers number	1
Effect typology	Shear
Application	Single side
Bending anchor	Nor efficacious
ηa	0.80
Ef [N/mm2]	194,800.00
ε fk [%]	1.50000
ε fd [%]	0.19867
f fdd [N/mm2]	258.0

Fig. 4.9 Reinforcement Parameters DS (Geosteel G600) Respectively OS (Geosteel G1200)

The URM test has shown good consistence between the real and the simulated specimen (Fig. 4.10). For the DS and DS tests, differences between 7 and 8% were

present between the maximum shear forces (Table 4-2). For the OS specimen the pre-peak softening was not present in the simulation, similarly to the DIANA environment. Considering the good fidelity of the obtained results, one can conclude that the calibrated material parameters could be used for further structural investigations.

Table 4-2 Maximum Shear for 3Muri Specimens

3Muri Specimen	**Maximum Simulated Shear F_{v3m} [daN]**	**Maximum Tested Shear F_{vm} [daN]**	**Difference from Tested Shear Value [%]**
URM	6029	5368	12
DS	18711	20140	-8
OS	11611	10923	6

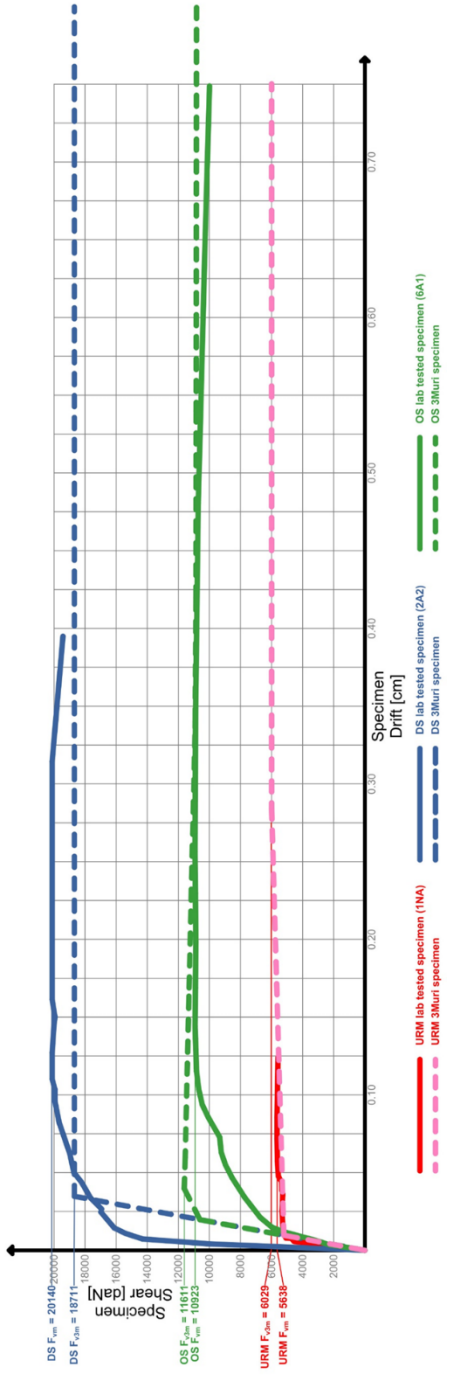


Fig. 4.10 Specimen scale simulation results

4.2.2 Structural Simulation Context

A simplified structural model is proposed to study the wall panel behaviour in a panel matrix with different geometrical shapes. The 3d Model consists of a tower structure with 3 levels and wall thicknesses as identified in case of the historical buildings in Timisoara. The buildings dimensions are modular, using 30 cm modules. The global plan dimensions of the tower are 480 cm for the North and South walls and 540 cm for the East and West walls (Fig. 4.11).

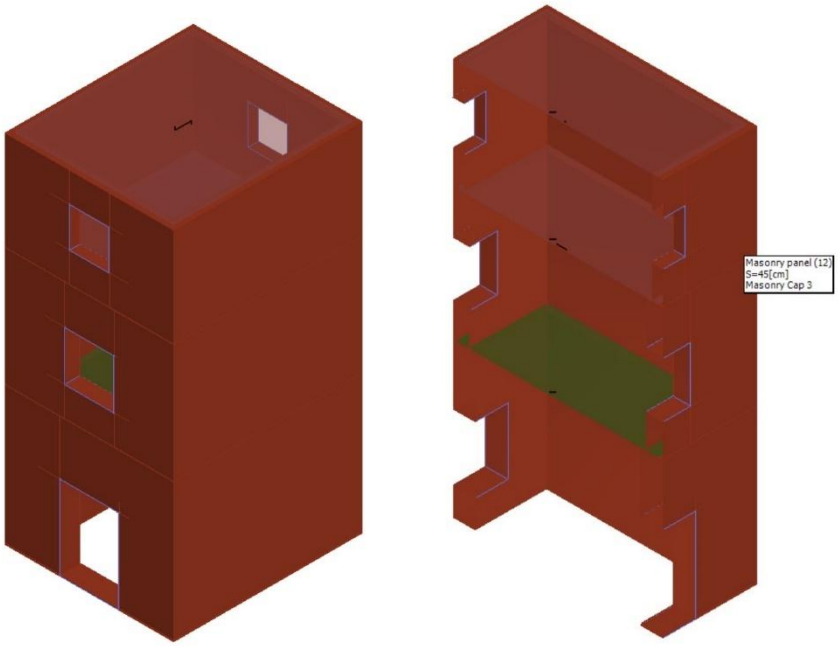


Fig. 4.11 Structural perspective and cross-section

The modelled building's levels are:

Level 1 (ground floor), with a height of 420 cm and having a window opening of 180x240 cm with a 75 cm sill to the north and a door opening of 180x315 cm to the south. This gives the model some eccentricity. The wall thickness on the ground floor is 60 cm, equivalent to two brick lengths. They are considered anchored at the base.

Level 2 that has a height 360 cm, reaching a top level of +780 cm, has two window openings of 150x210 cm with a 90 cm sill to the north and to the south. Its wall perimeter has a thickness of 45 cm, one and the half brick lengths, aligned to the outer face of the building. In fact, the walls of this level have the same thickness as the tested specimens. The outer face is flush with the ground floor wall.

Level 3 that has a height of 300 cm, its top-level reaching +1080 cm. It also has two smaller window openings of 120x150 cm with a 90 cm sill towards north and south. The wall thickness is 30 cm, one brick length, flush on the outside with the walls below.

Because the 3Muri tool accounts for the deformation of the horizontal structures, the floors have been modelled according to the real floor systems used in the building period: Over the ground level a barrel-vaulted structure resting on steel beams was modelled; Over the upper two levels a one-way timber floor with solid wood parallel beams topped by thick planks. For the barrel vaulted floor the steel beams were placed at 80 cm interval and were similar in size with the current IPE300. The ½ brick vaults were topped with a layer of C12/15 equivalent concrete. For the next floors, wooden beams with a dimension of 20x30cm were placed at 80 cm intervals and were topped by spruce planks. The last floor under the roof space is also built on wooden 20x30 cm beams placed at 80 cm intervals.

The loads on the floors were set to service loads values, but over the top floor a supplemental mass was added to simulate the presence of a roof structure. In the case of the first-floor barrel vault a permanent load of 532 daN/m^2 and a live load of 200 daN/m^2 was considered. For the second floor, a permanent load of 56 daN/m^2 and live load of 200 daN/m^2 was taken into consideration. Ultimately, for the floor under the roof space the same permanent and live load as in the previous floor, but to compensate for the roof structure mass, a supplemental 97 distributed load was also considered.

The focus of the FE analysis the south wall, named "Wall 4" in the simulations as it has the greatest opening area and from this point of view is considered the most vulnerable.

4.2.3 Seismic Characteristics and Material Model

For the current simulation the EN 1998-1 was used for the estimation of the seismic load. The seismic action type and soil parameters were selected closely to those of the Banat region of Timisoara, and the soil type D, according to Eurocode 8, was the most suitable, being predominantly a cohesive soil.

The seismic load was considered, and a pushover analysis was employed to evaluate the structural characteristics. This is finally consistent with the experimental loading performed on wallet specimens (see chapter 3). The seismic direction was selected parallel to the Wall 4 (X axis) as it provides the most disadvantageous in-plane loading for Wall 4. The displacement control node was selected on the top level.

Unreinforced masonry (URM), one-sided (OS) external strengthening and double-sided (DS) strengthening scenarios were simulated.

The masonry material was modelled as elastic-plastic materials considering the results obtained in experimental tests and seen in chapter 3 -

Table 3-7:

- shear modulus G = 1500N/mm^2,
- maximum shear strength f_{vlim} = 0.1N/mm^2
- compressive strength f_k=390N/cm^2 (as calculated in section 3.5.3 Masonry)

The strengthening was applied according to each context (single or two layers), using the reinforcement configuration interface, to be the same as in the tested specimens (bidirectional application of 300mm strips at 45cm intervals). Values for the Geosteel G600 and Geosteel G1200 reinforcement were used from the Kerakoll library (Table 4-3).

Table 4-3 Material properties of the reinforcement materials used in the numerical simulation

Property	Geosteel G600	Geosteel G1200
Equivalent thickness [mm]	0.084	0.169
Width of the strip [mm]	300	300
Tensile breaking load [kN]	35	70
Tensile strength [N/mm^2]	3073	2805
Elastic modulus [N/mm^2]	195200	194800
Characteristic deformation [%]	1.5	1.5

4.2.4 Global Structural Behaviour

The numerical simulation results can be seen in the figures below. They illustrate the Wall 4 state at the end of loading and the response curves lateral shear wall – top displacement of each model. The 3Muri damage on elements (Fig. 4.13; Fig. 4.14; Fig. 4.15) can be followed using the legend offered in Fig. 4.12.

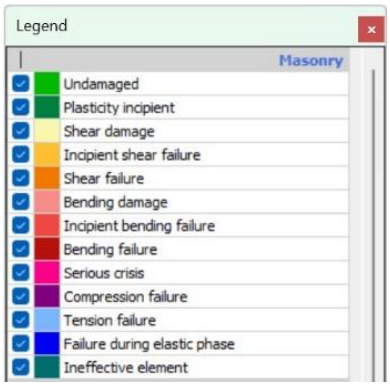


Fig. 4.12 Masonry damage legend

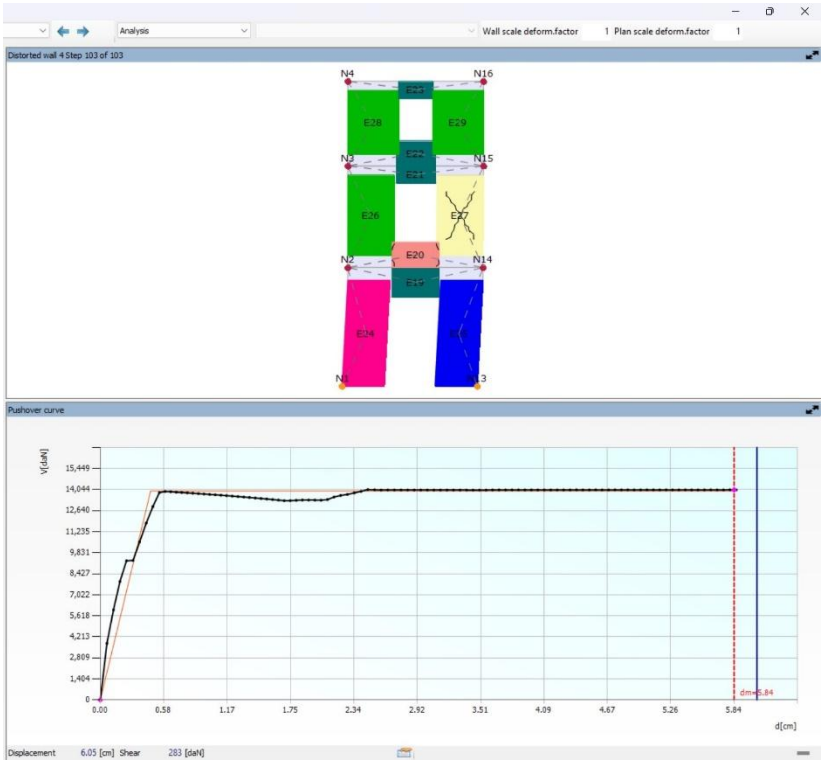


Fig. 4.13 Wall 4 URM up: final state of panel wall; down: pushover response curve (the pushover curve is presented in black, and the bilinear equivalent in orange)

The global behaviour of the Wall 4 in a standard non-consolidated state could be considered as elastic-plastic. After the shear failure, the entire wall behaviour is perfectly constant but showing low ductility. The failure is recorded at a top displacement of 5.84 cm. For the URM (Fig. 4.13) most of the damage occurs at ground level where the piers fail. The upper floor elements receive only a limited part of the lateral shear forces.

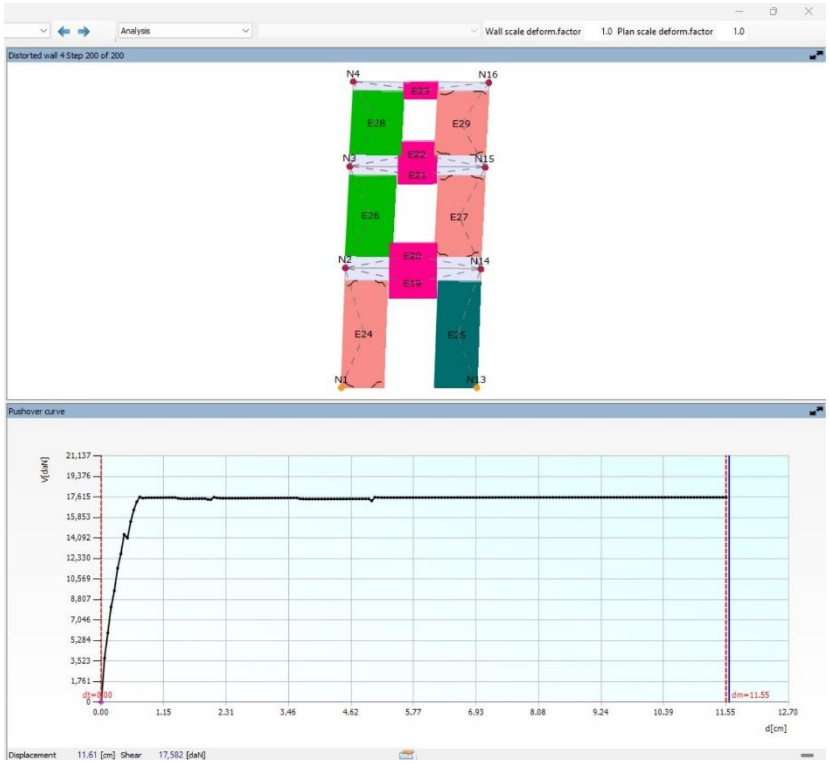


Fig. 4.14 Wall 4 DS up: final state of panel wall; down pushover response curve (the pushover curve is presented in black, and the bilinear equivalent in orange)

The response of the model strengthened on both sides (DS) can also be considered as elastic-plastic showing a very good ductility. The failure is recorded at a top displacement of 11.55 cm, presenting a significant, almost double increase of the top displacement compared the unreinforced masonry model.

The strengthening on both sides (Fig. 4.14) proves to be efficient in increasing and distributing the damage to all levels in a first step. However, in final states the spandrels, not the piers, are more loaded and are subjected to failure. Probably, a better connection between piers at each floor level could be thought.

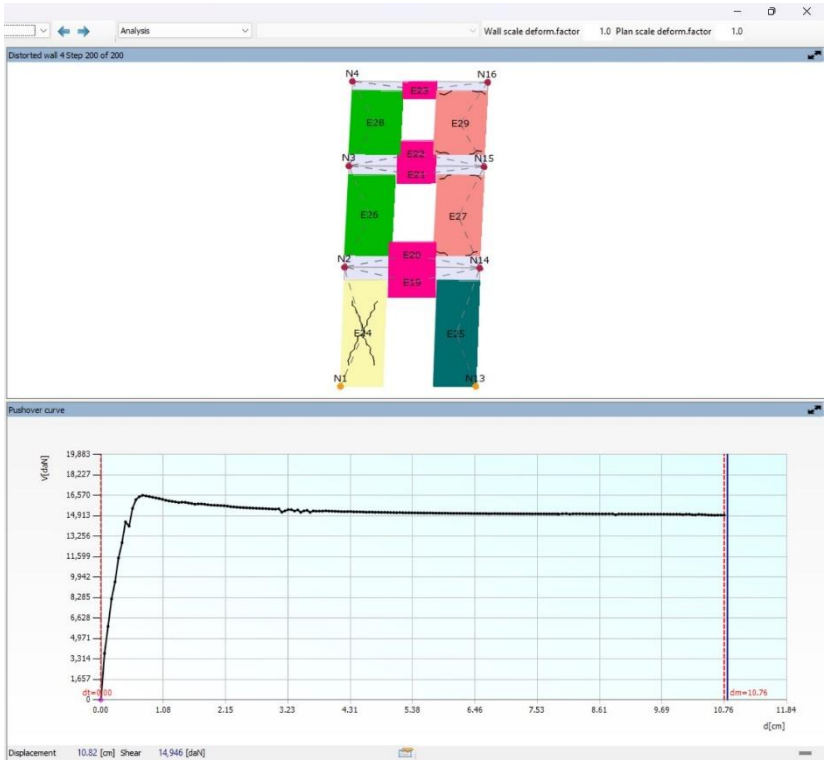


Fig. 4.15 Wall 4 OS up: final state of panel wall; down pushover response curve (the pushover curve is presented in black, and the bilinear equivalent in orange)

The response of the single-sided strengthened model (OS) can be considered elastic-plastic showing also a very good ductility. The failure is recorded at a top displacement of 10.76 cm, presenting also a double increase of the top displacement compared the unreinforced masonry model. According to the response curve a slight decrease of the shear strength can be observed after the elastic area.

The wall strengthened on one side (Fig. 4.15) received similar damage to the DS with some difference in damage cause at the lower level, where the damaged pier exhibits from cracks due to shear, not bending. The final displacement reached is similar, but at a lower force than the DS wall.

4.2.5 Interpretation of Numerical Results

For the three scenarios, the pushover curves were the most compelling and offer the best responses of the behaviour of wall panel. The maximum reached drift for the URM simulation was used as a reference point, at 5.84 cm. A comparison was made at this drift to evaluate the force for each scenario.

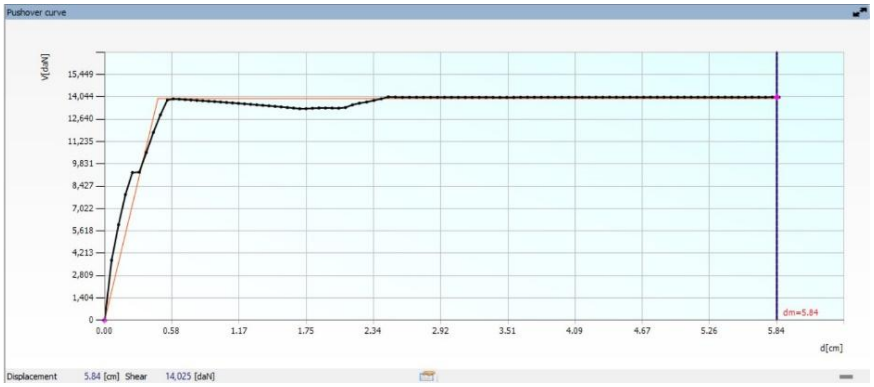


Fig. 4.16 URM Wall 4 at maximum 5.84cm drift

For the URM wall (Fig. 4.16), the last step before failure was at a drift of 5.84cm corresponding to a shear force of 14025daN.



Fig. 4.17 DS Wall 4 at 5.82cm drift

The DS simulation (Fig. 4.17) displayed a shear force of 17563daN at the similar drift of 5.82 cm that was selected from the simulation steps as closest to 5.84 cm.

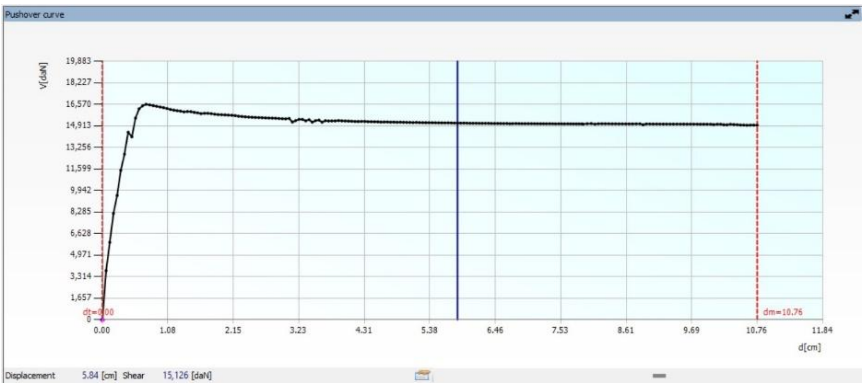


Fig. 4.18 OS Wall 4 at 5.84cm drift

The OS (Fig. 4.18) displayed a shear force of 15126 daN at the same 5.85 cm drift.

The comparative analysis shows that the double-sided strengthening is improving the initial rigidity of the masonry walls with 4 % compared to the unreinforced masonry wall while the one-sided strengthening solution is slightly decreasing its initial rigidity with 0.33 %. Yet, a significant improvement of 25 % can be observed in both maximum shear force and shear force at the 5.84 cm drift in the case of the double-sided reinforced solution. On the other hand, the one-sided strengthening solution is offering a 17 % increase of the maximum shear force compared to the unreinforced masonry model, and an approximately 8 % increase of the shear force at the 5.84 cm drift. The combined data can be read in the table below (Table 4-4; Fig. 4.19).

Table 4-4 Pushover analysis results

Analysis	Initial rigidity [daN/cm]	Maximum drift [cm]	Shear at maximum drift [daN]	Shear at 5.84cm drift [daN]	Shear improvement over URM at 5.84cm drift [%]	Maximum shear [daN]	Maximum shear improvement [%]
URM	6.306	5.84	14025	14025	-	14044	-
DS	6.590	11.55	17582	17563	25.22	17615	25.42
OS	6.285	10.76	14946	15126	7.85	16570	17.98

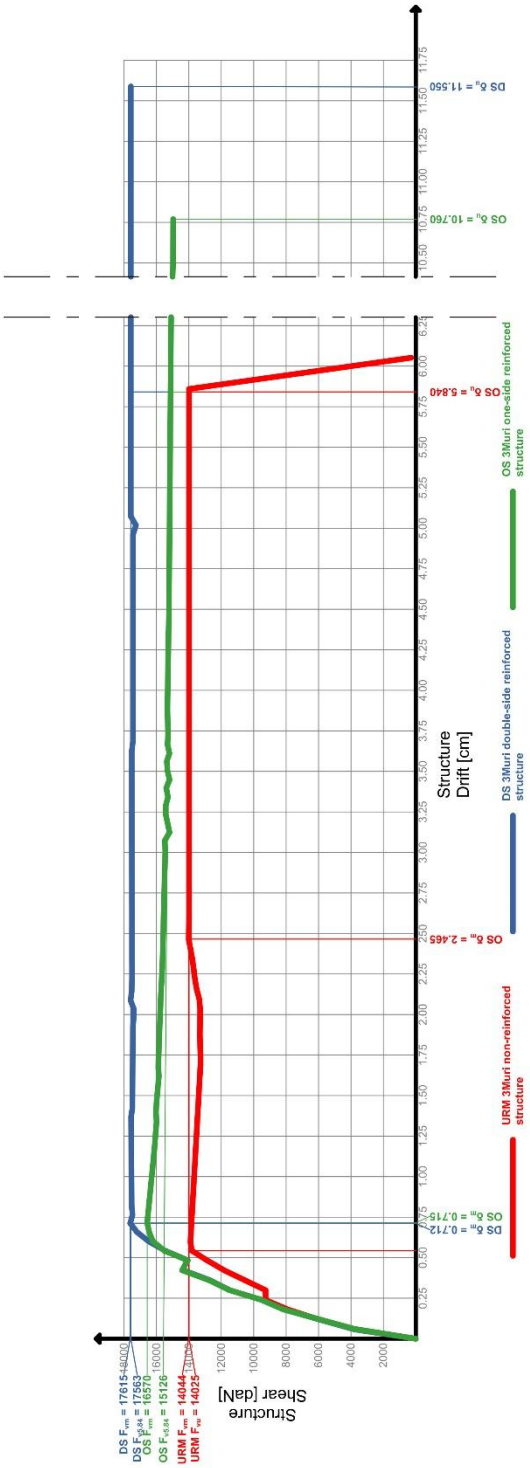


Fig. 4.19 Shear Drift comparison

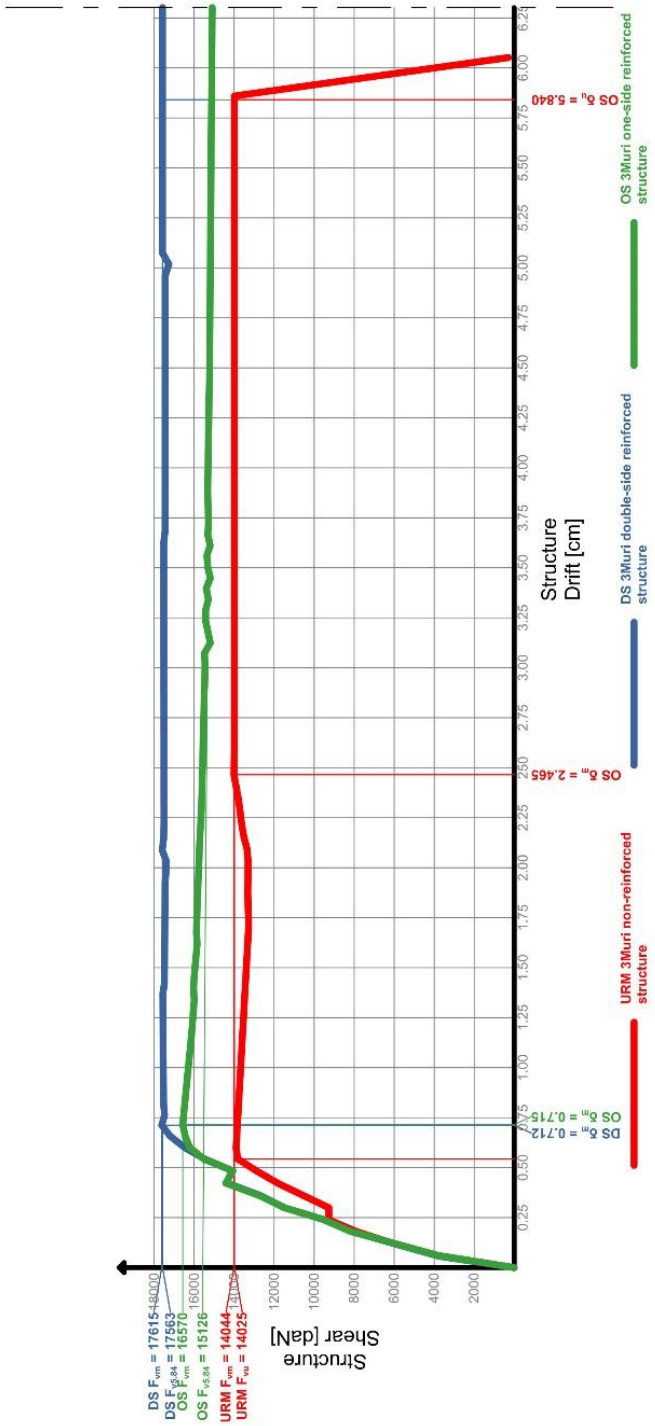


Fig. 4.20 Shear Drift Comparison - Enlarged First Part

4.3 Conclusions of the FE Simulations

The masonry reinforcement applied on the surfaces of walls provides results that improve the behaviour of a building. The one-sided approach can be used considering the lower benefits in comparison to the consecrated double-sided one. The difference from the non-reinforced masonry is most striking at the energy dissipation level which is clearly higher for the reinforced wall.

Besides the strength of the masonry elements, there are mechanisms that can lead to overall structural performance of a construction being lower than the elements' own strength increase due to reinforcement. They could be global system effects like stiffness modifications, alternate failure mechanisms, but in this model's case the load redistribution and weaker elements are most likely the cause. As soon as the masonry at element level is stronger, in the context of elastic floors, the spandrels as weaker elements get damaged and fail. This calls for a more complex investigation in case of intervention at building level to explore better connection between the masonry elements and to expose and propose adequate consolidation measures for the most vulnerable components.

BUPT

5 CONCLUSIONS

5.1 General Conclusions

The conservation and restoration of historic buildings is a complex problem which requires an interdisciplinary approach in order to increase the load-bearing capacity of the structure while preserving the authenticity and aesthetics of the building.

The study is focusing on the way that historic masonry structures characteristic for the western part of Romania, with a significant thickness, can be strengthened in order to reduce their vulnerability to seismic actions.

The proposed strengthening solution by reinforced mortar bring a significant difference in the behaviour of the wall specimens. While the URM failure was sudden and brittle, the reinforced specimens show an increased level of ductility, offering a significant opening of the cracks. The shear forces that the reinforced specimens took compared to the URM showed an increase by 85% for the one-sided strengthening respectively by 350% for the two-sided strengthening.

Besides, an important observation was the extraordinary bonding of the plaster matrix to the bricks which gives confidence in the applied method of strengthening. This seems to exceed the $1N/mm^2$ adhesion to substrate declared in the technical data and it is a value that could further be explored.

The stress-strain graphs show very little post-peak decrease compared to similar tests. This could be due to the use of steel fibre reinforcement, that stays elastic at the test strain values, the damage being localised in the masonry and binding mortar.

A detailed FE model was calibrated using a computer software tool dedicated to a detailed analysis. The calibrations give good results in terms of resistance, initial stiffness and ductility. These could serve in further parametric analyses to improved results, adapted for given structural interventions.

At structural level, a sophisticated model was developed using the 3Muri tool. Although the numerical case-study is a limited structure, it offers a good understanding of wall panel matrix behaviour.

Although the double-sided strengthening solution is showing a considerable influence on the shear strength of the masonry walls according to the laboratory test, the numerical simulations highlight that this might not be entirely applicable in real situations. The real effect of the strengthening can prove out to be inefficient if the corresponding strengthening solutions are not applied to all the load-bearing elements and proper connection between them can be ensured.

On the other hand, the analysis shows that in most situations the application of strengthening solutions on one side of the exterior load-bearing elements might be enough to ensure a sufficient improvement of their shear strength.

5.2 Practical Applications

The performed studies show that even the one-sided application of reinforcement is significant and can provide adequate levels of structural consolidation. Thus, the structural refurbishment with seismic and static upgrades is possible without moving the building inhabitants out is possible and can be considered for future projects. This kind of intervention has least impact on the image of the

BUPT

strengthened building which is crucial for the listed heritage buildings and historic zones within the cities.

The goal of finding a combined solution for reinforcement and thermal insulation proved elusive in case of controlling in plane shear damage. This is due to the elastic nature and softness of present thermal insulating materials. The most effective way of controlling diagonal shear failure is by using rigid materials intimately connected to the wall. They are readily available and can provide significant strengthening in just 10 mm of thickness, thus they are also compatible with the historic masonry. On top of the reinforcing layer a thermal solution layer can be applied. Depending on the cultural value of the façade surfaces, ETICS solutions can be applied, or other performant solutions such as aerogel mortars with reduced thicknesses. The later solution is useful where conservation of the outside appearance is important.

5.3 Personal Contributions

The main achievements and personal contributions are:

- A thorough analysis of similar studies performed on historic masonry structures, with emphasis on the single- and double-sided strengthening of these structures and reduction of seismic vulnerabilities.
- An extensive desk and on-site survey of characteristic masonry structures in the western part of Romania.
- Laboratory testing performed to determine the characteristic mechanical properties of the retrieved brick masonry and mortar specimens.
- Reconstruction of masonry specimens using historic bricks retrieved from a demolished building and a traditional mortar recipe using just lime, sand and water (1:3:1.25 ratio).
- Extensive laboratory shear testing on unreinforced masonry specimens and understanding of their shear behaviour considering the 45 cm thickness. This thickness is seldom used in practical studies.
- Laboratory analysis of the effect of single-sided and double-sided strengthening on the shear behaviour of the considered masonry specimens; analysis and comparison of the in-plane vertical and horizontal deformation measured on the masonry specimens.
- FE modelling of the tested unreinforced and reinforced masonry wallets and calibration of the models against the laboratory test results.
- Non-linear finite element modelling of a structure using the masonry material properties resulted from experimental testing.
- Analysis of the results obtained from the non-linear finite element model.

5.4 Future Developments

The thesis is opening a series of research topics which have to be further approached in order to ensure the preservation of heritage structures for future generations:

BUPT

Conclusions

- Future research is still necessary in order to fully understand the effect of contemporary reinforcement solutions, like vertical strips, rods or oblique helical bars, on the seismic behaviour of historic brick masonry structures.
- Laboratory tests have been performed until now on the 45cm thick wallets under in-plane diagonal compression. It is also important to explore the effect of the considered strengthening solutions on the out of plane behaviour.
- Cyclic load testing simulating the seismic reversals can be conducted to understand the efficacy of strengthening solutions on buildings.
- Numerical simulations have been calibrated considering the behaviour of the wallets and the calibrated values have been used until now in order to understand the behaviour of a small tower-like structure, it is important to perform non-linear dynamic simulations on characteristic existing buildings and understand the effect of the strengthening solution on its global seismic behaviour
- Integrated thermal and seismic retrofit solutions are rather few but the study shows that by using suitable materials improvement from both points of views can be achieved, especially for the out of plane loads. Further studies are still necessary in order to fully develop and understand the effect of the integrated solution on historic buildings.

5.5 Published Papers

5.5.1 Papers in Web of Science Indexed Journals

- D. Bocan, C. Bocan, A. Keller, A. Gruin, „Analysis of thermal rehabilitation and seismic strengthening solutions suitable for heritage structures", Sustainability, vol. 16(13), 2024. (WOS:001269917400001).

5.5.2 Papers in Web of Science Indexed Proceedings

- D. Bocan, A. Keller, C. Bocan, I. Apostol, M. Mosoarca, „Potential Results of Using Current Thermal Rehabilitation Techniques on a City Block of Timisoara and their Structural Strengthening Opportunities", IOP Conference Series: Materials Science and Engineering, vol. 471, 2019 (WOS:000465811802088).
- D. Bocan, C. Bocan, A. Keller, „Energy efficiency study applied on a monumental building", in Structures and Architecture-Bridging the Gap and Crossing Borders: Proceedings of the Fourth International Conference on Structures and Architecture (ICSA 2019), Lisbon, Portugal, July 2019, pp. 288-295, 2019 (WOS:000670758600035)
- D. Bocan, A. Keller, I. Apostol, M. Mosoarca, R. Bradeanu, „The impact of insulating plaster on the energy performance of historical buildings", Modern Technologies For The 3rd Millennium, pp. 179-184, 2018 (WOS:000491484600031).
- Apostol, M. Mosoarca, N. Chieffo, A. Keller, D. Bocan, C. Bocan, R. Bradeanu, „Solutions for improving seismic vulnerability of historic masonry buildings", Modern Technologies For The 3rd Millennium, pp. 131-136, 2018 (WOS:000491484600023).

5.5.1 Papers in International Database Indexed Proceedings

- C. Bocan, D. Bocan, M.H. Truță, „The Rehabilitation and Extension of the Old Arad's Casino – Case Study", RILEM Bookseries, vol 47, pp. 449–462, 2024 (Scopus)
- D. Bocan, A. Keller, M.Moșoarcă, C. Bocan, „ Experimental Investigation of One-Sided Strengthening Interventions on Historic Brick Masonry Walls", RILEM Bookseries, vol 47, pp. 485–495, 2024 (Scopus)
- D. Bocan, C. Bocan, A. Keller, „Possibilities of Using Fibre Reinforced Mortar and Textile Reinforced Mortar for Strengthening Masonry Columns in Rehabilitation Projects", RILEM Bookseries, vol 18, pp. 1651-1660, 2019 (Scopus)

BUPT

6 BIBLIOGRAPHY

[1] ASTM International, “Standard Test Method for Diagonal Tension (Shear) in Masonry Assemblages,” 2015, *ASTM International*.

[2] “History of Europe - Revolution, Industrial Society, 1789-1914 | Britannica.” Accessed: Oct. 06, 2024. [Online]. Available: https://www.britannica.com/topic/history-of-Europe/Revolution-and-the-growth-of-industrial-society-1789-1914

[3] Frampton Kenneth, “Frampton-Modern-Architecture-a-Critical-History,” 1982.

[4] Icomos, “International Charter for the conservation and restoration of monuments and sites (The Venice Charter 1964),” *IInd International Congress of Architects and Technicians of Historic Monuments*, 1964.

[5] ICOMOS, “The Declaration of Amsterdam,” Amsterdam, 1975.

[6] ICOMOS, “ICOMOS Nara document of authenticity 1994,” 1994.

[7] ICOMOS, *The Burra Charter : the Australia ICOMOS charter for places of cultural significance 2013*. Australia ICOMOS Incorporated, 2013.

[8] ICOMOS, “The Valletta Principles for the Safeguarding and Management of Historic Cities, Towns and Urban Areas Principes de la Valette pour la sauvegarde et la gestion des villes et ensembles urbains historiques,” 2011.

[9] D. Giardini, J. Wössner, and L. Danciu, “Mapping Europe’s Seismic Hazard,” *Eos (Washington DC)*, vol. 95, no. 29, pp. 261–268, 2014, doi: 10.12686/SED.

[10] A.-I. Keller, “A complex assessment methodology for historic roof structures,” Politehnica University Timisoara, Timisoara, 2020.

[11] D. Janotova and Z. Slížková, “Lime-based mortars with various binder composition: characterization and freeze-thaw resistance assessment,” *IOP Conf Ser Mater Sci Eng*, vol. 1205, p. 012009, Nov. 2021, doi: 10.1088/1757-899X/1205/1/012009.

[12] “Google Earth Image ~ 45°43’54.02"N , 21°13’27.98"E,” Feb. 16, 2023, *Google Earth, Timisoara*.

BUPT

[13] A. Narita *et al.*, “Behavior of Historic Buildings in Zones with Moderate Seismic Activity. Case Study: Banat Region, Romania,” *Procedia Eng*, vol. 161, pp. 729–737, 2016, doi: 10.1016/j.proeng.2016.08.754.

[14] “Austria-Hungary | History, Definition, Map, & Facts | Britannica.” Accessed: Feb. 16, 2023. [Online]. Available: https://www.britannica.com/place/Austria-Hungary

[15] M. Opris, *Timisoara Mica Monografie Urbanistica*. Bucuresti: Editura Tehnica, 1987.

[16] S. Dema, “Jimbolia și tradiția cărămizii.” Accessed: Dec. 05, 2024. [Online]. Available: https://www.jimboblog.com/post/jimbolia-%C8%99i-tradi%C8%9Bia-c%C4%83r%C4%83mizii

[17] L. Abel, T. Krones, and R. Rambausek, *Allgemeiner Bauratgeber Ein Hand- und Hilfsbuch für Bauherren, Architekten, Baunternehmer, Baumeister, Bautechniker, Bauhanweker, Landwirte und Rechnungsbeamte*, 2nd Edition. Wien und Leipzig: A. Hartlenben’s Verlag, 1908.

[18] C. Bocan, D. Bocan, and A. Keller, “Effects of Current Sunlight Exposure Regulations on New Housing,” in *IOP Conference Series: Materials Science and Engineering*, Institute of Physics Publishing, Feb. 2019. doi: 10.1088/1757-899X/471/8/082056.

[19] A. Narita *et al.*, “Behavior of Historic Buildings in Zones with Moderate Seismic Activity. Case Study: Banat Region, Romania,” *Procedia Eng*, vol. 161, pp. 729–737, 2016, doi: 10.1016/j.proeng.2016.08.754.

[20] Cornelius Radu and Victoria Oancea, “Source characteristics earthquake Banat”.

[21] F. Dinu, A. Stratan, D. Grecea, and D. Dubina, “Performance Based Design Criteria For Steel Mr Frames,” Oct. 2014. [Online]. Available: https://www.researchgate.net/publication/265011900

[22] N. Chieffo, A. Formisano, M. Mosoarca, and P. B. Lourenço, “SEISMIC VULNERABILITY ASSESSMENT OF A ROMANIAN HISTORICAL BUILDING UNDER NEAR-FIELD EARTHQUAKE,” 2020, pp. 4957–4971. doi: 10.47964/1120.9402.20351.

BUPT

[23] E. Oros, *Cercetări privind hazardul seismic pentru Banat Teza de Doctorat*. Editura Sfantul Ierarh Nicolae, 2022. [Online]. Available: https://www.researchgate.net/publication/360889045

[24] M. Mosoarca, M. Fofiu, and I. Onescu, "Failure mechanism of historic churches in Gorj county for shallow seismic action," *Eng Fail Anal*, vol. 152, no. May, p. 107502, 2023, doi: 10.1016/j.engfailanal.2023.107502.

[25] A. Benedetti, "In Plane Behaviour of Masonry Walls Reinforced with Mortar Coatings and Fibre Meshes," *International Journal of Architectural Heritage*, vol. 13, no. 7, pp. 1029–1041, 2019, doi: 10.1080/15583058.2019.1618972.

[26] ICOMOS, "Resolutions of the General Assembly 19GA Agenda item 1 Official Opening of the General Assembly," 2017.

[27] J. G. Rots and J. Blaauwendraad, "Blaauwendraad_1989 Crack models for concrete," *HERON*, no. 1, p. 34, 1989, Accessed: Jun. 28, 2024. [Online]. Available: http://resolver.tudelft.nl/uuid:0a401939-2938-4f9d-a395-b6a6652b2cd9

[28] P. B. Lourenco, P. Roca, J. L. González, E. Oñate, and P. B. Lourenço, "Experimental and numerical issues in the modelling of the mechanical behaviour of masonry STRUCTURAL ANALYSIS OF HISTORICAL CONSTRUCTIONS II EXPERIMENTAL AND NUMERICAL ISSUES IN THE MODELLING OF THE MECHANICAL BEHAVIOUR OF MASONRY." [Online]. Available: https://www.researchgate.net/publication/255606974

[29] L. Miccoli, A. Garofano, P. Fontana, and U. Müller, "Experimental testing and finite element modelling of earth block masonry," *Eng Struct*, vol. 104, pp. 80–94, Dec. 2015, doi: 10.1016/j.engstruct.2015.09.020.

[30] Y. Endo and K. Miyoshi, "Meso-scale numerical simulation of the mechanical behaviour of brick masonry in earth mortar," *Journal of Building Engineering*, vol. 74, Sep. 2023, doi: 10.1016/j.jobe.2023.106890.

[31] D. Bocan, A. Keller, C. Bocan, I. Onescu, and M. Marius, "Potential Results of Using Current Thermal Rehabilitation Techniques on a City Block of Timisoara and their Structural Strengthening Opportunities," *IOP Conf Ser Mater Sci Eng*, vol. 471, p. 062037, Feb. 2019, doi: 10.1088/1757-899X/471/6/062037.

[32] M. V. Requena-Garcia-Cruz, J. Díaz-Borrego, E. Romero-Sánchez, A. Morales-Esteban, and M. A. Campano, "Assessment of Integrated Solutions for the Combined Energy Efficiency Improvement and Seismic Strengthening of

BUPT

Existing URM Buildings," *Buildings*, vol. 12, no. 8, 2022, doi: 10.3390/buildings12081276.

[33] D. A. Pohoryles, D. A. Bournas, F. Da Porto, A. Caprino, G. Santarsiero, and T. Triantafillou, "Integrated seismic and energy retrofitting of existing buildings: A state-of-the-art review," 2022. doi: 10.1016/j.jobe.2022.105274.

[34] D. A. Pohoryles, C. Maduta, D. A. Bournas, and L. A. Kouris, "Energy performance of existing residential buildings in Europe: A novel approach combining energy with seismic retrofitting," *Energy Build*, vol. 223, 2020, doi: 10.1016/j.enbuild.2020.110024.

[35] V. Pertile, A. Stella, L. De Stefani, and R. Scotta, "Seismic and energy integrated retrofitting of existing buildings with an innovative icf-based system: Design principles and case studies," *Sustainability (Switzerland)*, vol. 13, no. 16, 2021, doi: 10.3390/su13169363.

[36] M. F. Junaid, Z. ur Rehman, N. Ijaz, R. Farooq, U. Khalid, and Z. Ijaz, "Performance evaluation of cement-based composites containing phase change materials from energy management and construction standpoints," 2024. doi: 10.1016/j.conbuildmat.2024.135108.

[37] S. Caprili, F. Del Carlo, and G. Salvadori, "An enhanced system for the combined seismic and energy retrofit of masonry buildings," in *Procedia Structural Integrity*, 2022. doi: 10.1016/j.prostr.2023.01.133.

[38] V. Pertile, L. De Stefani, and R. Scotta, "Development and characterization of a system for the seismic and energy retrofit of existing buildings," in *Procedia Structural Integrity*, 2018. doi: 10.1016/j.prostr.2018.11.045.

[39] Wienerberger, "Porotherm clay brick_technical data sheet." Accessed: Nov. 05, 2024. [Online]. Available: https://cdn.mathaus.ro/medias/sys_master/productPdfs/h01/hfa/h00/9467616198686.pdf?_gl=1*lsvx6i*_up*MQ..&gclid=Cj0KCQiA_qG5BhDTARIsAA0UHSL2rJJu6HGf7EidvGH77TcnZYZV9hs2VxwUCSsJDMBy1zjJOPCAs9gaAnc0EALw_wcB

[40] Wienerberger, "Porotherm multi-cellular clay block _ technica data sheet." Accessed: Nov. 05, 2024. [Online]. Available: https://www.wienerberger.ro/produse/zidarie-porotherm/blocuri-ceramice-porotherm/porotherm-30-sth.html

BUPT

[41] Xella, “Ytong_Technical data sheet.” Accessed: Nov. 05, 2024. [Online]. Available: https://storefrontapi.commerce.xella.com/medias/sys_master/images/h11/h2b/9203491340318/Fisa Tehnica Ytong/Fisa-Tehnica-Ytong.pdf

[42] E. Pavaje, “Concrete block_technical data sheet.” Accessed: Nov. 05, 2024. [Online]. Available: https://elis.ro/public/upload/pdf/product/ro_92_fisa_tehnica_Boltari_ZIDARIE_BZ3.pdf

[43] A. L. Webb, “Energy retrofits in historic and traditional buildings: A review of problems and methods,” 2017. doi: 10.1016/j.rser.2017.01.145.

[44] K. Fouseki, D. Newton, K. S. Murillo Camacho, S. Nandi, and T. Koukou, “Energy effciency, thermal comfort, and heritage conservation in residential historic buildings as dynamic and systemic socio-cultural practices,” *Atmosphere (Basel)*, vol. 11, no. 6, 2020, doi: 10.3390/atmos11060604.

[45] R. Agliata, A. Marino, L. Mollo, and P. Pariso, “Historic building energy audit and retrofit simulation with hemp-lime plaster-A case study,” *Sustainability (Switzerland)*, vol. 12, no. 11, 2020, doi: 10.3390/su12114620.

[46] M. Menconi, N. Painting, and P. Piroozfar, “Modelling and simulation of low-risk energy retrofit measures for Traditional Listed Dwellings in the UK,” *Journal of Building Engineering*, vol. 82, 2024, doi: 10.1016/j.jobe.2023.108346.

[47] C. D. Şahin, Z. D. Arsan, S. S. Tunçoku, T. Broström, and G. G. Akkurt, “A transdisciplinary approach on the energy efficient retrofitting of a historic building in the Aegean Region of Turkey,” *Energy Build*, vol. 96, 2015, doi: 10.1016/j.enbuild.2015.03.018.

[48] E. Roque, R. Vicente, R. M. S. F. Almeida, J. Mendes da Silva, and A. Vaz Ferreira, “Thermal characterisation of traditional wall solution of built heritage using the simple hot box-heat flow meter method: In situ measurements and numerical simulation,” *Appl Therm Eng*, vol. 169, 2020, doi: 10.1016/j.applthermaleng.2020.114935.

[49] P. Besen and P. Boarin, “Integrating energy retrofit with seismic upgrades to future-proof built heritage: Case studies of unreinforced masonry buildings in Aotearoa New Zealand,” *Build Environ*, vol. 241, 2023, doi: 10.1016/j.buildenv.2023.110512.

[50] Kerakoll Spa, “Lime mortar _ Technical data sheet.” Accessed: Nov. 05, 2024. [Online]. Available: https://products.kerakoll.com/yep-repository/kerakoll/media/Bio_muratura_0723_en.pdf

[51] Adeplast, “Cement mortar _ Technical data sheet.” Accessed: Nov. 05, 2024. [Online]. Available: https://www.adeplast.ro/storage/files/235/540 Fisa tehnica ADEPLAST MZ 5 - 2018.pdf

[52] Wienerberger, “Porotherm M50 mortar _ Technical data sheet.” Accessed: Nov. 05, 2024. [Online]. Available: https://cdn.mathaus.ro/medias/sys_master/productPdfs/h01/h5c/h00/9465783451678.pdf

[53] H. H. Jo, H. Yuk, Y. Kang, and S. Kim, “Conservation of architectural heritage: Innovative approaches to enhance thermal comfort and promote sustainable usage in historic buildings,” *Case Studies in Thermal Engineering*, vol. 51, 2023, doi: 10.1016/j.csite.2023.103500.

[54] A. Buda *et al.*, “Conservation-compatible retrofit solutions in historic buildings: An integrated approach,” 2021. doi: 10.3390/su13052927.

[55] S. Türkmen, B. T. De Vries, S. N. M. Wijte, and A. T. Vermeltfoort, *In-plane behaviour of clay brick masonry wallettes retrofitted with single-sided fabric-reinforced cementitious matrix and deep mounted carbon fibre strips*, vol. 18, no. 2. Springer Netherlands, 2020. doi: 10.1007/s10518-019-00596-2.

[56] L. D. Pereira, V. Tavares, and N. Soares, “Up-to-date challenges for the conservation, rehabilitation and energy retrofitting of higher education cultural heritage buildings,” *Sustainability (Switzerland)*, vol. 13, no. 4, 2021, doi: 10.3390/su13042061.

[57] Y. Chae and S. H. Kim, “Selection of retrofit measures for reasonable energy and hygrothermal performances of modern heritage building under dry cold and hot humid climate:A case of modern heritage school in Korea,” *Case Studies in Thermal Engineering*, vol. 36, 2022, doi: 10.1016/j.csite.2022.102243.

[58] E. Mustafaraj and Y. Yardim, “Retrofitting damaged unreinforced masonry using external shear strengthening techniques,” *Journal of Building Engineering*, vol. 26, 2019, doi: 10.1016/j.jobe.2019.100913.

[59] M. R. Valluzzi *et al.*, “Nested buildings: An innovative strategy for the integrated seismic and energy retrofit of existing masonry buildings with CLT

BUPT

panels," *Sustainability (Switzerland)*, vol. 13, no. 3, 2021, doi: 10.3390/su13031188.

[60] F. Longo, A. Cascardi, P. Lassandro, and M. A. Aiello, "Thermal and seismic capacity improvements for masonry building heritage: A unified retrofitting system," *Sustainability (Switzerland)*, vol. 13, no. 3, 2021, doi: 10.3390/su13031111.

[61] A. Ilki, M. Ispir, C. Demir, N. Kumbasar, and F. As, "FRP RETROFIT OF WALLS CONSTRUCTED WITH HISTORICAL BRICKS Risk Algılama / Risk Perception View project Bolted Moment Connection System for Precast Reinforced Concrete Members View project FRP RETROFIT OF WALLS CONSTRUCTED WITH HISTORICAL BRICKS," 2008. [Online]. Available: http://www.ins.itu.edu.tr/eers/labhome.htm

[62] Mapei, "Fiber-Reinforced Polymer (FRP) - Composite Systems," 2015. [Online]. Available: https://cdnmedia.mapei.com/docs/librariesprovider10/line-technical-documentation-documents/fiber-reinforced-polymer--frp--composite-systems-brochure.pdf?sfvrsn=8623879f_18

[63] M. Tomaževič, "Shear resistance of masonry walls and Eurocode 6: Shear versus tensile strength of masonry," *Mater Struct*, vol. 42, pp. 889–907, Aug. 2009, doi: 10.1617/s11527-008-9430-6.

[64] Mapei, "FRCM system MAPEGRID G," 2022. [Online]. Available: https://cdnmedia.mapei.com/docs/librariesprovider2/products-documents/22_06154_frcm-system-mapegrid-g_en_e8a385900adb4998b87427f32a2250c9.pdf?sfvrsn=16d4135e_0

[65] F. S. Murgo, F. Ferretti, and C. Mazzotti, "A discrete-cracking numerical model for the in-plane behavior of FRCM strengthened masonry panels," *Bulletin of Earthquake Engineering*, vol. 19, no. 11, 2021, doi: 10.1007/s10518-021-01129-6.

[66] Kerakoll Spa, "Rinforzo ARV 100," 2023, *Kerakoll Spa*.

[67] Kerakoll Spa, "Geosteel Grid 200," 2023, *Kerakoll Spa*. [Online]. Available: https://products.kerakoll.com/yep-repository/kerakoll/media/Geosteel_Grid_200_2023_en.pdf

[68] M. Del Zoppo, M. Di Ludovico, A. Balsamo, and A. Prota, "In-plane shear capacity of tuff masonry walls with traditional and innovative Composite

Reinforced Mortars (CRM)," *Constr Build Mater*, vol. 210, 2019, doi: 10.1016/j.conbuildmat.2019.03.133.

[69] Kerakoll Spa, "GeoSteel G600," Jun. 2018, *Kerakoll Spa, Sassuolo*. Accessed: Jul. 14, 2024. [Online]. Available: https://products.kerakoll.com/yep-repository/kerakoll/media/Geosteel_G600_2023_en.pdf

[70] F. Parisi, I. Iovinella, A. Balsamo, N. Augenti, and A. Prota, "In-plane behaviour of tuff masonry strengthened with inorganic matrix-grid composites," *Compos B Eng*, vol. 45, no. 1, 2013, doi: 10.1016/j.compositesb.2012.09.068.

[71] V. Alecci *et al.*, "Shear capacity of masonry panels repaired with composite materials: Experimental and analytical investigations," *Compos B Eng*, vol. 171, 2019, doi: 10.1016/j.compositesb.2019.04.013.

[72] L. Garcia-Ramonda, L. Pelá, P. Roca, and G. Camata, "In-plane shear behaviour by diagonal compression testing of brick masonry walls strengthened with basalt and steel textile reinforced mortars," *Constr Build Mater*, vol. 240, 2020, doi: 10.1016/j.conbuildmat.2019.117905.

[73] M. Shabdin, M. Zargaran, and N. K. A. Attari, "Experimental diagonal tension (shear) test of Un-Reinforced Masonry (URM) walls strengthened with textile reinforced mortar (TRM)," *Constr Build Mater*, vol. 164, 2018, doi: 10.1016/j.conbuildmat.2017.12.234.

[74] M. Busselli, D. Cassol, A. Prada, and I. Giongo, "Timber based integrated techniques to improve energy efficiency and seismic behaviour of existing masonry buildings," *Sustainability (Switzerland)*, vol. 13, no. 18, 2021, doi: 10.3390/su131810379.

[75] N. Gattesco and I. Boem, "Experimental and analytical study to evaluate the effectiveness of an in-plane reinforcement for masonry walls using GFRP meshes," *Constr Build Mater*, vol. 88, 2015, doi: 10.1016/j.conbuildmat.2015.04.014.

[76] N. Ismail, R. B. Petersen, M. J. Masia, and J. M. Ingham, "Diagonal shear behaviour of unreinforced masonry wallettes strengthened using twisted steel bars," *Constr Build Mater*, vol. 25, no. 12, 2011, doi: 10.1016/j.conbuildmat.2011.04.063.

[77] "EN 1052-3. Methods of test for masonry – Part 3: Determination of initial shear strength," 2007.

BUPT

[78] CEN, “BS EN 1052-4:2000 Methods of test for masonry Determination of shear strength including damp proof course,” 2000.

[79] P. B. Lourenço, J. O. Barros, and J. T. Oliveira, “Shear testing of stack bonded masonry,” *Constr Build Mater*, vol. 18, no. 2, pp. 125–132, Mar. 2004, doi: 10.1016/J.CONBUILDMAT.2003.08.018.

[80] Chácara C., Lourenço P. B., Cannizzaro F., Pantò B., and Caliò I., “Seismic Assessment of an Unreinforced Masonry Structure Subjected To Out-of-Plane Dynamic Excitations By Means of a Discrete Macro-Modelling Approach,” in *3rd International Conference on Protection of Historical Constructions*, 2017.

[81] A. Benedetti, “In Plane Behaviour of Masonry Walls Reinforced with Mortar Coatings and Fibre Meshes,” *International Journal of Architectural Heritage*, vol. 13, no. 7, pp. 1029–1041, 2019, doi: 10.1080/15583058.2019.1618972.

[82] P. Cassese, C. Balestrieri, L. Fenu, D. Asprone, and F. Parisi, “In-plane shear behaviour of adobe masonry wallets strengthened with textile reinforced mortar,” *Constr Build Mater*, vol. 306, 2021, doi: 10.1016/j.conbuildmat.2021.124832.

[83] S. Elmalyh, A. Bouyahyaoui, T. Cherradi, A. Rotaru, and P. Mihai, “Shear strength of unreinforced masonry walls retrofitted with CFRP,” *Advances in Science, Technology and Engineering Systems*, vol. 5, no. 2, 2020, doi: 10.25046/AJ050246.

[84] Z. Dong, M. Deng, J. Dai, and P. Ma, “Diagonal compressive behavior of unreinforced masonry walls strengthened with textile reinforced mortar added with short PVA fibers,” *Eng Struct*, vol. 246, 2021, doi: 10.1016/j.engstruct.2021.113034.

[85] J. Segura, L. Pelà, S. Saloustros, and P. Roca, “Experimental and numerical insights on the diagonal compression test for the shear characterisation of masonry,” *Constr Build Mater*, vol. 287, 2021, doi: 10.1016/j.conbuildmat.2021.122964.

[86] D. Bocan, C. Bocan, A. Keller, and A. Gruin, “Analysis of Thermal Rehabilitation and Seismic Strengthening Solutions Suitable for Heritage Structures,” *Sustainability 2024, Vol. 16, Page 5369*, vol. 16, no. 13, p. 5369, Jun. 2024, doi: 10.3390/SU16135369.

[87] A. Soleymani, M. A. Najafgholipour, A. Johari, and S. Jowkar, “In-plane shear strengthening of traditional unreinforced masonry walls with near surface

mounted GFRP bars," *Constr Build Mater*, vol. 367, 2023, doi: 10.1016/j.conbuildmat.2023.130362.

[88] D. Dizhur and J. M. Ingham, "Diagonal tension strength of vintage unreinforced clay brick masonry wall panels," *Constr Build Mater*, vol. 43, pp. 418–427, 2013, doi: 10.1016/j.conbuildmat.2013.02.015.

[89] N. Ismail, R. B. Petersen, M. J. Masia, and J. M. Ingham, "Diagonal shear behaviour of unreinforced masonry wallettes strengthened using twisted steel bars," *Constr Build Mater*, vol. 25, no. 12, pp. 4386–4393, 2011, doi: 10.1016/j.conbuildmat.2011.04.063.

[90] M. Mosoarca, I. Onescu, E. Onescu, and A. Anastasiadis, "Seismic vulnerability assessment methodology for historic masonry buildings in the near-field areas," *Eng Fail Anal*, vol. 115, Sep. 2020, doi: 10.1016/j.engfailanal.2020.104662.

[91] D. Dizhur and J. M. Ingham, "Diagonal tension strength of vintage unreinforced clay brick masonry wall panels," *Constr Build Mater*, vol. 43, pp. 418–427, 2013, doi: 10.1016/j.conbuildmat.2013.02.015.

[92] S. Türkmen, B. T. De Vries, S. N. M. Wijte, and A. T. Vermeltfoort, *In-plane behaviour of clay brick masonry wallettes retrofitted with single-sided fabric-reinforced cementitious matrix and deep mounted carbon fibre strips*, vol. 18, no. 2. Springer Netherlands, 2020. doi: 10.1007/s10518-019-00596-2.

[93] Kerakoll Spa, "GeoCalce ® F Antisismico," Apr. 2017, *Kerakoll Spa, Sassuolo*. Accessed: Jul. 14, 2024. [Online]. Available: https://products.kerakoll.com/yep-repository/kerakoll/media/GeoCalce_F_Antisismico_0723_en.pdf

[94] Kerakoll Spa, "GeoSteel G1200," Aug. 2018, *Kerakoll Spa, Sassuolo*. Accessed: Jul. 14, 2024. [Online]. Available: https://products.kerakoll.com/yep-repository/kerakoll/media/Geosteel_G1200_2023_en.pdf

[95] P. E. Mezrea, M. Ispir, I. A. Balci, I. E. Bal, and A. Ilki, "Diagonal tensile tests on historical brick masonry wallets strengthened with fabric reinforced cementitious mortar," *Structures*, vol. 33, no. October 2020, pp. 935–946, 2021, doi: 10.1016/j.istruc.2021.04.076.

[96] IDS, "Potentiometric Displacement Sensor." Accessed: Aug. 08, 2022. [Online]. Available: https://www.inds.co.uk/product/potentiometric-displacement-sensor/

BUPT

[97] D. Bocan, A. Keller, M. Mosoarca, and C. Bocan, “Experimental Investigation of One-Sided Strengthening Interventions on Historic Brick Masonry Walls,” in *RILEM Bookseries*, Springer Science and Business Media B.V., 2023, pp. 485–495.

[98] P. E. Mezrea, M. Ispir, I. A. Balci, I. E. Bal, and A. Ilki, “Diagonal tensile tests on historical brick masonry wallets strengthened with fabric reinforced cementitious mortar,” *Structures*, vol. 33, no. October 2020, pp. 935–946, 2021, doi: 10.1016/j.istruc.2021.04.076.

[99] A. Soleymani, M. A. Najafgholipour, A. Johari, and S. Jowkar, “In-plane shear strengthening of traditional unreinforced masonry walls with near surface mounted GFRP bars,” *Constr Build Mater*, vol. 367, no. January, p. 130362, 2023, doi: 10.1016/j.conbuildmat.2023.130362.

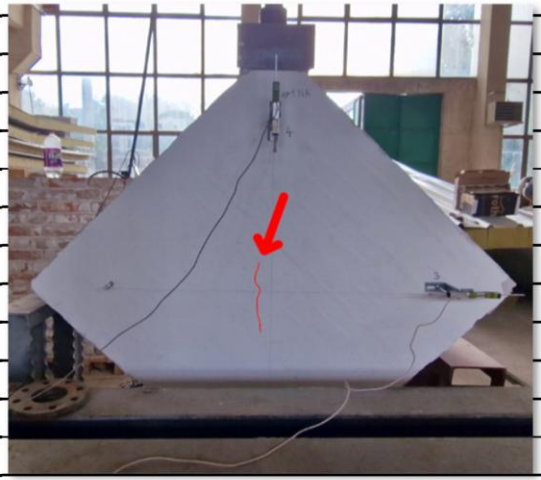
[100] F. Micelli, M. S. Sciolti, M. Leone, M. A. Aiello, and A. Dudine, “Shear behaviour of Fiber Reinforced Mortar strengthened masonry walls built with limestone blocks and hydraulic mortar,” in *Brick and Block Masonry: Trends, Innovations and Challenges - Proceedings of the 16th International Brick and Block Masonry Conference, IBMAC 2016*, C. Modena, F. da Porto, and M. R. Valluzzi, Eds., Padova, Italy: Taylor & Francis Group, 2016, pp. 2137–2146. doi: 10.1201/b21889-264.

BUPT

7 ANNEX A FAILURE MODES OF TESTED SPECIMENS

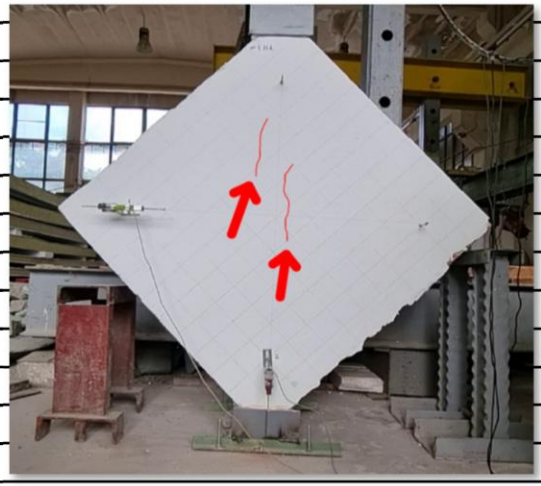
7.1 Unreinforced Specimen

Data Read Number	Actual Time	Event	Vertical Force P [kN]	Shear Stress S_s [Mpa=N/mm^2]- ASTM E519	Shear Strain γ - Average of faces ASTM E519 [mm/m]	Drift Percent δ [%]
37	8:54:07		0	0	0	0
38	8:54:10	Start of loading	0	0	0	0
39	8:54:12		0.05	6.5463E-05	0	0
354	9:06:48		73.35	0.096034167	0.128159802	0.012816
355	9:06:50	First crack on face 1 - diagonal tension cracking	74	0.096885185	0.159094927	0.015909
356	9:06:53		74.25	0.0972125	0.172352837	0.017235
357	9:06:55		74.45	0.097474352	0.198868658	0.019887
358	9:06:58		74.7	0.097801667	0.278416122	0.027842
359	9:07:00		75	0.098194444	0.300512639	0.030051
360	9:07:02		75.3	0.098587222	0.31377055	0.031377
361	9:07:05		74.8	0.097932593	0.335867067	0.033587
362	9:07:07		73.7	0.096492407	0.349124978	0.034912
363	9:07:10		72.25	0.094593981	0.393318013	0.039332
364	9:07:12		70.75	0.092630093	0.397737317	0.039774
365	9:07:14		71.25	0.093284722	0.410995227	0.0411
366	9:07:17		72.45	0.094855833	0.410995227	0.0411
367	9:07:19		74	0.096885185	0.415414531	0.041541
368	9:07:22		74.9	0.098063519	0.419833834	0.041983
369	9:07:24		75.2	0.098456296	0.424253138	0.042425
370	9:07:26		73.6	0.096361481	0.428672441	0.042867
371	9:07:29		71.6	0.093742963	0.433091745	0.043309
372	9:07:31		70.7	0.09256463	0.433091745	0.043309
373	9:07:34		70.4	0.092171852	0.433091745	0.043309



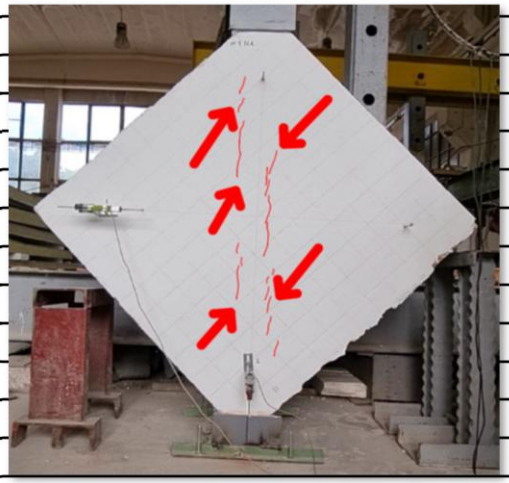
BUPT

Data Read Number	Actual Time	Event	Vertical Force P [kN]	Shear Stress S_s [Mpa=N/mm^2]- ASTM E519	Shear Strain γ - Average of faces ASTM E519 [mm/m]	Drift Percent δ [%]
374	9:07:36		70	0.091648148	0.437511048	0.043751
375	9:07:38		69.7	0.09125537	0.437511048	0.043751
376	9:07:41		69.45	0.090928056	0.437511048	0.043751
377	9:07:43		69.1	0.090469815	0.437511048	0.043751
378	9:07:46		68.8	0.090077037	0.437511048	0.043751
379	9:07:48	Second Crack on face 1 and 2 - diagonal tension cracking	68.5	0.089684259	0.437511048	0.043751
380	9:07:50		68.15	0.089226019	0.437511048	0.043751
381	9:07:53		67.9	0.088898704	0.437511048	0.043751
382	9:07:55		67.7	0.088636852	0.437511048	0.043751
383	9:07:58		67.5	0.088375	0.437511048	0.043751
384	9:08:00		67.35	0.088178611	0.437511048	0.043751
385	9:08:02		67.1	0.087851296	0.437511048	0.043751
386	9:08:05		66.85	0.087523981	0.437511048	0.043751
387	9:08:07		66.65	0.08726213	0.437511048	0.043751
388	9:08:10		66.45	0.087000278	0.437511048	0.043751
389	9:08:12		66.2	0.086672963	0.437511048	0.043751
390	9:08:14		66	0.086411111	0.437511048	0.043751
391	9:08:17		65.85	0.086214722	0.437511048	0.043751
392	9:08:19		65.7	0.086018333	0.441930352	0.044193
393	9:08:22		65.55	0.085821944	0.437511048	0.043751
394	9:08:24		65.4	0.085625556	0.441930352	0.044193
422	9:09:31		74.6	0.097670741	0.455188262	0.045519
423	9:09:34		74.65	0.097736204	0.455188262	0.045519



BUPT

Data Read Number	Actual Time	Event	Vertical Force P [kN]	Shear Stress S_s [Mpa=N/mm^2]- ASTM E519	Shear Strain γ - Average of faces ASTM E519 [mm/m]	Drift Percent δ [%]
424	9:09:36		74.6	0.097670741	0.459607566	0.045961
425	9:09:38		74.65	0.097736204	0.459607566	0.045961
426	9:09:41		74.65	0.097736204	0.459607566	0.045961
427	9:09:43		74.7	0.097801667	0.459607566	0.045961
428	9:09:46		74.7	0.097801667	0.459607566	0.045961
429	9:09:48	Multiple Cracks - diagonal tension cracking	74.65	0.097736204	0.459607566	0.045961
430	9:09:50		74.7	0.097801667	0.459607566	0.045961
431	9:09:53		74.8	0.097932593	0.464026869	0.046403
432	9:09:55		75.1	0.09832537	0.464026869	0.046403
433	9:09:58		75	0.098194444	0.464026869	0.046403
434	9:10:00		75	0.098194444	0.468446173	0.046845
435	9:10:02		75	0.098194444	0.472865476	0.047287
436	9:10:05		75.05	0.098259907	0.472865476	0.047287
437	9:10:07		75.05	0.098259907	0.472865476	0.047287
438	9:10:10		75.05	0.098259907	0.472865476	0.047287
439	9:10:12		75.1	0.09832537	0.472865476	0.047287
440	9:10:14		75.1	0.09832537	0.47728478	0.047728
441	9:10:17		75.15	0.098390833	0.47728478	0.047728
442	9:10:19		75.2	0.098456296	0.47728478	0.047728
443	9:10:22		75.25	0.098521759	0.481704083	0.04817
444	9:10:24		75.3	0.098587222	0.481704083	0.04817
445	9:10:26		75.3	0.098587222	0.481704083	0.04817
466	9:11:17		79.55	0.104151574	0.799893937	0.079989



BUPT

Data Read Number	Actual Time	Event	Vertical Force P [kN]	Shear Stress S_s [Mpa=N/mm^2]-ASTM E519	Shear Strain γ - Average of faces ASTM E519 [mm/m]	Drift Percent δ [%]
467	9:11:19		79.75	0.104413426	0.897118614	0.089712
468	9:11:22	Brittle collapse - complete loss of stability	79.75	0.104413426	1.069471451	0.106947
469	9:11:24		78.9	0.103300556	1.551175535	0.155118
470	9:11:26		-0.2	-0.000261852	10.23068764	1.023069
471	9:11:28		-0.4	-0.000523704	10.23068764	1.023069
472	9:11:30		-0.4	-0.000523704	10.23068764	1.023069
473	9:11:32		-0.4	-0.000523704	24.90719463	2.490719
474	9:11:34		-0.4	-0.000523704	7.296270108	0.729627
475	9:11:36		-0.4	-0.000523704	1.259501503	0.12595
476	9:11:38		-0.45	-0.000589167	10.23068764	1.023069
477	9:11:40		-0.45	-0.000589167	10.23068764	1.023069
478	9:11:42		-0.45	-0.000589167	10.23068764	1.023069
479	9:11:44		-0.45	-0.000589167	10.23068764	1.023069
480	9:11:46		-0.45	-0.000589167	10.23068764	1.023069
481	9:11:48		-0.45	-0.000589167	10.23068764	1.023069

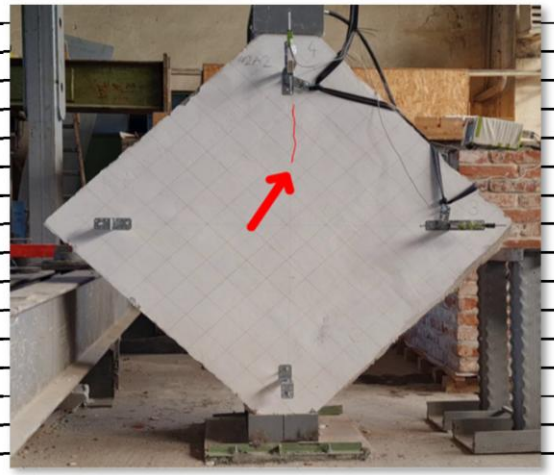


Fig. 7.1 Main events during 1NA unreinforced masonry specimen testing

7.2 Double-sided strengthened specimen

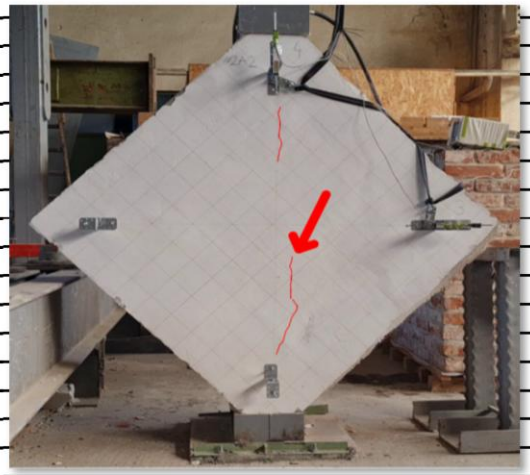
Data Read Number	Actual Time	Event	Vertical Force P [kN]	Shear Stress Ss [Mpa=N/mm2]-ASTM E519	Shear Strain γ - Average of faces ASTM E519 [mm/m]	Drift Percent δ [%]
543	9:34:59		0	0	0	0
544	9:35:02	Start of loading	0.125	0.000163657	0	0
545	9:35:04		0.25	0.000327315	0	0
805	9:45:28		157.5	0.206208333	0.066289553	0.006629
806	9:45:30		158.25	0.207190278	0.066289553	0.006629
807	9:45:33	Sound	159.125	0.20833588	0.066289553	0.006629
808	9:45:35		160	0.209481481	0.066289553	0.006629
809	9:45:38		161	0.210790741	0.066289553	0.006629
832	9:46:33		184.875	0.242049306	0.083966767	0.008397
833	9:46:35		185.875	0.243358565	0.083966767	0.008397
834	9:46:38		186.75	0.244504167	0.079547463	0.007955
835	9:46:40	Another sound, no visible cracks	187.75	0.245813426	0.083966767	0.008397
836	9:46:42		188.625	0.246959028	0.083966767	0.008397
837	9:46:45		189.5	0.24810463	0.083966767	0.008397
838	9:46:47		190.5	0.249413889	0.083966767	0.008397
839	9:46:50		191.375	0.250559491	0.08838607	0.008839
840	9:46:52		192.125	0.251541435	0.08838607	0.008839
841	9:46:54		193	0.252687037	0.08838607	0.008839
842	9:46:57		193.875	0.253832639	0.08838607	0.008839
843	9:46:59		194.625	0.254814583	0.08838607	0.008839
844	9:47:02		195.5	0.255960185	0.08838607	0.008839
845	9:47:04		196.375	0.257105787	0.08838607	0.008839
846	9:47:06		197.25	0.258251389	0.083966767	0.008397
847	9:47:09		198	0.259233333	0.08838607	0.008839
848	9:47:11		198.875	0.260378935	0.08838607	0.008839
849	9:47:14		199.75	0.261524537	0.08838607	0.008839
850	9:47:16	20 tons of loads	200.625	0.262670139	0.092805374	0.009281
851	9:47:18		201.375	0.263652083	0.097224677	0.009722
852	9:47:21		202.125	0.264634028	0.097224677	0.009722
853	9:47:23		203.125	0.265943287	0.097224677	0.009722

Data Read Number	Actual Time	Event	Vertical Force P [kN]	Shear Stress Ss [Mpa=N/mm2]- ASTM E519	Shear Strain γ - Average of faces ASTM E519 [mm/m]	Drift Percent δ [%]
854	9:47:26		204	0.267088889	0.097224677	0.009722
855	9:47:28		204.75	0.268070833	0.101643981	0.010164
856	9:47:30		205.5	0.269052778	0.106063284	0.010606
857	9:47:33		206.625	0.270525694	0.106063284	0.010606
858	9:47:35		208.25	0.272653241	0.110482588	0.011048
859	9:47:38		210	0.274944444	0.114901891	0.01149
860	9:47:40		211.625	0.277071991	0.123740498	0.012374
861	9:47:42		213.25	0.279199537	0.123740498	0.012374
862	9:47:45		214.75	0.281163426	0.123740498	0.012374
863	9:47:47		216	0.2828	0.128159802	0.012816
864	9:47:50		217.375	0.284600231	0.136998409	0.0137
865	9:47:52		218.75	0.286400463	0.136998409	0.0137
866	9:47:54		220	0.288037037	0.141417713	0.014142
867	9:47:57		221.25	0.289673611	0.145837016	0.014584
868	9:47:59		222.5	0.291310185	0.154675623	0.015468
869	9:48:02		223.5	0.292619444	0.154675623	0.015468
870	9:48:04		224.75	0.294256019	0.16351423	0.016351
871	9:48:06		226	0.295892593	0.167933534	0.016793
872	9:48:09		226.875	0.297038194	0.172352837	0.017235
873	9:48:11		227.75	0.298183796	0.176772141	0.017677
874	9:48:14		228.5	0.299165741	0.181191444	0.018119
875	9:48:16		229.125	0.299984028	0.185610748	0.018561
876	9:48:18		229.875	0.300965972	0.190030051	0.019003
877	9:48:21		230.625	0.301947917	0.198868658	0.019887
878	9:48:23		231.25	0.302766204	0.203287962	0.020329
879	9:48:26	First crack - diagonal tension crack along the load axis	231.75	0.303420833	0.216545872	0.021655
880	9:48:28		232.25	0.304075463	0.220965176	0.022097
881	9:48:30		233	0.305057407	0.225384479	0.022538
882	9:48:33		233.625	0.305875694	0.225384479	0.022538
883	9:48:35		234.125	0.306530324	0.234223086	0.023422



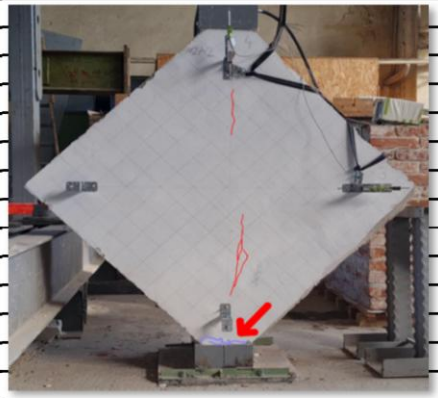
BUPT

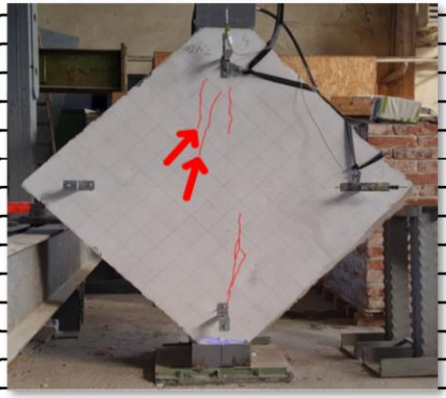
Data Read Number	Actual Time	Event	Vertical Force P [kN]	Shear Stress Ss [Mpa=N/mm2]- ASTM E519	Shear Strain γ - Average of faces ASTM E519 [mm/m]	Drift Percent δ [%]
884	9:48:38	Another crack - diagonal tension crack near the inferior loading shoe	234.625	0.307184954	0.23864239	0.023864
885	9:48:40		232.875	0.30489375	0.23864239	0.023864
886	9:48:42		231.875	0.303584491	0.243061693	0.024306
887	9:48:45		232.375	0.30423912	0.243061693	0.024306
888	9:48:47		234.375	0.306857639	0.247480997	0.024748
889	9:48:50		234.5	0.307021296	0.251900301	0.02519
890	9:48:52		235.125	0.307839583	0.256319604	0.025632
891	9:48:54		235.625	0.308494213	0.256319604	0.025632
892	9:48:57		236	0.308985185	0.265158211	0.026516
893	9:48:59		236.5	0.309639815	0.269577515	0.026958
894	9:49:02		236.75	0.30996713	0.278416122	0.027842
895	9:49:04		237.25	0.310621759	0.282835425	0.028284
896	9:49:06		237.625	0.311112731	0.287254729	0.028725
897	9:49:09		238.125	0.311767361	0.291674032	0.029167
898	9:49:11		238.625	0.312421991	0.296093336	0.029609
899	9:49:14		239.125	0.31307662	0.296093336	0.029609
900	9:49:16		239.75	0.313894907	0.300512639	0.030051
901	9:49:18		240	0.314222222	0.300512639	0.030051
902	9:49:21		240.375	0.314713194	0.309351246	0.030935
903	9:49:23	Further sounds	240.875	0.315367824	0.31377055	0.031377
904	9:49:26		241	0.315531481	0.31377055	0.031377
905	9:49:28		240.875	0.315367824	0.322609157	0.032261
906	9:49:30		239.75	0.313894907	0.322609157	0.032261



BUPT

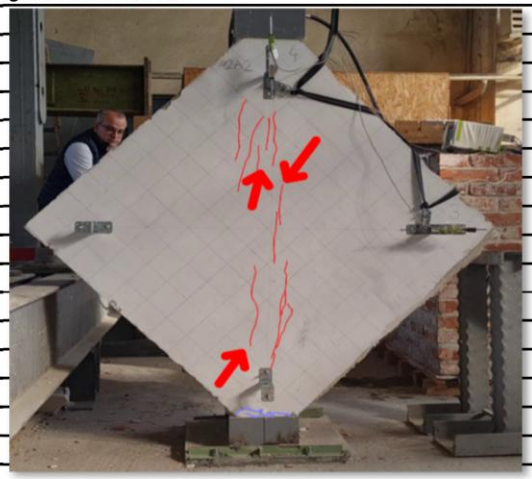
Data Read Number	Actual Time	Event	Vertical Force P [kN]	Shear Stress Ss [Mpa=N/mm2]- ASTM E519	Shear Strain γ - Average of faces ASTM E519 [mm/m]	Drift Percent δ [%]
907	9:49:33	Sounds - local crushing near the inferior loading shoe	239.75	0.313894907	0.32702846	0.032703
908	9:49:35		239.875	0.314058565	0.32702846	0.032703
909	9:49:38		238.5	0.312258333	0.331447764	0.033145
910	9:49:40		238.625	0.312421991	0.335867067	0.033587
911	9:49:42		238.875	0.312749306	0.340286371	0.034029
912	9:49:45		239.25	0.313240278	0.340286371	0.034029
913	9:49:47		239.625	0.31373125	0.344705674	0.034471
914	9:49:50		240	0.314222222	0.344705674	0.034471
915	9:49:52		240.5	0.314876852	0.344705674	0.034471
916	9:49:54		240.75	0.315204167	0.349124978	0.034912
917	9:49:57		241.125	0.315695139	0.349124978	0.034912
918	9:49:59		241.625	0.316349769	0.353544281	0.035354
919	9:50:02		242	0.316840741	0.357963585	0.035796
920	9:50:04		242.5	0.31749537	0.357963585	0.035796
921	9:50:06		242.75	0.317822685	0.362382888	0.036238
922	9:50:09	Further cracks - diagonal tension	243.125	0.318313657	0.366802192	0.03668
923	9:50:11		243.5	0.31880463	0.366802192	0.03668
924	9:50:14		243.875	0.319295602	0.371221495	0.037122
925	9:50:16		244.375	0.319950231	0.371221495	0.037122
926	9:50:18		244.5	0.320113889	0.375640799	0.037564
927	9:50:21		244.875	0.320604861	0.380060103	0.038006
928	9:50:23	Sounds	245.125	0.320932176	0.380060103	0.038006
929	9:50:26		245.375	0.321259491	0.38889871	0.03889
930	9:50:28		245.75	0.321750463	0.393318013	0.039332
931	9:50:30		246	0.322077778	0.397737317	0.039774
932	9:50:33		246.25	0.322405093	0.397737317	0.039774
933	9:50:35		246.5	0.322732407	0.40215662	0.040216
934	9:50:38		246.5	0.322732407	0.40215662	0.040216
935	9:50:40		247	0.323387037	0.406575924	0.040658
936	9:50:42		246.875	0.32322338	0.406575924	0.040658
937	9:50:45		240.375	0.314713194	0.410995227	0.0411





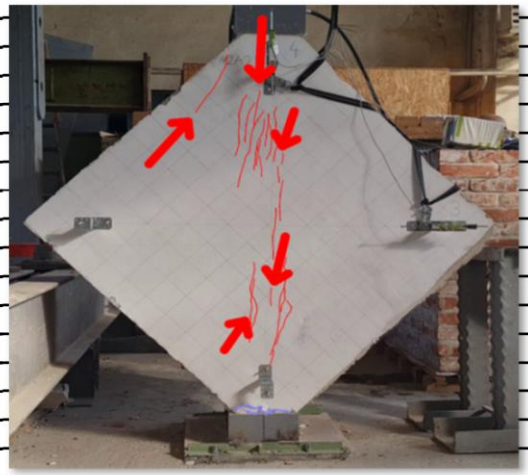
BUPT

Data Read Number	Actual Time	Event	Vertical Force P [kN]	Shear Stress Ss [Mpa=N/mm2]- ASTM E519	Shear Strain γ - Average of faces ASTM E519 [mm/m]	Drift Percent δ [%]
947	9:51:09		250.25	0.32764213	0.433091745	0.043309
948	9:51:11		251	0.328624074	0.437511048	0.043751
949	9:51:14		251.625	0.329442361	0.446349655	0.044635
950	9:51:16		252	0.329933333	0.450768959	0.045077
951	9:51:18		252.5	0.330587963	0.455188262	0.045519
952	9:51:21		252.75	0.330915278	0.459607566	0.045961
953	9:51:23		252.875	0.331078935	0.464026869	0.046403
954	9:51:26		250.625	0.328133102	0.468446173	0.046845
955	9:51:28		253.125	0.33140625	0.47728478	0.047728
956	9:51:30		253.625	0.33206088	0.481704083	0.04817
957	9:51:33		254.125	0.332715509	0.587767368	0.058777
958	9:51:35	New diagonal tension cracks	254.75	0.333533796	0.530316422	0.053032
959	9:51:38		255.125	0.334024769	0.534735726	0.053474
960	9:51:40		255.625	0.334679398	0.534735726	0.053474
961	9:51:42		256.125	0.335334028	0.539155029	0.053916
962	9:51:45		256.625	0.335988657	0.539155029	0.053916
963	9:51:47		257	0.33647963	0.543574333	0.054357
964	9:51:50		257.5	0.337134259	0.547993636	0.054799
965	9:51:52		258	0.337788889	0.547993636	0.054799
966	9:51:54		258.375	0.338279861	0.556832243	0.055683
967	9:51:57		258.875	0.338934491	0.561251547	0.056125
968	9:51:59		259.375	0.33958912	0.570090154	0.057009
969	9:52:02		259.875	0.34024375	0.578928761	0.057893
970	9:52:04		260.5	0.341062037	0.587767368	0.058777
971	9:52:06		261.125	0.341880324	0.587767368	0.058777
972	9:52:09		261.75	0.342698611	0.596605975	0.059661
973	9:52:11		262.25	0.343353241	0.601025278	0.060103
974	9:52:14		262.875	0.344171528	0.605444582	0.060544
975	9:52:16		263.5	0.344989815	0.614283189	0.061428
976	9:52:18		264	0.345644444	0.618702492	0.06187
977	9:52:21		264.75	0.346626389	0.6275411	0.062754



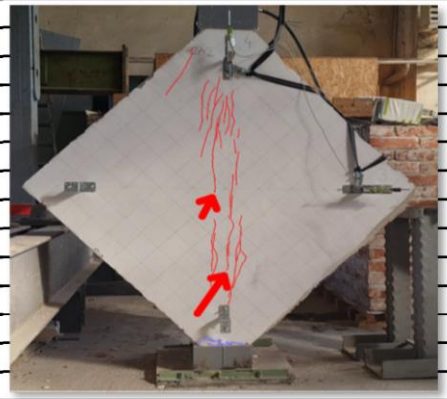
BUPT

Data Read Number	Actual Time	Event	Vertical Force P [kN]	Shear Stress Ss [Mpa=N/mm2]- ASTM E519	Shear Strain γ - Average of faces ASTM E519 [mm/m]	Drift Percent δ [%]
978	9:52:23		265.25	0.347281019	0.64079901	0.06408
979	9:52:26	New diagonal tension cracks	265.875	0.348099306	0.649637617	0.064964
980	9:52:28		266.375	0.348753935	0.676153438	0.067615
981	9:52:30		266.875	0.349408565	0.711507866	0.071151
982	9:52:33		267.375	0.350063194	0.733604384	0.07336
983	9:52:35		267.875	0.350717824	0.751281598	0.075128
984	9:52:38		268.25	0.351208796	0.768958812	0.076896
985	9:52:40		268.875	0.352027083	0.786636026	0.078664
986	9:52:42		269.25	0.352518056	0.799893937	0.079989
987	9:52:45		269.875	0.353336343	0.813151847	0.081315
988	9:52:47		270.375	0.353990972	0.826409758	0.082641
989	9:52:50		271	0.354809259	0.844086972	0.084409
990	9:52:52		271.5	0.355463889	0.857344882	0.085734
991	9:52:54		272	0.356118519	0.875022097	0.087502
992	9:52:57		272.625	0.356936806	0.875022097	0.087502
993	9:52:59		273.25	0.357755093	0.897118614	0.089712
994	9:53:02		273.875	0.35857338	0.914795828	0.09148
995	9:53:04		274.5	0.359391667	0.936892346	0.093689
996	9:53:06		275	0.360046296	0.941311649	0.094131
997	9:53:09		275.625	0.360864583	0.95456956	0.095457
998	9:53:11		276.25	0.36168287	0.96782747	0.096783
999	9:53:14		276.75	0.3623375	0.981085381	0.098109
1000	9:53:16		277.25	0.36299213	0.994343291	0.099434
1001	9:53:18		277.75	0.363646759	1.016439809	0.101644
1002	9:53:21		278.375	0.364465046	1.04295563	0.104296
1003	9:53:23		278.75	0.364956019	1.056213541	0.105621
1004	9:53:26		279.375	0.365774306	1.069471451	0.106947
1005	9:53:28		279.875	0.366428935	1.095987272	0.109599
1006	9:53:30		280.5	0.367247222	1.126922397	0.112692
1007	9:53:33		280.875	0.367738194	1.149018915	0.114902
1008	9:53:35		281.375	0.368392824	1.175534736	0.117553



BUPT

Data Read Number	Actual Time	Event	Vertical Force P [kN]	Shear Stress Ss [Mpa=N/mm2]- ASTM E519	Shear Strain γ - Average of faces ASTM E519 [mm/m]	Drift Percent δ [%]
1009	9:53:38		281.875	0.369047454	1.197631253	0.119763
1010	9:53:40		282.375	0.369702083	1.277178717	0.127718
1011	9:53:42		282.75	0.370193056	1.299275234	0.129928
1012	9:53:45		283.25	0.370847685	1.325791055	0.132579
1013	9:53:47		283.75	0.371502315	1.347887573	0.134789
1014	9:53:50		284.25	0.372156944	1.374403394	0.13744
1015	9:53:52		284.5	0.372484259	1.396499912	0.13965
1016	9:53:54		284.5	0.372484259	1.427435036	0.142744
1017	9:53:57		284.625	0.372647917	1.52024041	0.152024
1018	9:53:59		284.5	0.372484259	1.560014142	0.156001
1019	9:54:02	New diagonal tension cracks	284.625	0.372647917	1.586529963	0.158653
1020	9:54:04		284.625	0.372647917	1.60862648	0.160863
1021	9:54:06		283.875	0.371665972	1.643980909	0.164398
1022	9:54:09		283.625	0.371338657	1.661658123	0.166166
1023	9:54:11		282.375	0.369702083	1.674916033	0.167492
1024	9:54:14		283.375	0.371011343	1.688173944	0.168817
1025	9:54:16		283.25	0.370847685	1.701431854	0.170143
1026	9:54:18		281.125	0.368065509	1.714689765	0.171469
1027	9:54:21		282.375	0.369702083	1.785398621	0.17854
1028	9:54:23		283	0.37052037	1.798656532	0.179866
1029	9:54:26		277.25	0.36299213	1.807495139	0.18075
1030	9:54:28		272.375	0.356609491	1.820753049	0.182075
1031	9:54:30		267.75	0.350554167	1.838430263	0.183843
1032	9:54:33		271.75	0.355791204	1.851688174	0.185169
1033	9:54:35		277	0.362664815	1.851688174	0.185169
1034	9:54:38	The force seems to be decreasing	281.5	0.368556481	1.856107477	0.185611
1035	9:54:40		281.25	0.368229167	1.860526781	0.186053
1036	9:54:42		281.375	0.368392824	1.869365388	0.186937
1037	9:54:45		282	0.369211111	1.882623299	0.188262
1038	9:54:47		282.75	0.370193056	1.895881209	0.189588
1039	9:54:50		283.375	0.371011343	1.90913912	0.190914



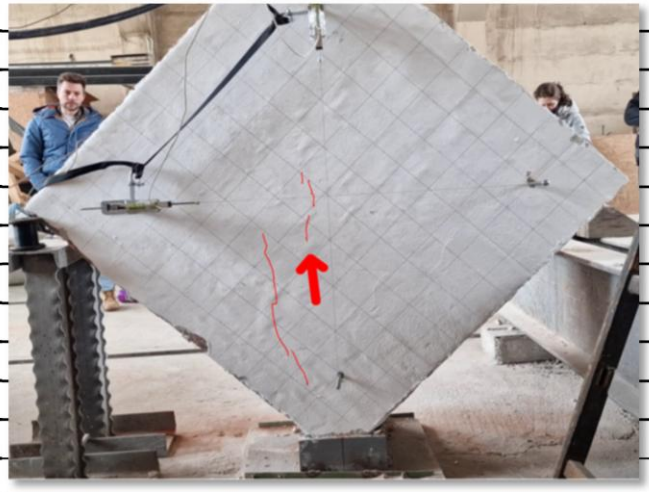
BUPT

Data Read Number	Actual Time	Event	Vertical Force P [kN]	Shear Stress Ss [Mpa=N/mm2]-ASTM E519	Shear Strain γ - Average of faces ASTM E519 [mm/m]	Drift Percent δ [%]
1040	9:54:52	New increase in force	283.625	0.371338657	1.931235637	0.193124
1041	9:54:54		284.25	0.372156944	2.015202404	0.20152
1042	9:54:57		284.75	0.372811574	3.933180131	0.393318
1043	9:54:59		284.875	0.372975231	3.972953862	0.397295
1044	9:55:02		284.625	0.372647917	4.030404808	0.40304
1045	9:55:04		283.125	0.370684028	3.84479406	0.384479
1046	9:55:06		7.25	0.00949213	2.929998232	0.293
1047	9:55:09	Cracking parallel to masonry plane	28.375	0.037150231	2.921159625	0.292116
1048	9:55:11		30.25	0.039605093	2.921159625	0.292116
1049	9:55:14	Loading was stopped to mark and study the cracks	32.25	0.042223611	2.921159625	0.292116
1050	9:55:16		34.25	0.04484213	2.925578929	0.292558
1051	9:55:18		36.25	0.047460648	2.921159625	0.292116
1052	9:55:21		38.25	0.050079167	2.921159625	0.292116
1053	9:55:23		40.25	0.052697685	2.921159625	0.292116
1054	9:55:26		42.125	0.055152546	2.921159625	0.292116
1055	9:55:28		44.125	0.057771065	2.921159625	0.292116
1056	9:55:30		46	0.060225926	2.938836839	0.293884
1057	9:55:33		48	0.062844444	2.929998232	0.293
1058	9:55:35		49.875	0.065299306	2.929998232	0.293
1059	9:55:38		51.75	0.067754167	2.929998232	0.293
1060	9:55:40		53.75	0.070372685	2.934417536	0.293442
1061	9:55:42		55.625	0.072827546	2.934417536	0.293442
1062	9:55:45		57.625	0.075446065	2.938836839	0.293884
1063	9:55:47		59.5	0.077900926	2.947675446	0.294768
1064	9:55:50		61.375	0.080355787	2.947675446	0.294768
1065	9:55:52		63.25	0.082810648	2.95209475	0.295209
1066	9:55:54		65.125	0.085265509	2.956514053	0.295651
1067	9:55:57		67	0.08772037	2.96535266	0.296535
1068	9:55:59		68.875	0.090175231	2.978610571	0.297861
1069	9:56:02		70.75	0.092630093	2.983029874	0.298303
1070	9:56:04		72.5	0.094921296	2.991868482	0.299187

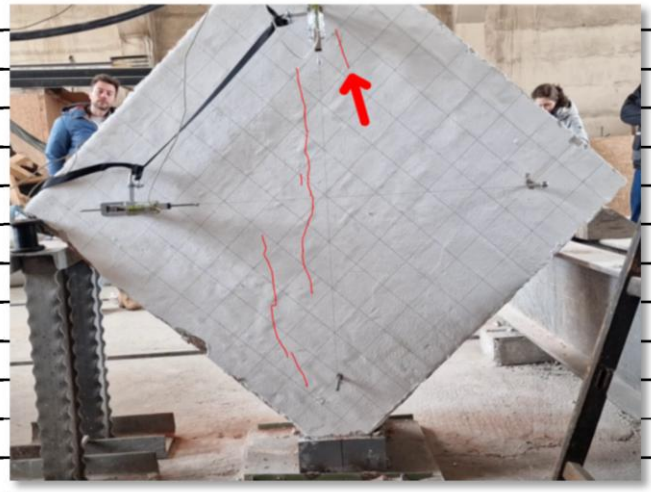
Fig. 7.2 Main events during 2A2 two-side strengthened specimen testing

7.3 Single-sided Strengthened Specimen

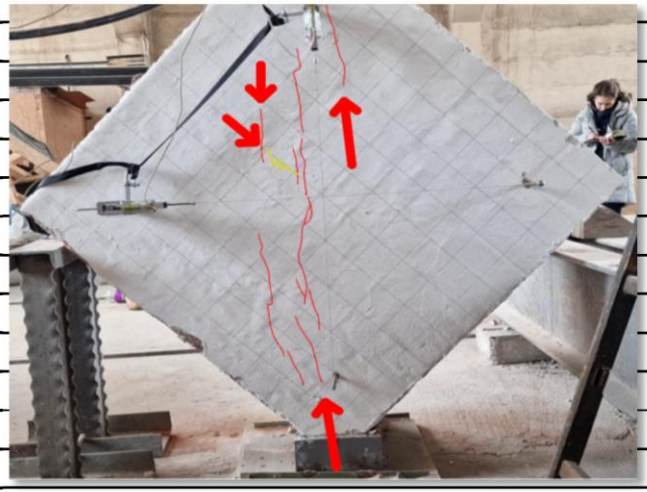
Data Read Number	Actual Time	Event	Vertical Force P [kN]	Shear Stress Ss [Mpa=N/mm2]-ASTM E519	Shear Strain γ - Average of faces ASTM E519 [mm/m]	Drift Percent δ [%]
1	12:59:58		0	0	0	0
90	13:03:32		0	0	-0.004419304	-0.00044
91	13:03:34	Beginning of load	0	0	0	0
92	13:03:37		0.125	0.000163657	-0.004419304	-0.00044
260	13:10:20		104.375	0.136653935	0.309351246	0.03094
261	13:10:22		104.875	0.137308565	0.322609157	0.03226
262	13:10:25		105.25	0.137799537	0.32702846	0.0327
263	13:10:27		105.625	0.138290509	0.335867067	0.03359
264	13:10:29		106.125	0.138945139	0.344705674	0.03447
265	13:10:32		106.5	0.139436111	0.353544281	0.03535
266	13:10:34		106.875	0.139927083	0.362382888	0.03624
267	13:10:37		107.375	0.140581713	0.366802192	0.03668
268	13:10:39		107.875	0.141236343	0.371221495	0.03712
269	13:10:41		108.25	0.141727315	0.371221495	0.03712
270	13:10:44		108.625	0.142218287	0.375640799	0.03756
271	13:10:46		109	0.142709259	0.384479406	0.03845
272	13:10:49		109.5	0.143363889	0.38889871	0.03889
273	13:10:51		109.875	0.143854861	0.410995227	0.0411
274	13:10:53		110.375	0.144509491	0.424253138	0.04243
275	13:10:56	Low intensity sounds	110.75	0.145000463	0.433091745	0.04331
276	13:10:58	A diagonal tension crack is beginning to form on the unreinforced face 2	111.25	0.145655093	0.441930352	0.04419
277	13:11:01		111.625	0.146146065	0.450768959	0.04508
278	13:11:03		112.125	0.146800694	0.455188262	0.04552

Data Read Number	Actual Time	Event	Vertical Force P [kN]	Shear Stress Ss [Mpa=N/mm2]- ASTM E519	Shear Strain γ - Average of faces ASTM E519 [mm/m]	Drift Percent δ [%]
290	13:11:32		116.75	0.152856019	0.55241294	0.05524
291	13:11:34	Cracks on unreinforced face 2	117.125	0.153346991	0.56567085	0.05657
292	13:11:37		117.5	0.153837963	0.578928761	0.05789
293	13:11:39		117.75	0.154165278	0.587767368	0.05878
294	13:11:41		118.125	0.15465625	0.601025278	0.0601
295	13:11:44		118.5	0.155147222	0.618702492	0.06187
296	13:11:46		118.75	0.155474537	0.6275411	0.06275
297	13:11:49		118.875	0.155638194	0.64079901	0.06408
298	13:11:51		119.125	0.155965509	0.645218314	0.06452
299	13:11:53		119.5	0.156456481	0.658476224	0.06585
300	13:11:56		119.625	0.156620139	0.671734135	0.06717
301	13:11:58		119.875	0.156947454	0.676153438	0.06762
302	13:12:01		120.125	0.157274769	0.680572742	0.06806
303	13:12:03		120.5	0.157765741	0.684992045	0.0685
304	13:12:05		120.75	0.158093056	0.698249956	0.06982
305	13:12:08		121	0.15842037	0.707088563	0.07071
306	13:12:10		121.375	0.158911343	0.720346473	0.07203
307	13:12:13		121.5	0.159075	0.733604384	0.07336
308	13:12:15		121.875	0.159565972	0.742442991	0.07424
309	13:12:17		122.125	0.159893287	0.751281598	0.07513
310	13:12:20		122.5	0.160384259	0.755700902	0.07557
311	13:12:22		122.75	0.160711574	0.768958812	0.0769
312	13:12:25		123	0.161038889	0.782216723	0.07822

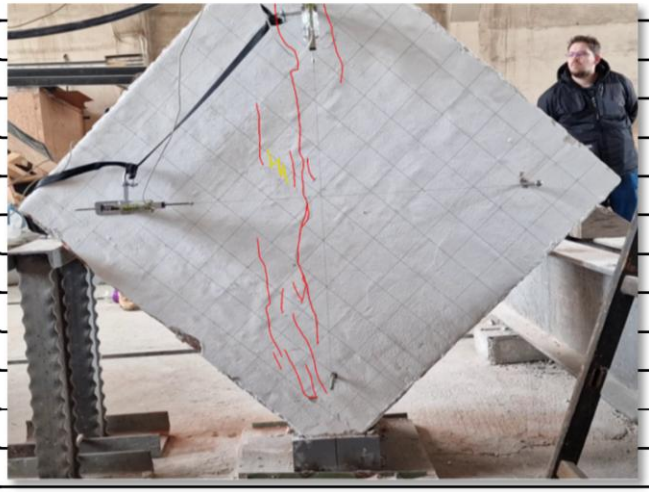
BUPT

Data Read Number	Actual Time	Event	Vertical Force P [kN]	Shear Stress Ss [Mpa=N/mm2]- ASTM E519	Shear Strain γ - Average of faces ASTM E519 [mm/m]	Drift Percent δ [%]
317	13:12:37		124.625	0.163166435	0.821990454	0.0822
318	13:12:39	Cracks are opening, third diagonal tension crack on unreinforced face 2	125	0.163657407	0.835248365	0.08352
319	13:12:41	Still no damage on face 1	125.25	0.163984722	0.848506275	0.08485
320	13:12:44		125.625	0.164475694	0.857344882	0.08573
321	13:12:46		125.875	0.164803009	0.870602793	0.08706
322	13:12:49		126.125	0.165130324	0.883860704	0.08839
323	13:12:51		126.5	0.165621296	0.892699311	0.08927
324	13:12:53		126.75	0.165948611	0.910376525	0.09104
325	13:12:56		127	0.166275926	0.914795828	0.09148
326	13:12:58		127.375	0.166766898	0.932473042	0.09325
327	13:13:01		127.75	0.16725787	0.945730953	0.09457
328	13:13:03		127.75	0.16725787	0.958988863	0.0959
329	13:13:05		127	0.166275926	0.96782747	0.09678
330	13:13:08		125.375	0.16414838	0.976666077	0.09767
331	13:13:10		125.125	0.163821065	0.985504684	0.09855
332	13:13:13		126.25	0.165293981	0.989923988	0.09899
333	13:13:15		127.5	0.166930556	0.998762595	0.09988
334	13:13:17		127.5	0.166930556	1.007601202	0.10076
335	13:13:20		127.875	0.167421528	1.012020506	0.1012
336	13:13:22		128	0.167585185	1.016439809	0.10164
337	13:13:25		128.125	0.167748843	1.025278416	0.10253
338	13:13:27		128.375	0.168076157	1.034117023	0.10341
339	13:13:29		128.5	0.168239815	1.04295563	0.1043

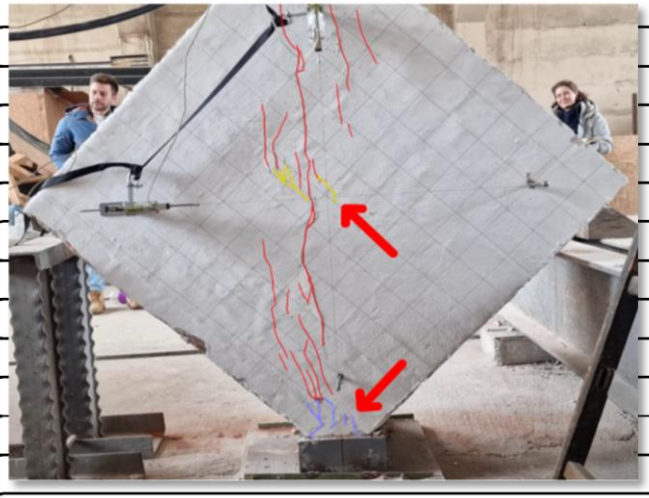
BUPT

Data Read Number	Actual Time	Event	Vertical Force P [kN]	Shear Stress Ss [Mpa=N/mm2]- ASTM E519	Shear Strain γ - Average of faces ASTM E519 [mm/m]	Drift Percent δ [%]
345	13:13:44		129.625	0.169712731	1.104825879	0.11048
346	13:13:46	Diagonal tension cracking on the whole diagonal unreinforced face 2	129.875	0.170040046	1.113664486	0.11137
347	13:13:49	A local joint sliding crack. No sign of damage on the reinforced face 1	130.125	0.170367361	1.131341701	0.11313
348	13:13:51		130.25	0.170531019	1.149018915	0.1149
349	13:13:53		130.625	0.171021991	1.162276825	0.11623
350	13:13:56		130.75	0.171185648	1.179954039	0.118
351	13:13:58		130.875	0.171349306	1.202050557	0.12021
352	13:14:01		131.125	0.17167662	1.215308467	0.12153
353	13:14:03		131.375	0.172003935	1.232985681	0.1233
354	13:14:05		131.5	0.172167593	1.241824288	0.12418
355	13:14:08		131.5	0.172167593	1.255082199	0.12551
356	13:14:10		131.625	0.17233125	1.263920806	0.12639
357	13:14:13		131.875	0.172658565	1.272759413	0.12728
358	13:14:15		132	0.172822222	1.286017324	0.1286
359	13:14:17		131.875	0.172658565	1.299275234	0.12993
360	13:14:20		132	0.172822222	1.303694538	0.13037
361	13:14:22		132.375	0.173313194	1.321371752	0.13214
362	13:14:25		132.375	0.173313194	1.321371752	0.13214
363	13:14:27		132.375	0.173313194	1.330210359	0.13302
364	13:14:29		132.5	0.173476852	1.339048966	0.1339
365	13:14:32		132.75	0.173804167	1.352306876	0.13523
366	13:14:34		132.75	0.173804167	1.361145483	0.13611
367	13:14:37		132.75	0.173804167	1.383242001	0.13832

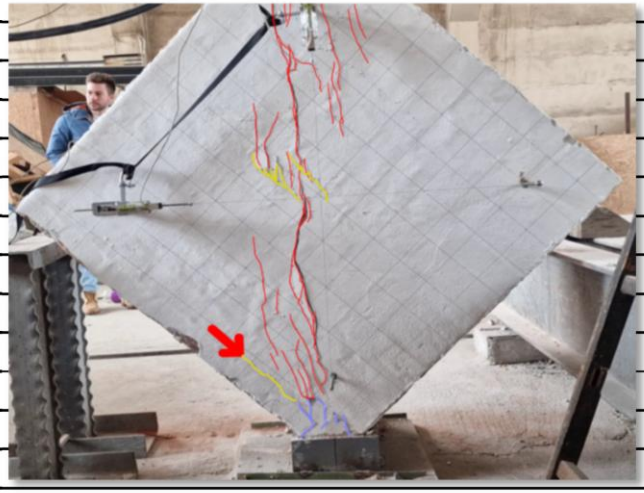
BUPT

Data Read Number	Actual Time	Event	Vertical Force P [kN]	Shear Stress Ss [Mpa=N/mm2]- ASTM E519	Shear Strain γ - Average of faces ASTM E519 [mm/m]	Drift Percent δ [%]
399	13:15:53		136.125	0.178222917	1.679335337	0.16793
400	13:15:56	Main crack widened on unreinforced face 2	136.25	0.178386574	1.688173944	0.16882
401	13:15:58	No crack on reinforced face 1	136.5	0.178713889	1.701431854	0.17014
402	13:16:01		136.625	0.178877546	1.710270461	0.17103
403	13:16:03		136.625	0.178877546	1.719109068	0.17191
404	13:16:05		136.75	0.179041204	1.732366979	0.17324
405	13:16:08		137.125	0.179532176	1.736786282	0.17368
406	13:16:10		137.125	0.179532176	1.74562489	0.17456
407	13:16:13		137.25	0.179695833	1.750044193	0.175
408	13:16:15		137.375	0.179859491	1.763302104	0.17633
409	13:16:17		137.75	0.180350463	1.772140711	0.17721
410	13:16:20		137.75	0.180350463	1.780979318	0.1781
411	13:16:22		138	0.180677778	1.780979318	0.1781
412	13:16:25		138	0.180677778	1.785398621	0.17854
413	13:16:27		138.25	0.181005093	1.794237228	0.17942
414	13:16:29		138.25	0.181005093	1.807495139	0.18075
415	13:16:32		138.375	0.18116875	1.816333746	0.18163
416	13:16:34		138.5	0.181332407	1.820753049	0.18208
417	13:16:37		138.5	0.181332407	1.825172353	0.18252
418	13:16:39		138.875	0.18182338	1.829591656	0.18296
419	13:16:41		138.75	0.181659722	1.83401096	0.1834
420	13:16:44		138.875	0.18182338	1.842849567	0.18428
421	13:16:46		139.125	0.182150694	1.851688174	0.18517

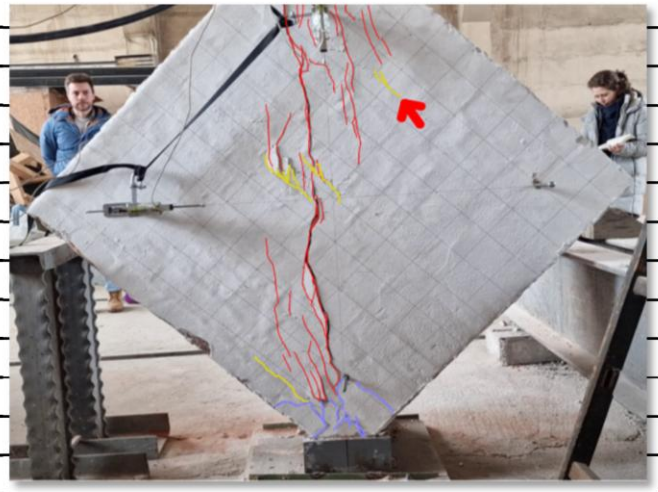
BUPT

Data Read Number	Actual Time	Event	Vertical Force P [kN]	Shear Stress Ss [Mpa=N/mm2]-ASTM E519	Shear Strain γ - Average of faces ASTM E519 [mm/m]	Drift Percent δ [%]
461	13:18:22		147	0.192461111	2.837192858	0.28372
462	13:18:25	Powerful sudden sound, main crack on face 2 open at approx. 3mm	147.375	0.192952083	2.885805197	0.28858
463	13:18:27	Crushing cracks near the lower shoe. No crack on reinforced face 1	147.75	0.193443056	2.947675446	0.29477
464	13:18:29		147.875	0.193606713	3.013964999	0.3014
465	13:18:32		148.125	0.193934028	3.093512462	0.30935
466	13:18:34		148	0.19377037	3.20399505	0.3204
467	13:18:37		147.75	0.193443056	3.451476047	0.34515
468	13:18:39		146.75	0.192133796	3.725472865	0.37255
469	13:18:41		145.875	0.190988194	3.915502917	0.39155
470	13:18:44		145.25	0.190169907	4.052501326	0.40525
471	13:18:46		143.375	0.187715046	4.167403217	0.41674
472	13:18:49		141.625	0.185423843	4.251369984	0.42514
473	13:18:51		140.125	0.183459954	4.32207884	0.43221
474	13:18:53		139.125	0.182150694	4.379529786	0.43795
475	13:18:56		138	0.180677778	4.428142125	0.44281
476	13:18:58		136.875	0.179204861	4.467915856	0.44679
477	13:19:01		135.625	0.177568287	4.507689588	0.45077
478	13:19:03		134.125	0.175604398	4.543044016	0.4543
479	13:19:05		133.5	0.174786111	4.569559837	0.45696
480	13:19:08		133	0.174131481	4.604914266	0.46049
481	13:19:10		132.375	0.173313194	4.631430087	0.46314
482	13:19:13		132	0.172822222	4.662365211	0.46624
483	13:19:15		131.875	0.172658565	4.684461729	0.46845

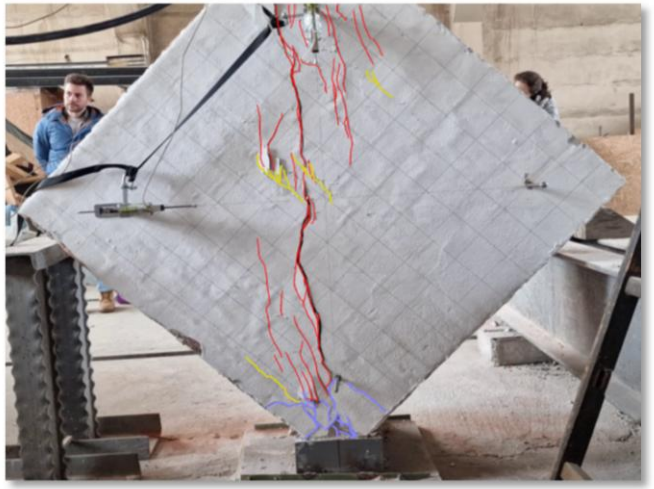
BUPT

Data Read Number	Actual Time	Event	Vertical Force P [kN]	Shear Stress Ss [Mpa=N/mm2]- ASTM E519	Shear Strain γ - Average of faces ASTM E519 [mm/m]	Drift Percent δ [%]
484	13:19:17	Force stays constant. Deformations grow on unreinforced face 2	131.875	0.172658565	4.71097755	0.4711
485	13:19:20		131.625	0.17233125	4.728654764	0.47287
547	13:21:49		133.375	0.174622454	5.329680042	0.53297
548	13:21:51	Force beginning to increase again	135	0.17675	5.334099346	0.53341
549	13:21:53		135.75	0.177731944	5.338518649	0.53385
550	13:21:56		136.125	0.178222917	5.342937953	0.53429
551	13:21:58		135.875	0.177895602	5.347357256	0.53474
552	13:22:01		135.5	0.17740463	5.35177656	0.53518
553	13:22:03		135	0.17675	5.356195864	0.53562
554	13:22:05		134.875	0.176586343	5.360615167	0.53606
555	13:22:08		134.375	0.175931713	5.365034471	0.5365
556	13:22:10		134	0.175440741	5.365034471	0.5365
557	13:22:13		133.5	0.174786111	5.369453774	0.53695
558	13:22:15		133.125	0.174295139	5.373873078	0.53739
559	13:22:17		132.875	0.173967824	5.378292381	0.53783
560	13:22:20		132.75	0.173804167	5.382711685	0.53827
561	13:22:22		132.625	0.173640509	5.382711685	0.53827
562	13:22:25		132.375	0.173313194	5.387130988	0.53871
563	13:22:27		131.875	0.172658565	5.391550292	0.53916
564	13:22:29		132.375	0.173313194	5.395969595	0.5396
565	13:22:32		132.625	0.173640509	5.395969595	0.5396
566	13:22:34		132.875	0.173967824	5.400388899	0.54004
567	13:22:37		133.125	0.174295139	5.409227506	0.54092

BUPT

Data Read Number	Actual Time	Event	Vertical Force P [kN]	Shear Stress Ss [Mpa=N/mm2]-ASTM E519	Shear Strain γ - Average of faces ASTM E519 [mm/m]	Drift Percent δ [%]
619	13:24:41		129.625	0.169712731	5.563903129	0.55639
620	13:24:44	Still no damage on reinforced face 1	129.625	0.169712731	5.563903129	0.55639
621	13:24:46		130.875	0.171349306	5.568322432	0.55683
778	13:31:03		137.5	0.180023148	5.811384126	0.58114
779	13:31:05		137.375	0.179859491	5.811384126	0.58114
780	13:31:08		137.5	0.180023148	5.815803429	0.58158
781	13:31:10		137.875	0.18051412	5.815803429	0.58158
782	13:31:13		137.625	0.180186806	5.820222733	0.58202
783	13:31:15		137.75	0.180350463	5.820222733	0.58202
784	13:31:17		137.875	0.18051412	5.82906134	0.58291
785	13:31:20		138.25	0.181005093	5.837899947	0.58379
786	13:31:22		138.75	0.181659722	5.851157858	0.58512
787	13:31:25		139.5	0.182641667	5.864415768	0.58644
788	13:31:27		140.25	0.183623611	5.899770196	0.58998
789	13:31:29		140.875	0.184441898	5.939543928	0.59395
790	13:31:32		141.5	0.185260185	5.99257557	0.59926
791	13:31:34		142.125	0.186078472	6.06770373	0.60677
792	13:31:37	Deformation grows at a rate of approx. 0.4mm/s on face 2	142.5	0.186569444	6.160509104	0.61605
793	13:31:39	Existing cracks open wide	142.875	0.187060417	6.270991692	0.6271
794	13:31:41		143	0.187224074	6.377054976	0.63771
795	13:31:44		143.375	0.187715046	6.487537564	0.64875
796	13:31:46		143.5	0.187878704	6.615697366	0.66157
797	13:31:49		143.5	0.187878704	6.748276472	0.67483

BUPT

Data Read Number	Actual Time	Event	Vertical Force P [kN]	Shear Stress Ss [Mpa=N/mm2]- ASTM E519	Shear Strain γ - Average of faces ASTM E519 [mm/m]	Drift Percent δ [%]
801	13:31:58	Horizontal crack of approx. 6mm on unreinforced face 2	143.625	0.188042361	7.380236875	0.73802
802	13:32:01		143.375	0.187715046	7.561428319	0.75614
803	13:32:03		143.125	0.187387731	7.773554888	0.77736
804	13:32:05		142.75	0.186896759	8.007777974	0.80078
805	13:32:08		142.25	0.18624213	8.272936185	0.82729
806	13:32:10		141.625	0.185423843	8.569029521	0.8569
807	13:32:13		140.75	0.184278241	8.935831713	0.89358
808	13:32:15		139.25	0.182314352	9.598727241	0.95987
809	13:32:17		135.75	0.177731944	10.72564964	1.07256

BUPT

Data Read Number	Actual Time	Event	Vertical Force P [kN]	Shear Stress Ss [Mpa=N/mm2]-ASTM E519	Shear Strain γ - Average of faces ASTM E519 [mm/m]	Drift Percent δ [%]
810	13:32:20		129.5	0.169549074	11.87908786	1.18791
811	13:32:22	Long joint sliding crack on unreinforced face 2, force dropped.	125.625	0.164475694	12.51988687	1.25199
812	13:32:25	Horizontal crack of approx. 10mm on unreinforced face 2	123.625	0.161857176	13.01484886	1.30148
813	13:32:27		121.875	0.159565972	13.4479406	1.34479

BUPT

ANNEX A Failure modes of tested specimens

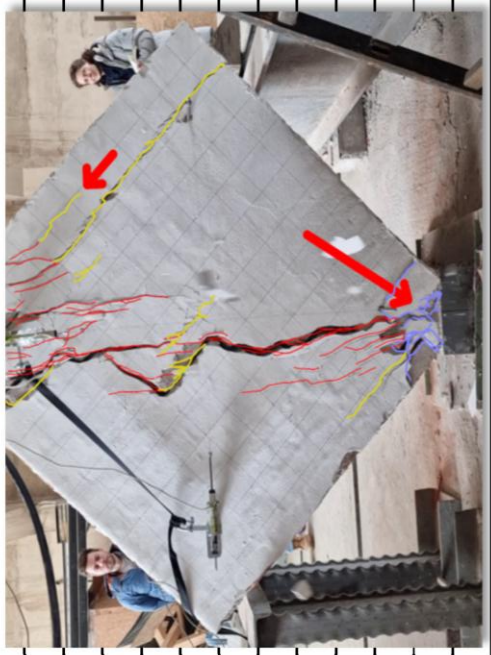
Data Read Number	Actual Time	Event	Vertical Force P [kN]	Shear Stress Ss [Mpa=N/mm2]- ASTM E519	Shear Strain γ - Average of faces ASTM E519 [mm/m]	Drift Percent δ [%]
814	13:32:29		120.5	0.157765741	13.91638678	1.39164
815	13:32:32	Stability lost from crushing near inferior loading shoe on face 2.	118.875	0.155638194	14.40692947	1.44069
816	13:32:34	Only the testing rig keeps the sample in place.	117.125	0.153346991	15.18472689	1.51847
817	13:32:37		112.125	0.146800694	19.93547817	1.99355
818	13:32:39		40.375	0.052861343	16.54587237	1.65459
819	13:32:41		32.375	0.042387269	16.44864769	1.64486
820	13:32:44		26.25	0.034368056	16.37793884	1.63779
821	13:32:46		21.625	0.028312731	16.32490719	1.63249
822	13:32:49		18	0.023566667	16.27629486	1.62763
823	13:32:51		15.375	0.020129861	16.21442461	1.62144
824	13:32:53		13.25	0.017347685	16.16581227	1.61658
825	13:32:56		11.75	0.015383796	16.13929645	1.61393
826	13:32:58		10.875	0.014238194	16.12161923	1.61216
827	13:33:01		10.75	0.014074537	16.11278063	1.61128
828	13:33:03		0.5	0.00065463	16.09510341	1.60951
829	13:33:05		0.5	0.00065463	16.05974898	1.60597
830	13:33:08		0.375	0.000490972	16.03323316	1.60332
831	13:33:10		0.375	0.000490972	15.90949266	1.59095
832	13:33:12		0.125	0.000163657	22.72847799	2.27285
833	13:33:14		0	0	19.14442284	1.91444
834	13:33:16		0	0	15.59572211	1.55957
835	13:33:18		3.125	0.004091435	15.5824642	1.55825
836	13:33:19		3.125	0.004091435	-16.97012551	-1.69701

Fig. 7.3 Main events during 4A1 one-side strengthened wall testing